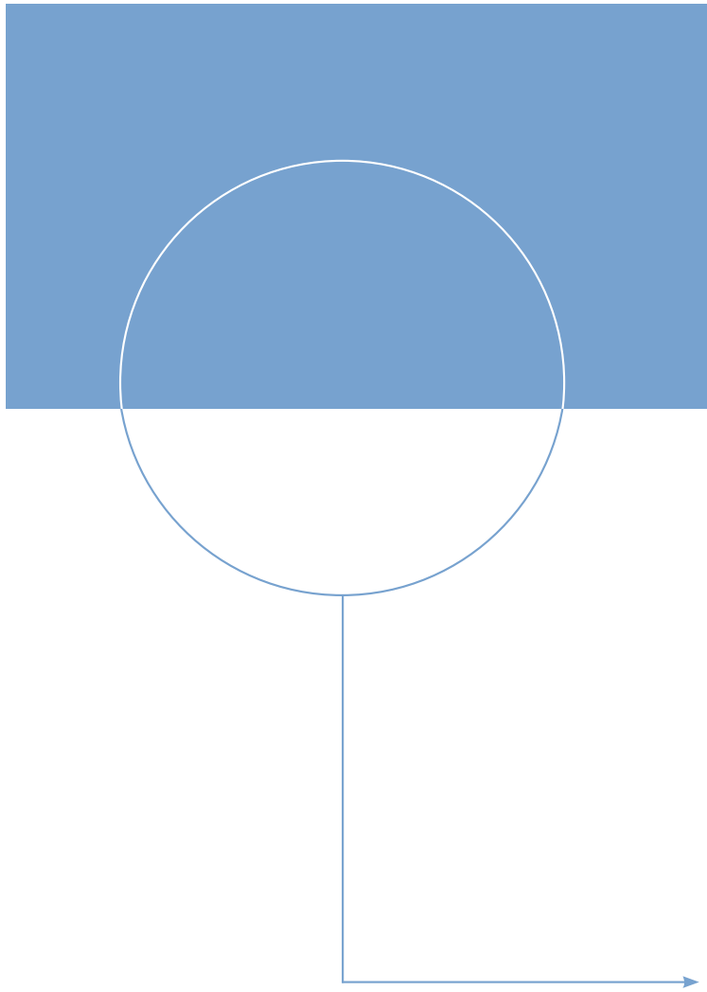

Master's thesis

2022

André Oppegård

NTNU
Norwegian University of
Science and Technology
Faculty of Information Technology and Electrical
Engineering
Department of Electric Power Engineering

André Oppegård

Modeling Optical Current Transformers in a Digital Substation.

May 2022

NTNU
Norwegian University of
Science and Technology

NTNU
Norwegian University of
Science and Technology

NTNU
Norwegian University of
Science and Technology

Modeling Optical Current Transformers in a Digital Substation.

André Oppegård

Electrical Power Engineering
Submission date: May 2022
Supervisor: Irina Oleinikova
Co-supervisor: Mohammad Khalili Katoulaei

Norwegian University of Science and Technology
Department of Electric Power Engineering

Preface

The following thesis concludes my master's degree in electrical power engineering at the Norwegian University of Science and Technology, within the department of Electric Power Engineering. The thesis is a continuance of a specialization project on the same topic, done the year before. This master's thesis has been done by the guidance of Irina Oleinikova and Mohammad Khalili Katoulaei. During the work on this thesis an extended abstract of its content was submitted to the SEST 2022 conference, aswell as a full scientific article following the acceptance of the abstract. The content of the thesis was chosen based of my professional interest in protection and control systems, I work as a protection relay engineer and keep a great interest of the topics discussed in this thesis. The thesis was completed in may of the spring semester in 2022.

Student, André Oppegård

Acknowledgement

I would like to thank the following persons and institutions for making the completion of this thesis possible:

- My supervisor Irina Oleinikova at NTNU, for great guidance during the work of producing the thesis.
- My co-supervisor Mohammad Khalili Katoulaei at NTNU, for great guidance and support on the subject.
- Bane NOR, for giving me the possibility to pursue further education while employed full-time.

Abstract

This work is focused on digital substation technologies, with a further attention to optical current transformers and their performance and interoperability in a differential protection setting. Optical current transformers have become a more accessible technology the last two decades. This transition from a conventional current transformer design to an optical one stimulates the requirement to develop a complete model of a OPCT. The model would define the performance, interoperability and error sources that could possibly occur in a digital substation.

This thesis maps the present current transducer technologies used in substations, with focus on their pitfalls and positive aspects. Following the mapping of the present and future technology a optical model of an open-core bulk-glass optical current transformer is developed and presented. This complete model is based of an optical model modelled by the use of a finite element method in a 2D environment. The thesis also presents an electrical model based on data experimentally obtained frequency response data from an actual optical current transformer. FEM modelling is chosen as the preferred optical modelling technique because of its ability to simulate more non-ideal and non-linear aspects of the optical current transformer.

The complete model is a combination of the optical and electrical model. This complete model is deployed in a protection and control system, and examined in different operational scenarios. The model is examined for optical non-linearities caused by external sources. The external sources examined are: Vibration, temperature changes and stray magnetic fields. In addition to the optical phenomena, the performance and interoperability of the model is examined in a real-world differential protection scenario where it's compared to a conventional current transformer design. The differential protection relay tests are done by injecting a stream of IEC61850 Sample Values as measurements to a *Siemens Siprotec 5 7UT82* transformer differential protection relay.

The conclusion is that open-core bulk-glass optical current transformers are well suited for application in a digital substation system, for accurate current measurements used for protection and metering purposes. The complete model shows a good representation of the non-linearities, and represent an optical current transformer well. The optical current transformer shows great promise in increasing the accuracy and sensitivity of differential protection relays, by delivering high linearity and bandwidth compared to conventional current transformer technologies. A drawback shown in the open-core bulk-glass model is the vulnerability to external stressors. These stresses have to be compensated or improved upon on to ensure a reliable operation of the optical current transformer.

Sammendrag

Denne masteroppgaven fokuserer på teknologier i en digital transformatorstasjon , med et videre fokus på optiske strømtransformatorer og strømtransformatorers ytelse og interoperabilitetet som mating til et transformator differensialstrømsvern. Optiske strømtransformatorer har blitt mer tilgjengelig de siste to siste tiår. Denne overgangen fra konvensjonelle strømtransformatorer til optiske strømtransformatorer utløser behovet for å utvikle komplette modeller av optiske strøm transformatorer. En slik model ville kunne definere ytelsen og interoperabiliteten til en slik teknologi før det blir tatt i bruk. Modellen vil også bli brukt til å undersøke feilkilder i det optiske systemet.

Denne oppgaven kartlegger de tradisjonelle og utradisjonelle strøm målemetodene som blir brukt i dagens kraftsystemer. Fordeler og ulemper ved disse målemetodene blir undersøkt. Etter kartleggingen så blir en komplett modell av en åpen-kjerne massiv-glass optisk strømtransformator utviklet og representert. Den optiske delen av modellen er basert på en modellering i "finite element method" (FEM) i et 2D-miljø. Den elektriske delen av modellen er basert på eksperimentellt utvinnet frekvensrespons data som grunnlag for en transferfunksjon. FEM modellering er valgt som foretrukket optisk modelleringsteknikk da det leverer et mer fleksibelt modelleringsverktøy, og tillater modellering og simulering av flere ulinearitetter som oppstår i optiske systemer.

Den komplette optiske strømtransformatormodellen er basert på en sammensetting av den elektriske og den optiske modellen. Denne komplette modellen er plassert i en kraftsystemmodel og undersøkt i forskjellige driftsscenarier. Modellens optiske ulinerariteter forårsaket av eksterne kilder er undersøkt. De eksterne kildene som har hatt fokus er: magnetiske felt på avveie, temperaturvariasjoner og vibrasjon. I tillegg til disse optiske fenomenene så er ytelsen og interoperabiliteten til modellen undersøkt i en faktisk differensialstrøms oppsett. I denne settingen er den komplette modellen av en optisk strømstransformator sammenlignet med en konvensjonell strømtransformator. Differensialtestene er utført ved å injisere en strøm av IEC61850 Sample Values inn til et *Siemens Siprotec 5 7UT82* transformatorvern som måleverdier.

Oppgaven konkluderer med at åpen-kjerne massiv-glass optiske strømtransformatorer er godt egnet for bruk i en digital transformatorstasjon. Det er godt egnet for å erstatte både målekjerner og vernkjerner i en transformatorstasjon. Den komplette modellen gir en god representasjon av optiske ulinearitetter og ytelsen til en optisk strømtransformator. Den komplette modellen viser gode resultater i å øke nøyaktigheten og sensitiviteten i et transformator differensialvern. Dette gjør den ved å levere en høyere linearitet og båndbredde, sammenlignet med konvensjonelle strømtransformatorer. Åpen-kjerne massiv-glass optisk strømstransformatorer viser også store sårbarheter til eksterne stress kilder, noe som må kompenseres for å få et driftssikkert anlegg.

Contents

List of Figures

List of Tables

List of Abbreviations

CCT Conventional Current Transformer
ε Ratio Error
εC Composite Error
ALF Accuracy Limit Factor
HV High Voltage
LV Low Voltage
FEM Finite Element Method
HMI Human Machine Interface
FBG Fibre Bragg Grating
MO Magneto-Optical
IED Intelligent Electronic Device
CT Current Transformer
OCT Optical Current Transformer
IT Instrument Transformer
NCIT Non-conventional Instrument Transformer
HMI Human Machine Interface
MU Merging Unit
GOOSE Generic Object Oriented System Event
SV Sample Values
MMS Manufacturing Message Specification
P2P Peer To Peer
RTU Remote Terminal Unit
ASCI Abstract Communication Service Interface
BER Basic Encoding Rules
ASN.1 Abstract Syntax Notation One
PDU Protocol Data Unit
P&C Protection And Control
COMTRADE Common Format For Transient Data Exchange For Power Systems

1 Introduction

As the society develops into a more digitized age, the requirements for reliability and safety in the power systems increases. This transition results in a further increased focus on fault handling, automation of substation events, data handling and overall reliability. The added requirements forces the power system design into a modernization, presenting new possibilities and problems that have to be solved to meet the demands of the development. Figure 1 visualizes the development from a traditional centralized grid to a decentralized "smart grid".

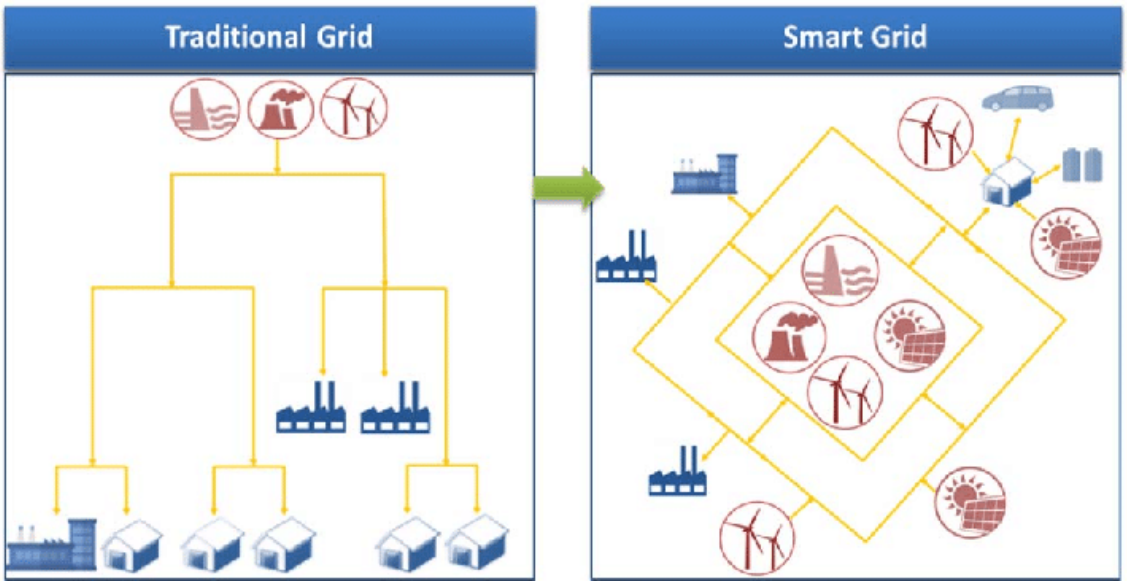

Figure 1: Transition from Traditional Grid to Smart Grid.[1]

The traditional power system design with centralized power production and constant loads, develops at a rapid pace towards a decentralized design. This transition is mainly due to increased small scale decentralized renewable power generation. A result of the decentralization of the power grid is that the once constant loads, becomes participating in producing power and contributing to the load flow of the power system. A transition from a uni-directional load flow to a multi-directional load flow demands more from the substation automation systems. To fulfill the increasingly intricate demands of a decentralized power grid, a more digital substation is proposed. A digital substation establishes a more sophisticated monitoring and control system compared to a traditional substation. [2] [3]

The development of a digitized insturment transformer technology is motivated to accomodate the digital transition. Conventional instrument transformer technology is mainly based on a magnetic core transformer, that transforms the voltage or current down to a secondary level. The secondary level is then injected into a hardwired secondary circuit in the substation. Figure 2 shows three medium voltage conventional current transformers operating in a substation. This instrument transformer design has innate compromises when it comes to accuracy and response, these compromises are especially noticeable compared to more modern digitized technology.
In a digital substation non-conventional instrument transformers are used. Non-conventional instrument transformers have emerged as a new technology in power system protection- and control of digital substations. When compared to the conventional measurement transformer, non-conventional transformer methods may deliver advantages and increased performance. The primary

Figure 2: Medium voltage current transformer application.[4]

working principle of NCITs and CCTs are based on the same method; transforming primary values into proportionally measurable secondary values. The main difference is between the transformation technology and the secondary injection. An optical current transformer, for instance uses a linear optical effect to measure the current, and the secondary current is injected into a substation automation system using a network protocol; IEC61850 Sample values.[5]

The thesis explores the impacts of optical current transformers. The Optical current transformer promises significant advantages compared to conventional current transformers.
These advantages include but are not limited to [6]:

- Non-intrusive installation
- No induced secondary voltage
- Wide dynamic range, with great dc capabilities.
- Better transient response

These advantages are further analyzed in this thesis.

1.1 Scope of the Thesis

Whilst the transition to a digital substation offers alot of new technology, it also brings new problems to be addressed. Accurate measurements are the core of a safe and reliable operation of a high-voltage system. The development from conventional substation design to digital substation designs enables the use of more modern measurement technologies. The focus is current measurement technologies with optical current transformers as a primary focal area.

The scope of this work is limited to the current measurement technology in substations. The thesis performs an extensive literature review on conventional- as well as unconventional technologies for current measurement. The literature review is done with focus on optical current transformers and their workings. The review forms a groundwork to design and develop a complete model of a bulk-glass open-core optical current transformer, as well as gaining a basis for comparison of this model to other technologies.

The model is limited to a bulk-glass open-core optical current model due to the intricacy of modelling a more sophisticated optical design in COMSOL. The model review is limited to a differential protection setting in a real-world differential protection scenario, as well as an optical simulation to map the optical non-linearities and non-ideal scenarios of the model.

The goal of this thesis is to examine the performance, behavior and interoperability of optical current transformers, especially in a differential protection setting. This will be done by modelling a complete model of a OPCT with the optical part modelled in FEM and the electrical part modelled in Matlab, all based on a thorough literature review.

2 Power System Protection and Control

To fully understand the impact of the digital substation, some background information has to be given. This chapter presents necessary groundwork, regarding the development of power system protection and control.
The main points of the chapter is split into four sub-chapters. As an introduction the two first sub-chapters explains the difference and development between conventional and digital substations. The third sub-chapter explores the performance aspect of conventional current transformers in a protection and control perspective. The fourth sub-chapter examines a few other non-conventional current transformer designs regarding substation protection- and control. And lastly a transformer differential protection is evaluated based on the conventional CTs limitations and the development of the substation.

2.1 Conventional Substation

Protection and control of a high-voltage grid is mostly handled in substations. The substations may fill multiple roles in a network. These roles may be as a voltage transforming substation, transforming the incoming voltage level into another, or as a pure switching substation used to sectionize and protect the power lines. Substations may also be equipped with instruments to provide voltage regulation, reactive power regulation and regulation of power flow.[7]
All equipment related to controlling and operating the high-voltage system is divided into two groups, primary equipment and secondary equipment. Primary equipment eg.:

- Circuit breakers
- Instrument Transformers
- Generators
- Transformers

Primary equipment consists of components that directly influence the power flow, production or distribution of the electrical energy in the high voltage system of a substation. [8]
Secondary equipment Eg.:

- IEDs
- Power measurement equipment
- Secondary circuits

Secondary equipment consist of equipment that does not directly influence the power flow of the system, but adds a layer of protection and control to the primary equipment. The secondary system is important in delivering safe and reliable power. [8]

To increase the reliability and secure a safe power flow, the secondary protection and control system has to make operational decisions based on the measured values from the instrument transformers in the power system. The communication interface between the secondary system and the primary system is hardwired in a conventional substation. This connection is done using copper

wires, where each copper wire is able to carry a single signal. This signal may be a state indication, or trip signal from the IED to the breaker. In a substation system there will be multiple signals per breaker per phase. This transferred amount of data requires a great number of copper cables to be installed between the primary and secondary equipment. [9][10]
Usually there is a notable distance between the two systems, making the overall amount of cables required to transfer all signals from the primary equipment to the secondary side even greater. Figure 3 shows the signal exchange in a conventional substation.

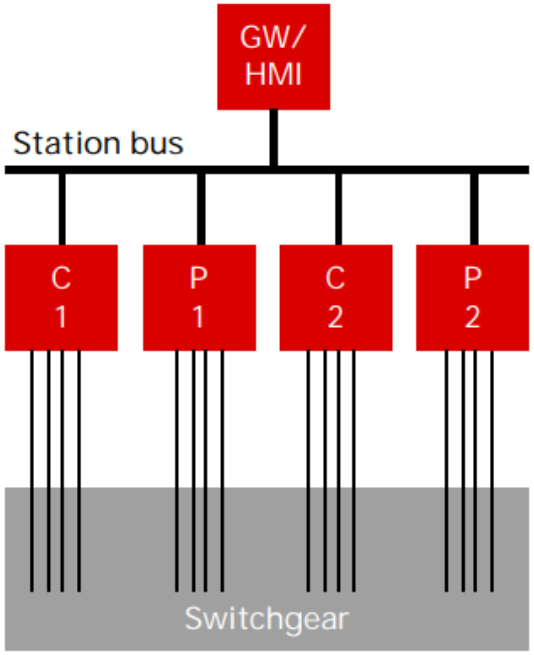

Figure 3: Conventional substation communication interface.[11]

The secondary circuits in a conventional substation can be categorized based on the information they are carrying.
The three primary groups are:

- Binary signals
- Analog signals
- Power supply

Binary signals carry information of all 0 and 1 states possible in the substation. These states may be state indication of breakers and switches, interlocking, trip signals and Buchholz-relays.
Analog signals carry all dynamic information throughout the substation. Examples of analog signals may be current measurements from current transformers, temperature measurements from transformers or generators, fan speeds, oil levels etc. All non-binary signals in a substation.
Lastly the power supply secondary circuits supply voltage to secondary equipment. This supply voltage is used to power circuit breaker coils, protection relay, power quality equipment as well as all other voltage dependant

2.2 Digital Substation

The transition between a conventional and digital substation results in many changes to the substation architecture. One of the main physical differences in the design is the use of communication protocols in place of copper wires. Figure 4 shows a communication architecture in place of the conventional substation architecture shown in fig3.

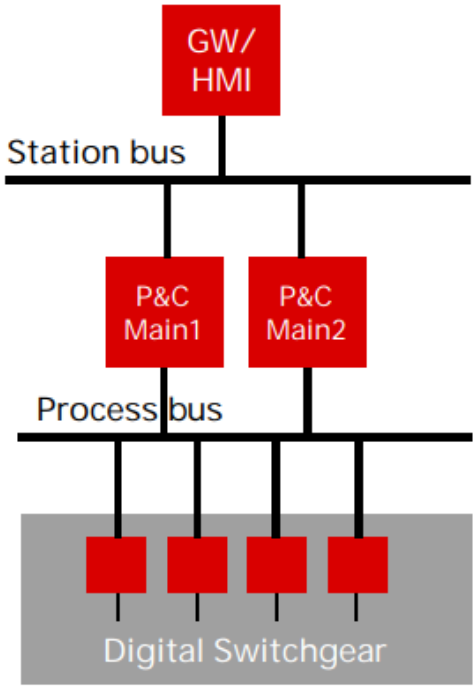

Figure 4: Digital substation communication interface.[11]

The conversion to communication protocol has a benefit of reducing the total amount of copper used in a substation between the control system and control devices. There might be some distance between primary equipment in a switch-yard to the secondary equipment, resulting in a substantial amount of copper cables. In [10] it was shown that the transition to communication protocols from copper cables could reduce the overall amount of cabling in a substation approaching 90% of the conventional amount.

The overall physical size required to establish a digital substation logical control compared to a conventional one is significantly reduced. This reduction is due to the digital substation being controlled by micro-controllers and IEDs compared to a electromechanical or electronic design from conventional substation. In addition to this, a single micro controller has the processing power to cover the roles of multiple electromechanical devices. This results in a significant possible decrease in overall physical space requirement as compared to a conventional design.[10]

Compacting the control system into smaller and fewer physical devices delivers a few benefits to the substation design beyond physical space requirements. The reduction of number of components has a benefit of possibly reducing outage times due to less points of failure. During a fault the outage times could be reduced due to the reduced amount of physical devices, reducing the troubleshooting times. A more compact substation would require less cabling during building, reducing the overall build times of a new substation.

Maintenance costs would be reduced in a fully digital substation. Modern IEDs and PLCs use self-monitoring systems as internal fault signals and watchdog functions to check each others health. By having a reliable and modern self-supervision systems in a substation it is possible to increase the length of maintenance intervals of the control system, reducing operational costs. [10][12].

The communication system in a digital substation is a network split into multiple layers and separate networks. The main layers in a digital substation are: the station control bus, process bus and the bay bus. The two separate networks are the station networks, and the process network. This network topography is shown in figure 5.

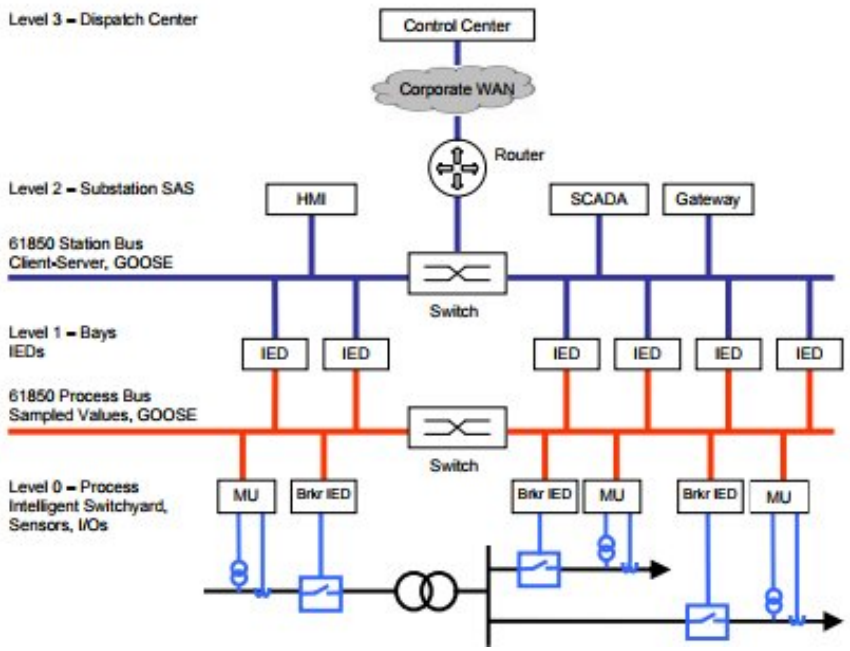

Figure 5: Network layers in a a digital substation..[13]

The two networks are split up into the process network and the station network. The station network is a IEC61850 MMS network connecting the bay level and the station level. [14]
The process layer network is a IEC61850 network between the bay-level and the process-level, this includes services as sample values and GOOSE [8].
Station control layer is the primary supervisory network, that contains communication and control devices to operate the substation. The devices in the station control layer are usually human machine interfaces for control systems, industrial remote communication or telecontrol equipment, time synchronizations and GPS clocks and as well as other external supervisory systems such as data acquisition and ventilation etc.

The bay layer contains the intelligent devices that control and monitor the primary equipment directly. These devices are predominantly consisting of all intelligent electronical devices as protection relays, logical control or power quality meters. A benefit of having the bay layer with all logical control separate from the station control layer is the self contained automation provided by the bay layer. This means that if you lose control over the station control layer, the protection relays would still control the process layer during a fault, providing a slight safety buffer.
The lower layer, the process layer contains all the primary equipment that directly influences the primary power flow in the substation. When comparing a digital substation process layer and a

conventional one the main physical differences are the use of digital voltage and current transformers. This modernization of instrument transformers are further explored in this thesis.
Table 1 compares the main advantages and changes going from a conventional design to a optical design of instrument transformers. [8][12].

Variable	Conventional	Optical
Saturation	Saturable	Linear
Dynamic range	Narrow	Wide
Output	Analog	Digital
Open secondary circuit	Induced voltage	No induced voltage
Insulation	Complex insulation	Simple insulation

Table 1: Comparison of CT and OPCT

2.2.1 IEC61850 Communication Standard

The communication system for digital substations is covered by the IEC standard 61850. The aim of IEC61850 is to ensure interoperability between different systems. This interoperability is ensured by defining a standard for all aspects of the digital substation. The IEC61850 cover every aspect between design and operation of a digital substation. The primary focus of this chapter is the communication protocol defined by the IEC61850 standard, its workings and limitations. The communication protocols defined in IEC61850 are separated into three main categories: GOOSE, Sample values and Manufacturing Message Specification. [5]

GOOSE Generic object oriented substation event, also abbreviated into GOOSE, is a P2P type communication based on a publisher- and subscriber topography. This communication protocol is commonly used in the station bus layer between protection relays. A GOOSE message is published from a protection relay to the station bus without any specified receiver. Only the receiver knows what it looks for by subscribing to specific types of messages. To ensure high-speed relaying, the GOOSE messages have no two way communication or verification of received message. To ensure that the packet reaches its subscriber, a protection relay will repeatedly publish its message in a burst after the occurrence. The main goal of the GOOSE messages is to be precise and as fast as possible to ensure safe operation of the substation. Goose messages may contain interlocking, breaker positions and other crucial operational data. A GOOSE network topology is visualized in figure 6. [15]

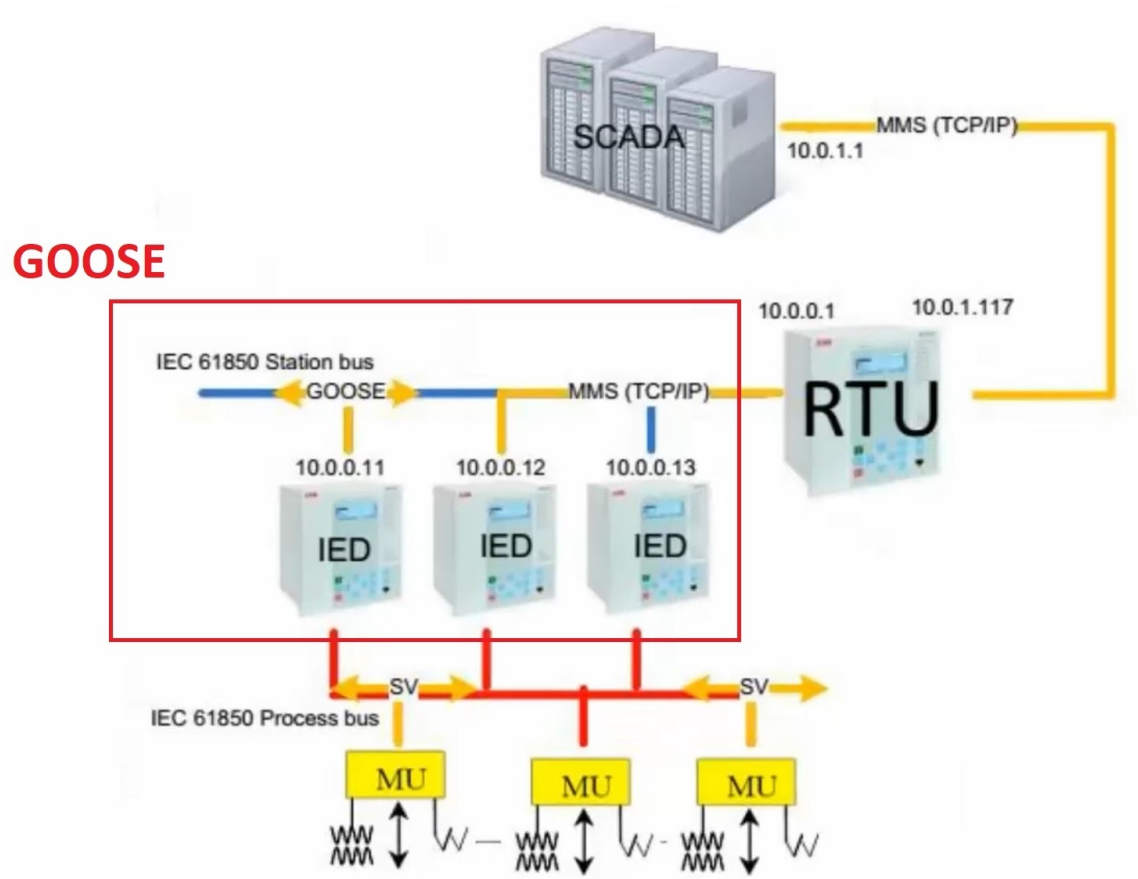

Figure 6: GOOSE network topology. [12][16]

These GOOSE messages are sent over a conventional ethernet system, but the communication is happening without the use of the traditional TCP IP model. GOOSE messages uses a different data structure called BER of ASN.1. ASN.1 is a standard that defines a structure for representing, transmitting, encoding and decoding packets. BER is the encoding structure defined in ASN.1.[17] The BER structure is based of a composition of three data sets:

- TYPE
- LENGTH
- VALUE

The composition of type length and value is referenced as TLV in the BER definition. [18][19]

The protocol data unit (PDU) that defines the data structure used by GOOSE is defined as shown in figure 7. The allData in goose is further based on a separate PDU shown in figure 8. The TLV is not a replica of ASN.1 BER, but an adaption for IEC61850. [18][20]

```
IECGoosePdu ::= SEQUENCE {
  gocbRef            [0] IMPLICIT VisibleString,
  timeAllowedtoLive  [1] IMPLICIT INTEGER,
  datSet             [2] IMPLICIT VisibleString,
  goID               [3] IMPLICIT VisibleString OPTIONAL,
  t                  [4] IMPLICIT UtcTime,
  stNum              [5] IMPLICIT INTEGER,
  sqNum              [6] IMPLICIT INTEGER,
  test               [7] IMPLICIT BOOLEAN DEFAULT FALSE,
  confRev            [8] IMPLICIT INTEGER,
  ndsCom             [9] IMPLICIT BOOLEAN DEFAULT FALSE,
  numDatSetEntries   [10] IMPLICIT INTEGER,
  allData            [11] IMPLICIT SEQUENCE OF Data,
  security           [12]  OCTET STRING OPTIONAL
  -- reserved for digital signature--}
```

Figure 7: Protocol data unit structure GOOSE.[19]

Figure 7 represents the overall data transferred in a goose message. Eg. The variable t contains the time stamp of the message in the UtcTime format, by looking at the data set in the goose PDU its also possible to observe that the t variable has a tag number of 7. The GoosePDU only transfers the bare-bones info as the time, whether or not the message is a test message etc. The actual transferred data is contained in the *allData* variable.
The *allData* variable has its own data structure shown in 8. This variable is used to transfer values between the IEDs. The all data variable can be used to transfer *BIT STRING* in form of interlockings and breaker indications, *FloatingPoints* representing currents or temperatures, etc. These variables are possible to transfer at the same time in the same goose package.

```
Data ::= CHOICE {
  -- context tag     [0] is reserved for AccessResult
  array              [1] IMPLICIT SEQUENCE OF Data,
  structure          [2] IMPLICIT SEQUENCE OF Data,
  boolean            [3] IMPLICIT BOOLEAN,
  bit-string         [4] IMPLICIT BIT STRING,
  integer            [5] IMPLICIT INTEGER,
  unsigned           [6] IMPLICIT INTEGER, -- shall not be negative
  floating-point     [7] IMPLICIT FloatingPoint,
  --                 [8]                              is reserved
  octet-string       [9] IMPLICIT OCTET STRING,
  visible-string     [10] IMPLICIT VisibleString,
  generalized-time   [11] IMPLICIT GeneralizedTime,
  binary-time        [12] IMPLICIT TimeOfDay,
  bcd                [13] IMPLICIT INTEGER, -- shall not be negative
  booleanArray       [14] IMPLICIT BIT STRING,
  objId              [15] IMPLICIT OBJECT IDENTIFIER,
  ...,
  mMSString          [16] IMPLICIT MMSString,
  utc-time           [17] IMPLICIT UtcTime -- added by IEC61850 8.1 G3--}
```

Figure 8: allData data structure.[19]

Analyzing the packets sent in a GOOSE network shows the data translation done by the BER ASN.1. A screen dump from a packet sniffer in a goose network is shown in figure 9. In this a

goose message is shown with informational tags. The message starts with a TLV or Tag Length Data in this figure. This TLV belongs to the first part of the goose message is the gocbRef with tag 0. The second part of the GOOSE PDU is the *timeAllowedToLive* with tag number 1, its possible to observe in the packet sniffer that this is the next published packet in the BER ASN.1. translation. The further tags as *datSet*, *goID* and *t* is following after in order as shown in figure 7.

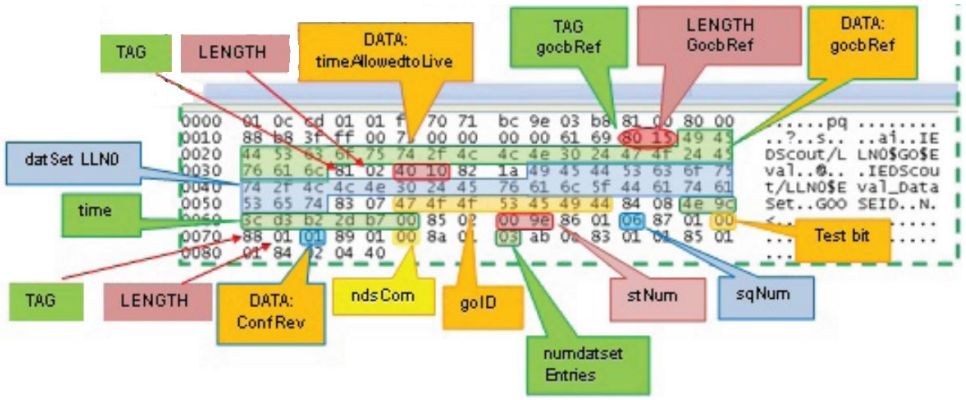

Figure 9: GOOSE packet sniffer. [19]

The gocbRef is short for GOOSE control block reference. This data has a tag of 0, in ASN.1 this is translated to 0x80. Looking at the packet sniffer in figure 9 is possible to observe and verify the expected ASN.1 translation by looking at the gocbRef. [18][19].

Sample Values Sample values are another part of the IEC61850 communication standard. This standard is used to transfer measured values from all digitized sensors in the substation. These measured values are translated from the sensor value into a Sample value standard and published in the process bus network. A sample value network topology is shown in figure 10.

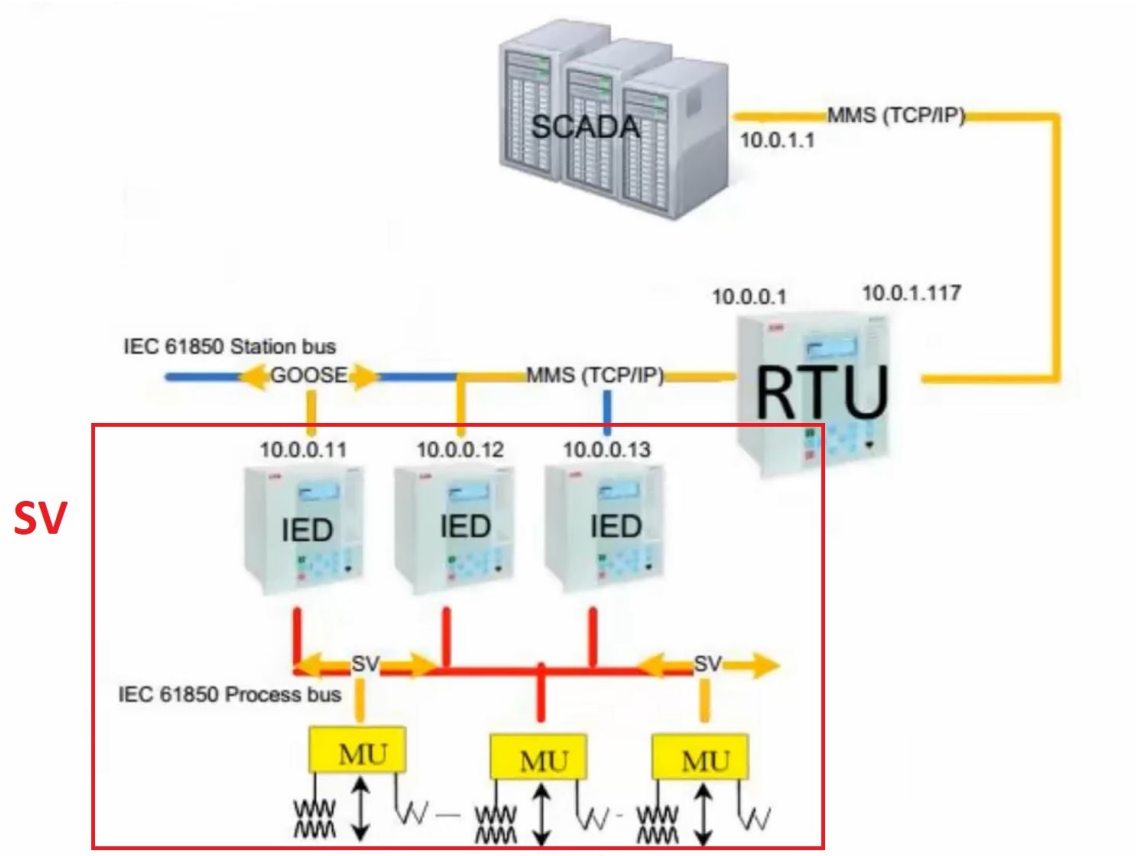

Figure 10: Sample value topology in a substation. [12][16]

Sample values are based on the same data structure as GOOSE, but is mainly used for measured values. All measured values published in the SV standard is time stamped and verified by the IEDs. An IED publishes a measured value from a buffer of measured values, the expected subscriber listens to the network and reads the defined value from a local buffer. Doing this is a way to verify the validity of the transferred value by looking at the time stamps and comparing. [5]

Manufacturer Message Specification Lastly manufacturer message specification is based of a client - server network standard. The MMS protocol is unlike SV and GOOSE based of a TCP IP structure. MMS data packets are further standardized by a international communication packet standard, defined in IEC9506. Due to the standardization of the MMS protocol it's used in all types of industrial applications. The MMS domain in a substation is shown in figure 11.

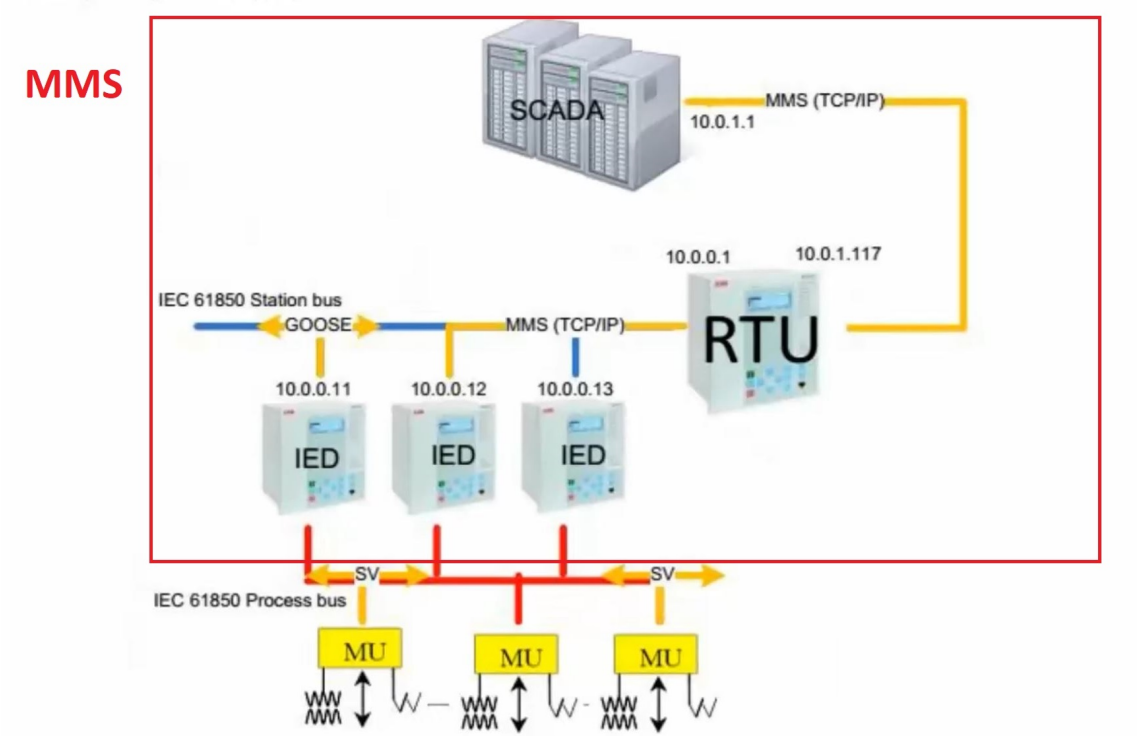

Figure 11: MMS domain in a substation. [12][16]

MMS handles all communication between the SCADA system, the RTU and the station bus. The IEC61850 MMS is based of the IEC9506 standard that defines the MMS structure. [21]
To enable the use of a IEC9506 standard in a IEC61850 network the MMS protocol has to be mapped to the IEC61850 abstract service communication interface (ASCI) of the IEDs. The ASCI is a interface connected to the IED, enabling control and monitoring of the device.

An example of this translation is shown in table 2.

ASCI Service	MMS Service
Associate	Initiate
GetServerDirectory	GetNamedList
SetLogicalDeviceDirectory	GetNamedList
GetDatasetDirectory	GetNamedList
GetDataDefinition	GetVariableAccessAttribute
GetDataDirectory	GetVariableAccessAttribute
GetDataValue	Read
SetDataValue	Write
Release	Conclude

Table 2: ASCI to MMS mappings. [22]

IEC61850 MMS messages are separated into two main groups of data types, these are buffered and non buffered reports. The buffered reports are used for remote-signaling and the non buffered reports are used as remote-measuring.
A MMS report is triggered by a change. To limit the amount of messages the change to the measured value has to surpass a user-defined level. [14]

2.3 Conventional Current Transformer

The most common way of measuring primary current in a conventional substation is the use of a magnetic iron core current transformer. A conventional current transformer has a main goal of transforming the primary current down to a scaled down secondary current which is proportional to the primary current. [23]
This transform scales down the primary current to a standardized value, given in IEC61869-2 [24]. The secondary current values are most often either scaled to 5A or 1A.
The primary current is scaled down based on one of the given values from IEC61869-2;

$$\underline{10} - 12{,}5 - \underline{15} - \underline{20} - 25 - \underline{30} - 40 - \underline{50} - 60 - \underline{75}\ \text{A}$$

Along with all decimal multiples or fractions of these numbers. The most frequently used values are underlined. [16]
Eg. A 500/5A current transformer would scale down the current in magnitude of 500 to 5A or 1/100 of the primary value.

Magnetic current transformers operation is based on a core enclosing a magnetic field produced by a current carrying conductor. A secondary winding is wrapped around the core a certain amount of turns to ensure the proper scaling. Figure 12 shows a common design of the conventional current transformer. Some designs are multi-core based transformers, with different core designed to achieve different levels of accuracy and range.

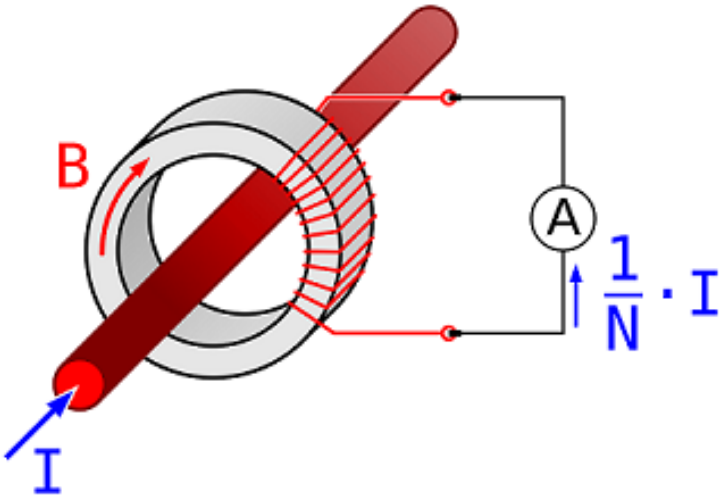

Figure 12: Basic design of a ring core current transformer.[25]

The resulting secondary current output in these designs are a result of the number of turns the secondary winding has completed around the iron core. Equation 1 shows the relation ship between windings and output secondary current. [24]

$$I_s = I_p(\frac{N_p}{N_s}) \tag{1}$$

I_s = Secondary current
I_p = Primary current
N_p = Number of primary windings
N_S = Number of secondary windings

Current transducers are sorted and categorized into accuracy classes. These classes are conditionally sorted after the measured error at different current levels, mostly based on the rated primary current. This classification is established in a IEC standard, IEC61869-2 [24]. The IEC standard is split into two sub groups containing a classification for current transformers used for measurement and a separate classification for current transformers used for protection. For measuring cores this Standard uses the following accuracy groups:

0.1 - 0.2 - 0.2S - 0.5 - 0.5S - 1 - 3 - 5

These classes explains the level of accuracy of a given current transformer at a given current level as mentioned, also called the ratio error shown in equation 2. For instance a current transformer rated as a 0.2 accuracy class, would have a expected maximum error margin of 0.2% at rated current. The **S** added to some of the standardized numbers also further defines a rule to the categorizations. All accuracy classes defined with a **S** will also be required to keep the accuracy at 1% of the maximum rated current. This means that a 1200A current transformer rated as a 0.2S categorization would be required to both be 0.2% accurate at maximum current of 1200A, and at 12A. This categorization is mostly adapted by measurement cores of current transformers, which

have greater demands to accuracy of the measurement. [16] [26]

The ratio error of a current transformer is calculated as shown in equation2.[24]

$$\varepsilon = \frac{K_r I_s - I_p}{I_p} x100\% \tag{2}$$

Where:
K_r = Winding ratio.
I_s = Measured Secondary current.
I_p = Measured primary current.

For protection a separate accuracy classification is used. This classification contains accuracy info at rated currents just as the measurement classification, but it also keeps information of the ALF or accuracy limiting factor of the current transformer. To show the error of a protection current transformer the composite error is evaluated. This error is based of a collection of error sources as ratio error, error due to harmonics and phase error. The composite error is shown in equation 3.

$$\varepsilon_c = \frac{\sqrt{\frac{1}{T}\int_0^T (K_r i_s - i_p)^2 dt}}{I_p} x100\% \tag{3}$$

Where:
K_r = Winding ratio of the transformer
I_p = RMS value of primary current
i_p = Instantaneous value of primary current.
i_s = Instantaneous value of secondary current.
T = The duration of a full cycle.

The composite error calculated gives basis to categorize the protection transformers, this is done in two main groups given in the IEC standard:

5P - 10P

These values represent the error margin of the current transformer, Eg. a 5P transformer would be accurate within 5% of the ideal measurement. Due to the non-linearities in the conventional current transformer this classification would not apply to all current levels possible, but is limited by the accuracy limiting factor. The ALF sets a upper limit to the accuracy range by adding a multiplier at the end of the accuracy classifications. An example of this would be 5P20, meaning that the current transformer would be 5% accurate within 20 times the rated current.
The accuracy limiting factor values are also standardized withing the IEC standard [24], the following values are the normalized values used:

5 - 10 - 15 - 20 - 30

The higher load levels a protection transformer is exposed to results in a more protruded set of non-linearities causing error in the measurements. These non linearities are mostly caused by core

saturation, hysteresis loss and eddy current losses. These are primarily non-linearities caused by the use of an iron core in the transformer.

The core magnetization of a current transformer is the primary limiting source of its ALF. The iron-core of a conventional current transformer is saturable, meaning that the core gets saturated a certain level of magnetic field strength causing a skew of the measurements. This core magnetization curve can be shown in a B-H curve, shown in figure 13.

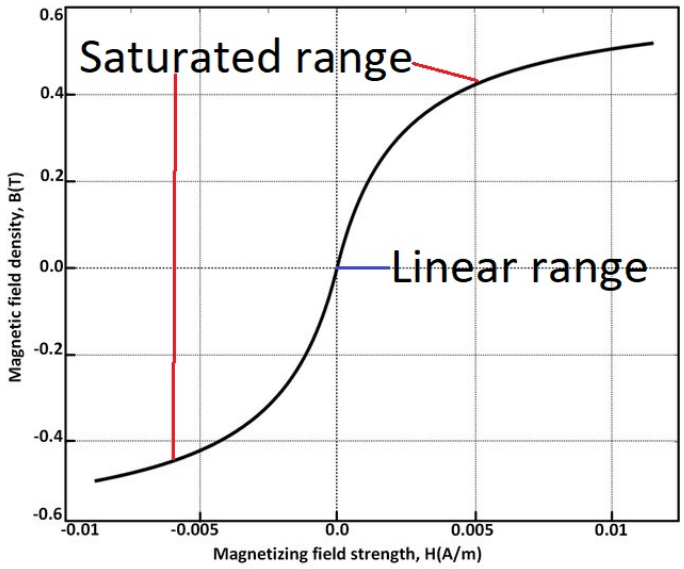

Figure 13: Magnetization curve of a iron core transformer.[27]

In the middle of the figure the current transformer operates in the linear range, meaning within the accuracy rating given to the current transformer. At higher current levels the magnetisation increases and the core starts to saturate. This pushes the current transformer out of the accuracy rating.
To modify or optimize the B-H curve the reluctance of the core has to be changed. A way of doing this is to implement an air gap in the core, resulting in a change in the core's reluctance, further changing the B-H curve. [28]

The core saturation is a function of induced voltage in the core and the variable magnetization impedance. In a saturated scenario the magnetization impedance is significantly lower than the secondary circuits impedance, causing the current to pass through the magnetization circuit instead of the secondary circuit, causing a measurement error. In a regular load scenario the magnetization impedance is far greater than the burden of the secondary current, causing the secondary current to fully pass through the secondary current circuits in the substation.[29]
The saturation effect may also be a result of an open secondary circuit. In a conventional substation the secondary circuits are hardwired as aforementioned. If one of the terminal blocks in the secondary circuit is opened, the secondary burden would go to infinity and the current transformer would eventually saturate. During this effect a high voltage may be induced over the magnetization resistance in the current transformer. This induced voltage will also result in a high voltage potential at the open terminal block. This may cause arcing in the terminal, and the voltage induced could be high enough to cause personnel injury. [30]

The most common wave form phenomena caused by the saturation effect is clipping of peaks in the wave form, this is illustrated in figure 14.

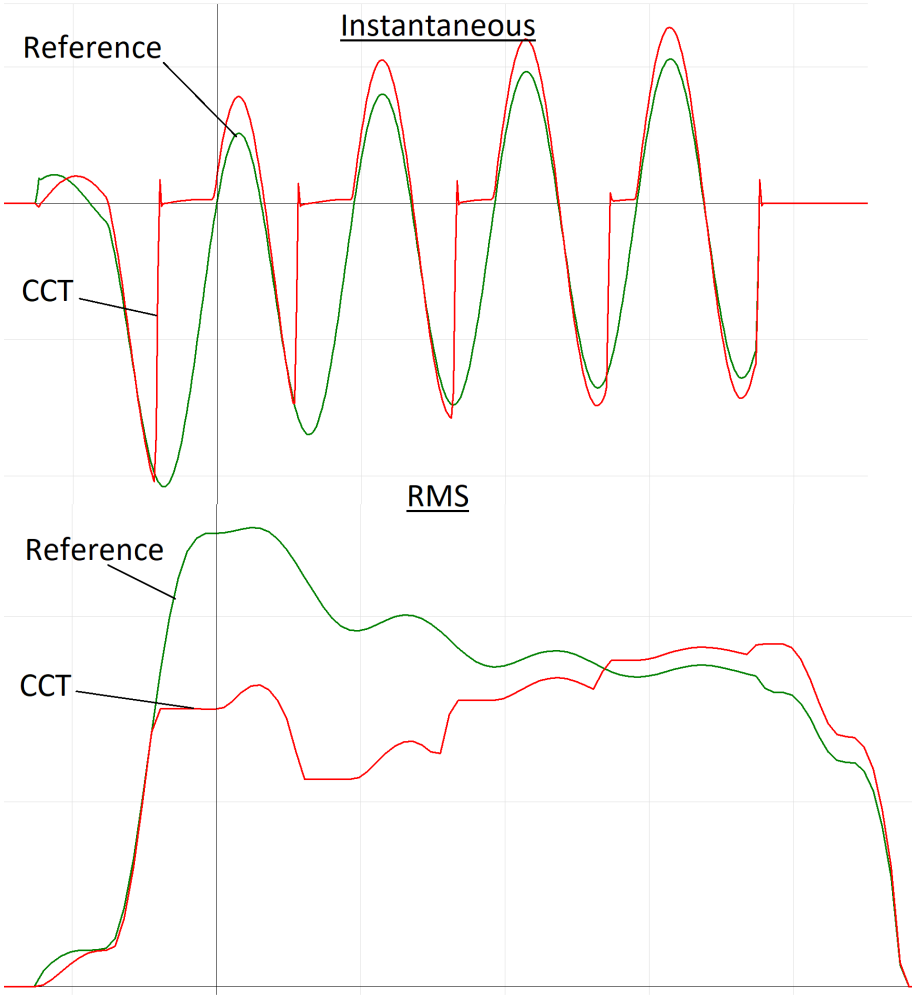

Figure 14: Core saturation of current transformer, Instantaneous values and RMS values.

The figure above shows the effect of magnetic core current transformer compared to a reference current in a fault scenario causing a current to exceed the ALF of the CCT. The transformer saturates at the current peaks, clipping the measurement and reducing the overall measured RMS value. This effect can have significant impact on protection and control system in the substation. This may cause erroneous tripping by the protection relay and power quality measurement issues. Among the different constituents of the protection and control system, the differential protection relay is especially affected by current transformer saturation. A transformer differential protection relay would be especially sensitive to this effect. This is due to the use of two different current transformers of different rated load and accuracy values measuring the current of each side of the transformer. In the case of an external fault, one of the current transformers might saturate, simulating the current values of an internal transformer fault, causing the protection relay to trip. [31]

2.4 Unconventional CT

This chapter aims to uncover and examine the most popular non-conventional current transformers. Some magnetic field sensors are also examined due to their ability to measure indirectly measure current.

2.4.1 Rogowski coil

The Rogowski coil is an old design used for current measuring. The Rogowski coil has either air-core or non-magnetic core design. The current transformer is usually represented with two different designs. One design is based of a helicaly wound wire wound in a circle, with the lead wire returning through the center of the helicaly wound wire. This results in a Rogowski coil with two terminals on the same side of the coil. The second design is a complete toroid design with terminals at one point on the toroid.[32]
To measure current with both these designs, the circularly wound coil is mounted around the conductor which one wishes to measure the current in. The primary workings are visualized in figure 15.

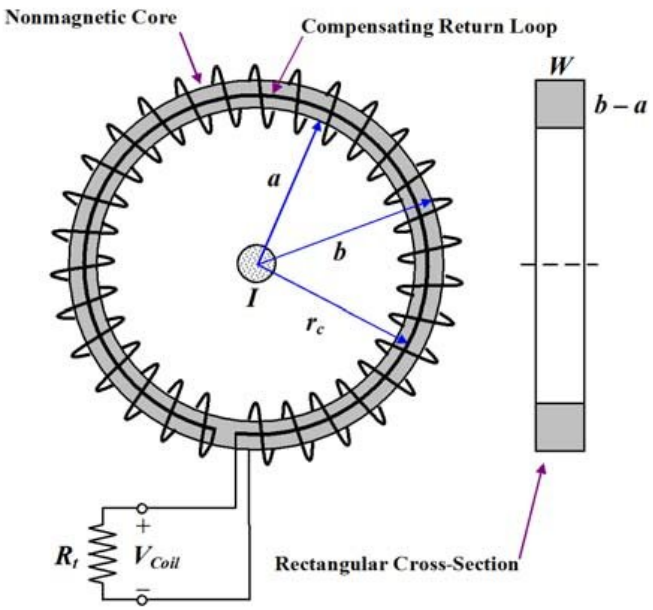

Figure 15: Design of a Rogowski coil.[33]

The Rogowski coil is based on the fact that the induced voltage in the coil is proportional to the derivative of the current in the primary conductor it's applied to. This induced voltage is converted into a measured current by an electronic sensing circuit. [34]
Compared to a conventional current transformer the Rogowski coil brings a few advantages;

- Ease of integration
- Fast response to transients
- Large linear range

- No induced secondary voltage

The Rogowski coil is not a solid loop, making it easy to install on a already existing conductor compared to a CCT. The low inductance of the coil results in a fast response to current transients. The current transformer has no core, making is less susceptible to non-linearities such as core saturation. This greatly increases the linear range compared to a CCT. The Rogowski coil is a simple design, making it cheap to manufacture. Lastly, the Rogowski coil eliminates the use of secondary current circuits, eliminating the danger of opening a secondary current circuit and making the overall operation safer. [35]

2.4.2 Search-coil magneto meter

Search-coil is an umbrella term for all magnetic field sensors based on capturing magnetic field by enclosing it in one or more loops of conducting wire. The magnetic field **B** generates a voltage, in accordance with Faraday's law of induction. A basic search-coil setup is shown in 16. [36]

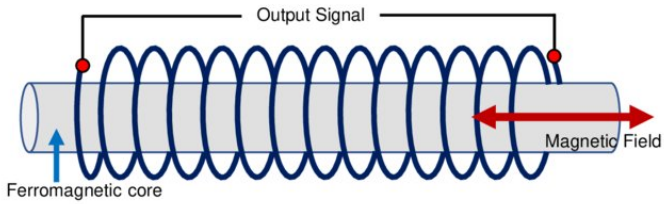

Figure 16: Search-coil setup.[37]

To measure magnetic fields a search coil is either wrapped around a conductor directly, or wrapped around a ferromagnetic core to enhance the effect of the magnetic field. When the magnetic field flux in the wrapped core or conductor changes, a resulting change of voltage with the same rate of change as the current is induced in the coiled conductor. This sensor design has a wide measurement range, but it can only measure the rate of change of the current based on Faraday's induction law. And therefore it is not suitable to measure stationary DC currents. [36]

2.4.3 Shunt resistor

A commonly used low voltage, current measurement technology is the use of a shunt resistor. This technique is based of sensing a voltage drop over a resistor which is then measured and translated to applied current. These shunt resistors are low ohmic components that are implemented in series with the primary current. Shunts are implemented directly into the circuit. For this reason they are not used in high-current situations due to low efficiency. [38] Shunt based current measuring methods does not provide any galvanic separation, and are not very power-efficient due to its low efficiency.[39]

2.4.4 Hall effect Sensor

A current measurement based on the hall effect uses a hall effect sensor to measure the change and amplitude of a magnetic field. To measure current of a conductor using a hall effect sensor a

magnetic core is wrapped around the conductor, and a hall effect sensor is placed within a small air gap in the core, as visualized in figure 17.[39]

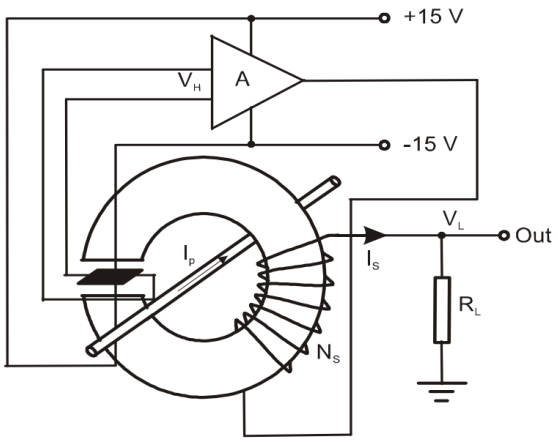

Figure 17: Setup of a hall effect sensor.[40]

The hall effect sensor itself is a sensor that outputs a voltage level proportional to the magnetic field strength. The magnetic field of the core is also proportional to the current applied, making this design able to proportionally measure the primary current based on the output voltage of the sensor. The output signal is processed by external circuitry to relate the voltage to the current. This circuitry might differ in complexity, from a regular amplification circuit to a more sophisticated design to increase accuracy.[41]
The air-gap of the core is used to regulate the reluctance of the core, this is useful when measuring higher currents to change the saturation point of the core. Increasing the length of the air-gap might result in a fringing flux effect in the air-gap, this has to be negated by increasing the surface area of the core or else the fringing flux will lead to a lower reading of the hall effect sensor than the actual applied value. An additional benefit of the air-gap design is the resulting galvanic separation it provides. [41]

2.4.5 Flux-Gate

A Flux-gate based current sensor uses a flux-gate magnetometer to measure the magnetic field. The flux-gate magnetometer is primarily based on two conductors coiled around a magnetic core. These coils are called drive- and sense coils. a flux-gate magnetometer is shown in 18. [38]

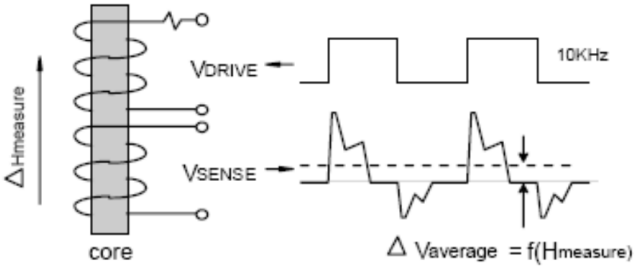

Figure 18: Flux-gate operation principle.[42]

The Drive coil applies a voltage signal to stimulate a oscillating core saturation. The Sensing coil outputs a signal based of the drive coil signal, and the permeability of the magnetic core. This means that any change in the external magnetic field will change the perceived permeability and change the output signal. This change is possible to relate to the magnetic field strength the core has been exposed to, and further the current of a conductor. [43]

2.5 Differential Protection

Electrical machines and transformers deployed in a power systems relies on high-speed fault clearing and detection to minimize equipment damage during a fault, while still being highly accurate to minimize downtime. This demand is primarily filled by the use of differential protection relays. The differential protection relay uses current measurements of multiple sides of an electrical device to evaluate if the current passing into the transformer is equally large as the current leaving the device. If the current entering the device does not leave the device, the protection relay evaluates the scenario as an internal fault, and rapidly trips the adjacent circuit breakers. [44]
Differential protection relays are most commonly used to protect:

- Lines
- Transformers
- Busbars
- Motors
- Generators

In short the differential protection could be used to protect any section installed between two or more current measuring transformers. A typical installation of differential protection relay is shown in figure 19.

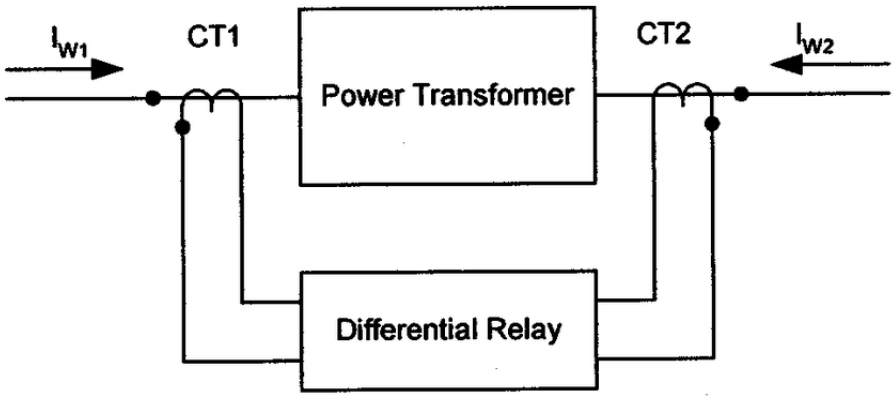

Figure 19: Setup of a differential protection relay.[45]

A Transformer differential protection relay as shown in figure 19, measures the currents going into and out of the transformer as aforementioned. Based on these measurements the protection relay computes a differential current value *Idiff*. This value is evaluated compared to user-defined protection parameters.
The primary mission of a differential protection relay is to detect internal faults at a high-speed.

Because this function is independent of current passing through the protection relay, it is not required to be time or current selective to downstream protection. Differential protection algorithms are highly responsive and sensitive to changes, enabling them to react to internal fault currents at low current magnitudes. A inter-turn fault at the windings has a possibility to produce a low fault current—a current low enough that an earth fault or overcurrent relay would not detect them as a trip scenario. A differential protection relay would rapidly, within a cycle of the fault appearing, detect and react to the fault current. [44] [16]

The core of the transformer differential protection is the user-defined settings, that decides the trip conditions. These values are calculated to restrain the differential protection for all foreseeable error sources, except for internal faults in the protected unit.
To fulfill this role the differential protection parameters must take into account following parameters:

- Nominal voltages of the transformer.
- Tap changers
- Auxiliary windings
- Vector group
- Current transformer ratios and accuracy.

These parameters are all crucial to know while evaluating the differential current, this is because all these parameters influates the resulting secondary current of a power transformer. Nominal voltages and current transformer ratios decides the expected current magnitude of the secondary and primary side of the transformer. The vector group of the transformer has to be known to compensate for the phase angle rotation caused by the transformer. Tap changers, auxiliary windings and current transformer accuracies are sources of allowed inaccuracies in the power transformer, and has to be accounted for. A tap changer may change the rated voltage of either side, resulting in a constant increase of error. Auxiliary windings results in a third current outlet on the power transformer, and if not accounted for will be evaluated as an internal fault by the differential protection. Lastly the current transformer accuracies have to be accounted for, so as not to trip due to foreseen measurement error as mentioned in previous chapters. [44]
The differential characteristic is a result of all these parameters, and shows a restraint area and a trip region. An example of a differential protection characteristic is shown in figure 20.

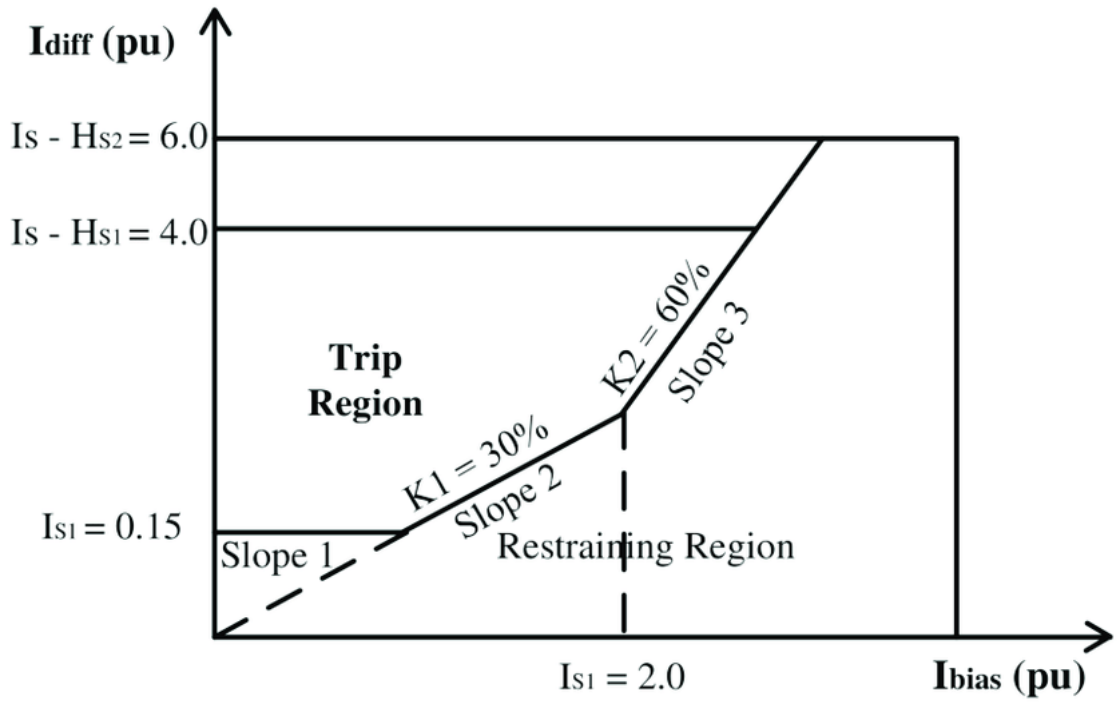

Figure 20: Tripping characteristic of a differential relay.[46]

The differential protection characteristic as visualized in figure 20 evaluates the Idiff in relation to the Ibias. Ibias is a transformation of load current, this transform can be done in different ways depending on the wished sensitivity of the protection relay. Equation 4 and equation 5 shows two common ways of calculating bias currents from load currents; [44]

$$Bias_{avg} = \frac{|Il_{HV}| + |Il_{LV}|}{2} \tag{4}$$

$$Bias_{max} = max(|Il_{HV}|, |Il_{LV}|) \tag{5}$$

, where
$\mathrm{Il_{HV}}$ = Phase current high voltage side.
$\mathrm{Il_{HV}}$ = Phase current low voltage side.

Bias average shown in equation 4 calculates the bias current based on the average value of the secondary and primary current. Bias max shown in equation 5 calculates the bias current based on the maximum value of either primary or secondary current. The different use of bias current results in different sensitivity levels of the differential protection relay. An average bias current results in a more sensitive differential protection relay. Max bias results in a more approximate calculation of bias current, causing the protection relay to become less sensitive to differential currents. The most commonly used way of calculating Ibias in newer numerical protection relays is average bias current. [44]

As mentioned the differential protection's task is to detect all abnormalities beyond the expected error sources. To do this one has to account for all the sources of expected error in the power transformer. These sources are;

- Current transformer inaccuracy.
- Relay measurement inaccuracy.
- Core magnetizing current.
- Tapchanger setting.

By summing up the error margins of these sources, with an added margin of error one can calculate the expected error. This is done in equation 6.

$$I_{uncertainty} = \frac{Abs_{uncertainty}}{Abs_{measurement}} x100 \tag{6}$$

$\text{Abs}_{\text{measurement}}$ = Absolute measurement
$\text{Abs}_{\text{uncertainty}}$ = Absolute uncertainty
$\text{I}_{\text{uncertainty}}$ = Maximum uncertainty from all sources

The absolute measurement is the sum of the nominal value and the highest value of tap changer error.
The absolute uncertainty is the uncertainty summation of the current transformer errors, the highest value of the tap changer error and the multiplication of secondary current transformer error and tap changer error.[44]
Inserting these values into equation 6, results in the following equation 7;

$$I_{uncertainty} = \frac{CT_p + CT_s + Tap + (CT_s Tap)}{I_n + Tap} x100 \tag{7}$$

, where
CT_p = Error primary CT
CT_s = Error secondary CT
Tap = Maximal tap changer error
I_n = Nominal current p.u.

The resulting current uncertainty is used as a pickup value for *Idiff* >. Meaning that no values lower than the total uncertainty of the system would be reacted to by the protection relay. The differential characteristic in figure 20 has used 0.15 or 15% as its pickup value.
Further, the differential characteristic consists of multiple slopes and turning points. These change based on the bias current flowing through the transformer in order to account for the non-linear phenomena that occurs at an increasing load current.
The first turning point between pickup and slope 2 is used to set the sensitivity of the differential protection. The goal of this value is to get as close to the error current as possible without resulting in a incorrect tripping of the breaker at regular load current. The exact position of the turning point is decided by the aforementioned pickup value. [44] Slope 1 in figure 20 is replaced by the pickup value of the differential protection, but the figure has plotted the relative error based on

load current from zero. The reason for the use of a static pickup value until a certain bias current is to remove any chance of a incorrect breaker trip at lower current due to high sensitivity.

After the first turning point the first slope starts, or slope 2 as its referred to in figure 20. With a higher load current, the overall error from all error sources increases. When this error margin surpasses the Idiff pickup value, it has to be increased proportional to the load current to inhibit incorrect operation.

The second slope starts at the second turning point, and is referred to as slope 3 in figure 20. This slope is implemented to account for greater error sources associated with higher load current. These high current scenarios might be external or internal faults where the current transformers might enter saturated states as mentioned in previous chapters. [44]
Idiff>> and *Idiff*>>> are both differential steps with a higher and faster setting than the first differential stage. These stages only take into account the differential current, and ignores the bias current. These stages are parameterised to cover all internal faults, while not reacting to any other operational disruptions. The non-bias differential levels should be parameterised to not react to any external faults, even in a scenario where the current transformer is saturated. [44]
Beyond the expected errors and internal faults there are a few harmonic phenomena a differential protection relay has to account for. These harmonic phenomena are the presence of 2nd and 5th overharmonic currents. These overharmonic phenomena will trip a differential protection relay if not accounted for, resulting in a incorrect trip of the circuit breaker. To counteract this misoperation modern differential protection relays analyses the harmonic content of the current, detects these phenomena and blocks the differential trip signal based on size of the overharmonic part in percent of load current.
The second harmonic is a result of inrush currents in power systems. Energizing a power transformer with no energy from the start results in a large current skewed with a DC component and a large 2nd harmonic component. The size of the 2nd harmonic depends on the positioning of the remanence flux in the transformer and the instant of the feeder voltage sinusoidal the energizing takes place.

The 5th harmonic is a result of overexcitation of transformers. Transformers are designed for a certain frequency and voltage level, and are vulnerable to saturating if these are exceeded. During a frequency or voltage swing the transformer might overexcite resulting in fifth harmonic components in the load current.
Both these overharmonic currents are common, and has to be detected and blocked for a reliable operation of a differential protection relay in the power system. [44]
Because the differential protection is so sensitive to error sources a more linear and accurate current source would greatly increase its performance. Optical current transformers show great potential in this area.

3 Optical current transformer

Optical current transformers are one of the most popular non-conventional current transformers. This is a further developed version of the conventional current transformer. The basic principle of the OPCT is to replace the magnetic core of the CCT with a optical transducer, based on the Faraday effect. This chapter will explore related phenomena and inner workings corresponding to optical current transformers, to lay a ground work for developing an optical model.

3.1 Core concepts

The optical current transformer brings a few new concepts and is based on core components one has to be familiar with to understand its inner workings. This sub-chapter will establish the core concepts.

3.1.1 Polarized light

Polarized light is the result of passing a incident light beam through a polarization medium "filtering out" components of the applied light, as visualised in figure 21. Dependant on the polarization medium's properties the resulting mode of polarization can differ. Polarization can be sectioned into three main modes of, dependant on the direction of the polarized light:

- Vertical Polarization
- Circular Polarization
- Elliptical Polarization

These modes of polarization are based on the appearance of the light wave compared to the Z-axis. A vertical polarization will look like it propagates in a straight line through the Z-Axis while looking straight down the axis, a circular polarization will look like a the light vector is propagating circularly around the Z-axis while an elliptical polarization would look like the light is propagating in a elliptical shape around the Z-axis. This phenomena is visualized in figure 21. [47]

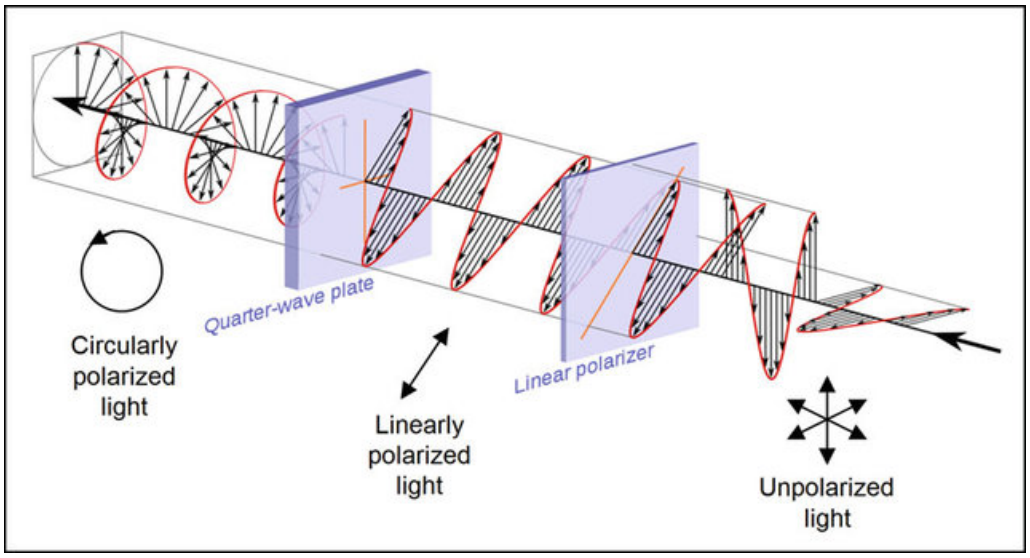

Figure 21: Incident light, linearly polarized light and circularly polarized light. As well as quarter-wave plates and a linear polarizer. [48]

The fundamentals of polarization and polarization modes can be separated into a different combination of X and Y-component amplitudes, as well as the phase shift between the two. Linearly polarized light is a combination of equal magnitudes and no phase shift between the X and Y-component of the light. A circular light has the same amplitudes as linearly polarized light, but with a phase shift between the two. The last mode, elliptically polarized light, comprises all other combinations of amplitudes and phase shift, making a uneven rotation around the Z-axis. [49]

3.1.2 Refractive Index

Refractive index describes a materials optical properties, mainly how fast light is able to travel through the material. The refractive index of materials is seen as one of the primary and most important optical properties, this is mainly due to the fact that it exhibits the optical properties and behaviors of a given material. [50]

Refractive index is defined as the following equation [51]:

$$n = \frac{c}{v} \tag{8}$$

Where:
n = Refractive Index.
c = Speed of light in vacuum.
v = Velocity of light in the optical medium.

The equations shows the relationship between the speed of light in a vacuum and the velocity of light in a optical medium, directly relating the refractive index to the speed of light through the medium. An increased refractive index implies a decrease in the speed of light through the material, likewise a reduced refractive index implies an increase in the overall speed of light through the material.[52]

The refractive index also plays a part in determining the change of light path when a light source is applied to a material. This phenomena is also referred to as refraction. The principle of refraction is visualised in figure 22. [53]

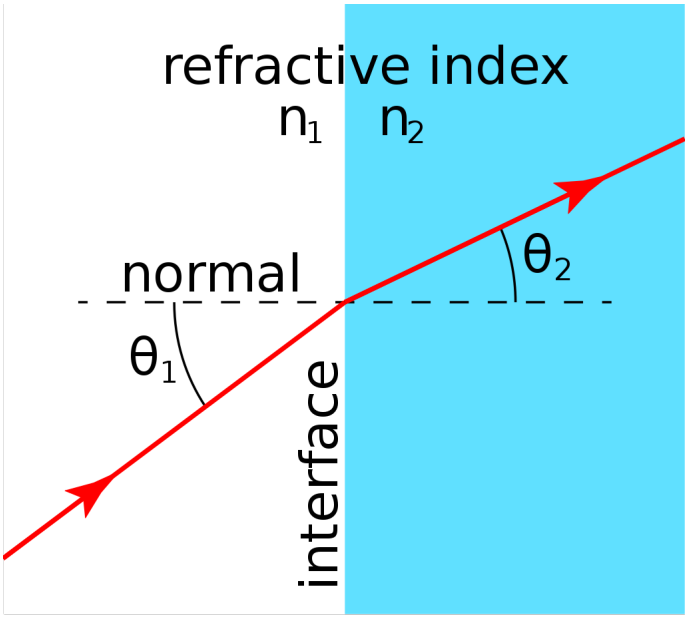

Figure 22: Refraction of light. [53]

The refraction effect defines the change of direction light is subjected to when facing a boundary between materials with different refractive index. Equation 9 shows the relationship between refraction angle and refractive indexes.

$$n_1 sin\theta_1 = n_2 sin\theta_2 \tag{9}$$

Where:
n_1 = Refractive Index 1st material.
n_2 = Refractive Index 2nd material.
θ_1 = Incident angle.
θ_2 = Refraction angle.
When the light source changes from a material with n_1 as refractive index to a material with n_2, the resulting angle of the light is based on the incident angle at which the light enters the medium.[54] This effect is the basis for the birefringence effect which accounts for most of optical current transformers error sources.

3.1.3 Birefringence

All optical materials with a refractive index have an optical property called birefringence. [55] Birefringence (birefraction) is the resulting refraction of the applied light compared to the refractive index of the material, taken together with the direction and speed of the incident light source. This makes a optical material that is anisotropic able to refract or split the applied light into polarized waves, traveling at different speeds and new trajectories. In the original direction of the applied

light this effect results in an overall loss of light intensity, as shown in figure 23. [56]

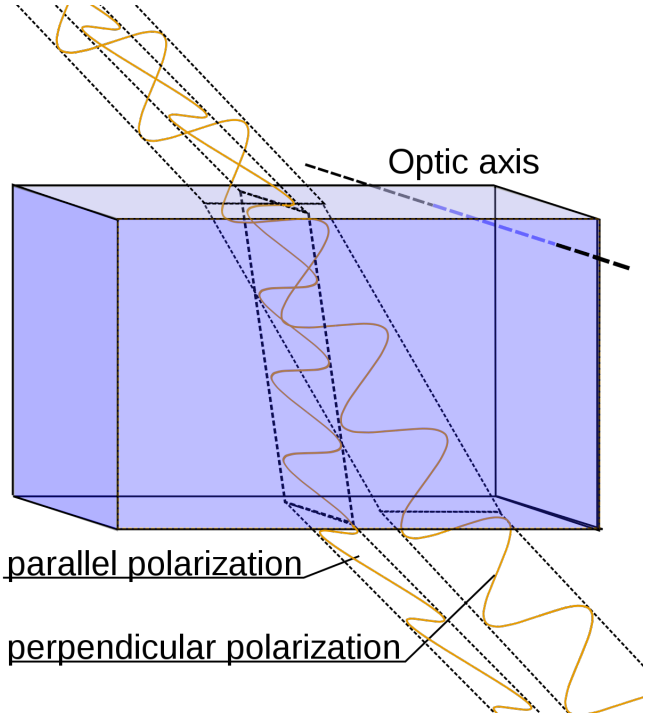

Figure 23: Birefringence effect through a material. [57]

Birefringence may result in all three polarization-modes, depending on the mode of the applied light and the type of birefringence of the material. Applying a linearly polarized light only consisting of X-component perpendicularly to a linearly birefringent material will not result in a change of polarization on the output light, this is dependant on how the applied light hits the anisotropic axis of the material. However, by applying a linearly polarized light consisting of equal X and Y-component to a birefringent material will cause a phase shift between the two. This is because a linearly birefringent material has a "slow"-axis and a "fast"-axis. This makes the orthogonal Y-component in the polarized light experience a different refractive index compared to the X-component in the same applied light.

Circular birefringence is based on the same principle as linear birefringence, but here applied to circularly polarized light. In this scenario the difference in experienced refractive index will be the difference between right-hand circularly polarized light and left-hand circularly polarized light. If a right-hand circularly polarized light is applied to a circularly-birefringent material the resulting light will be unchanged, but if a left and right CPL is applied to a circularly birefringent material, a phase shift will occur between the two. Applying a linearly polarized light to a circularly birefringent material will cause the light to change into circular polarization. [57]

According to the usage in optical systems this effect can be both promoted and suppressed. The birefringence effect is the main source of error in optical systems, but it also is the basis for multiple optical components such as quarter-wave plates, turning LP into CPL, or linear polarizers converting incident light to LP.[58]

3.1.4 Faraday Effect

The Faraday effect and its resulting Faraday rotation, is the primary magneto-optical phenomena that optical current transformers are based on.[59]
The Faraday effect manipulates polarization states of light traveling through a magneto-optic medium, proportional to the applied magnetic field strength. This rotation happens along the direction of the applied magnetic field. [60] This effect mimics an aforementioned circular birefringence, causing linearly polarized light that propagates through a magneto-optic medium to rotate proportional to the applied magnetic field. The effect is shown in figure 24.

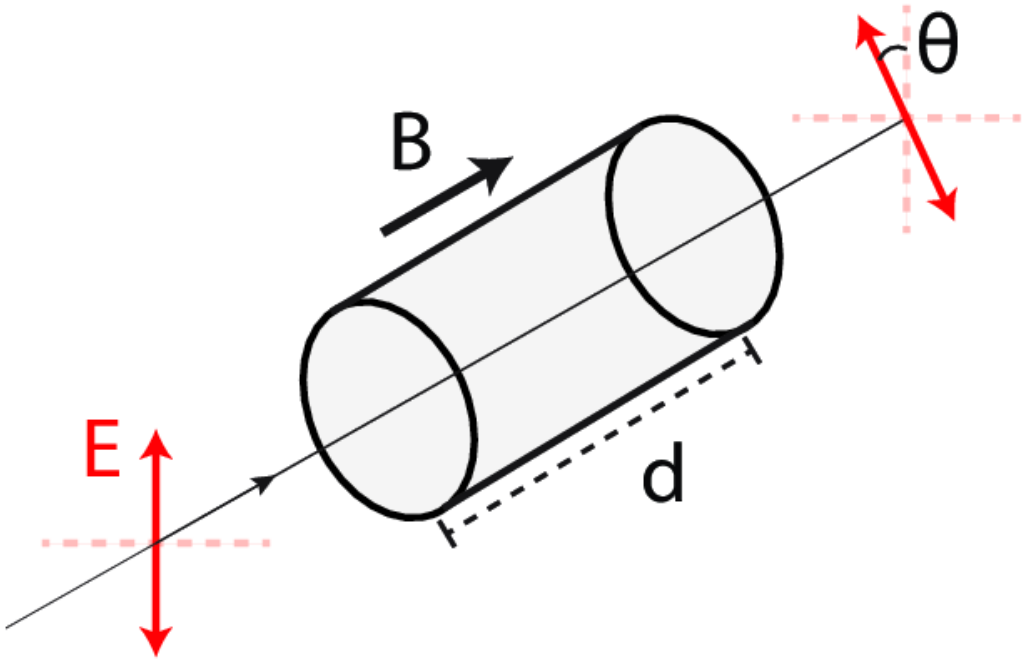

Figure 24: Faraday effect on LPL. [61]

The amount of rotation a polarization state is manipulated by the field strength and the Verdet constant of the material [62]. The Verdet constant relates the amount of applied field strength to the resulting shift in polarization rotation, therefore it's possible to say that the Verdet constant defines the strength of the Faraday rotation effect in a material. Equation 10 shows the relationship between the three factors.

$$\theta = V \int \mathbf{B} d\mathbf{l} \tag{10}$$

Where:
B = Applied magnetic field
θ = Resulting phase difference
V = Verdet constant

The Faraday effect is based on the proportional relationship of applied conductor current and perceived magnetic field strength **B** on the optical medium. Equation 10 shows the relationship between Verdet constant, the line integral of the magnetic field and the resulting polarization rotation. This whole relationship is proportional to the applied current, making us able to call the applied conductor current proportional with the resulting polarization rotation. [63]

The polarization rotation of the applied light is the result of a induced circular birefringence. This circular birefringence will act as if the material has a circular birefringence, affecting the applied light. This rotation of polarization is as mentioned linear with the applied magnetic field strength.[16] This effect affects both linearly polarized light and circular polarized light in a linear way. By applying a linear light, it's possible to observe a rotation of the linear light at the output of the magneto-optical medium. By applying a circularly polarized light, it's possible to observe a phase shift between the RCPL and LCPL at the output of the magneto-optical medium. This is the core principle of optical current transformers.[64]

One property of the Faraday rotation is that the resulting rotational effect is non-reciprocal. This means that the light will rotate with the applied magnetic field, and the sign of the resulting rotation will not change by changing the direction of the applied light, but only by changing the direction of the magnetic field.[65][66]
This effect is used as a indicator of successful modelling of the Faraday rotational effect in this thesis.

3.2 Optical Current Transformer Designs

As mentioned, to harness the effect of the Faraday rotation one has to apply light through a magneto-optical medium, and record the changes in the given light. Optical current transformers are mainly produced in two main designs based on its magneto-optical medium. These two categories are optical fiber and bulk-glass based. As well as different magneto-optical mediums used, a variety of detection methods are different as well. This chapter will explore the main main advantages and disadvantages of the two optical mediums and detection methods.

3.2.1 Polarimetric detection

Polarimetric detection is based on measuring the change of rotation in an applied linearly polarized light, and translating it into conductor current. A simple polarimetric detection scheme is shown in 25. [67]

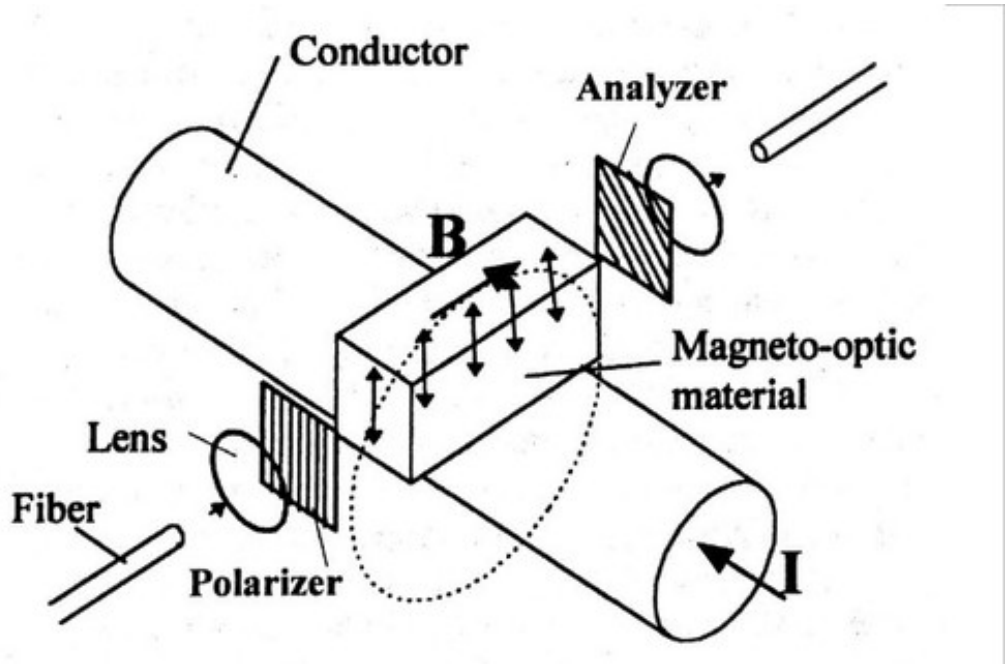

Figure 25: Polarimetric detection type. [67]

In the setup shown in figure 25, an incident light is inserted into a linear polarizer, making the light LP. The LP light is further moved into a magneto-optical material exposed to a magnetic field. The applied field will affect the polarization rotation, rotating it slightly with the direction of the magnetic field. The rotated LP-light is then inserted into the analyzer (polarizer) at an angle difference compared to the first, this rotational angle may be changed to increase or decrease the sensitivity of the current transformer. Lastly the output light intensity is measured and correlated to current. To calculate the expected output light intensity Malus law can be used, as shown in equation 11. [65]

$$I_{out} = I_{p1}\cos^2(\alpha) \tag{11}$$

Where:
I_{out} = Intensity of output light.
I_{p1} = Intensity of the LP light.
α = Angle difference between the polarizer and analyzer.

In a case where the polarizer and analyzer are configured to its most sensitive setting (45 degrees), the output light intensity can be shown by equation 12;

$$I_{out} = \frac{I_{in}}{2}[1 + \sin(2\theta_f)] \tag{12}$$

, where
θ_f = Rotational angle caused by the Faraday rotation.

The output signal **S** can then again be related to the Faraday rotation by equation 13. [65]

$$S_{ac} = \sin(2\theta_f) \tag{13}$$

As mentioned, the regulation method of a polarimetric scheme is most sensitive at a $\alpha = 45°$ angle difference between the polarizer and the analyzer. In this setup a change in the rotation of the LP-light will result in changes of the measured values that are very large compared to the average light intensity passing through the analyser, making the sensor more sensitive to changes. Measuring the angle difference based on the light intensity might cause additional error sources in the sensor. The main error source that this method brings is the varying of the input light intensity, meaning that any change of the light intensity would result in a false reading of polarization rotation at the sensor. This light change can come from all kinds of external sources, vibration, dust etc. To counteract this effect a further development of the polarimetric sensor is developed.

The further development of the polarimetric sensor is the polarimetric dual-quadrature detection scheme. The primary change in this design is the use of a Wollaston prism in place of the analyzer, as shown in figure 26. This analyzer method divides the output waves into orthogonally displaced waves, negating the effect of input light but instead looking at the difference in light intensity between the two orthogonally displaced waves. [65]

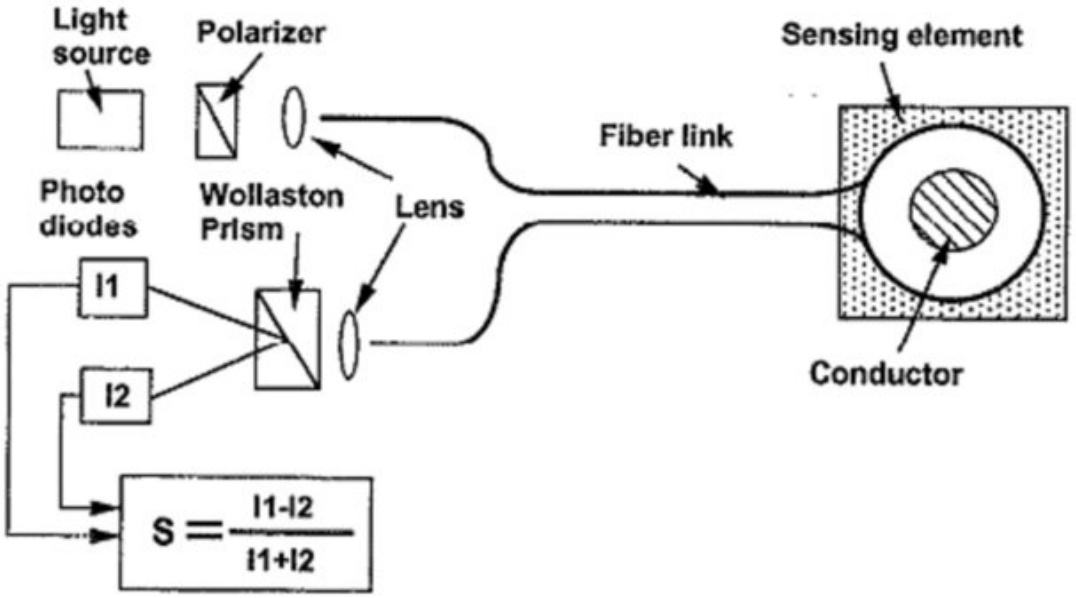

Figure 26: Polarimetric dual quadrature detection [68]

Dual-quadrature detection offers improved noise suppression compared to a regular polarimetic detection, especially when it comes to changes in input light intensity. Linear birefringence does not get accounted for in these designs, and has to be accounted for if it poses a great error source. The resulting signal of a dual-quadrature sensor is shown in equation 16 and 17, dependant on the amount of linear birefringence in the system.[16]

Equation 16 shows polarimetric dual quadrature detection with noticeable linear birefringence.

$$S_{ac} = 2\theta_f \frac{sin\beta}{\beta} \qquad \beta >> 2\theta_f \tag{14}$$

Equation 17 shows polarimetric dual quadrature detection with negatable linear birefringence.

$$S_{ac} = 2\theta_f \qquad \beta << 2\theta_f \tag{15}$$

where:
β = Linear Birefringence.

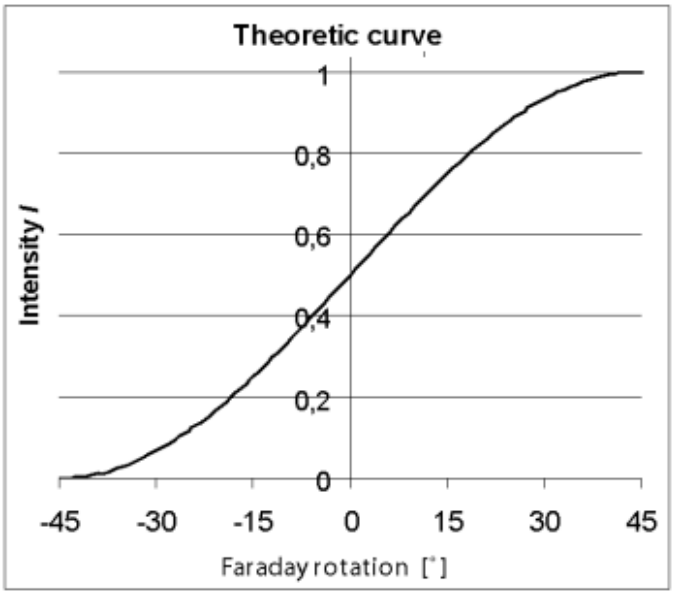

Figure 27: Theoretical linearity OPCT. [38]

The linearity of the sensor is not indefinite as shown in figure 27, making these equations false at higher rotational values.[69] As equation 17 shows, the linear birefringence can impose a great error source to a polarimetric system. To combat the effects of the linear birefringence compensation methods or a further developed sensor system is needed. [65].

3.2.2 Bulk-Glass

Bulk glass optical current transformers are based on a fully, or partially enclosed block of magneto-optical material. The main principle of a bulk glass OPCT is injecting a linearly polarized light into the bulk glass by the input fiber as shown in figure 28. When inside the bulk-glass the light will bounce around one rotation and get influenced by the Faraday effect. When the rotation is completed, an output fiber returns the light to a polarizer and is processed by a polarimetric sensor. One of the advantages of bulk-glass sensors is a high Verdet constant of the Faraday material, reducing the need for multiple rotations around the conductor. The bulk glass sensor is also possible to implement as a split core or partially enclosed core, making installation easy.[16]

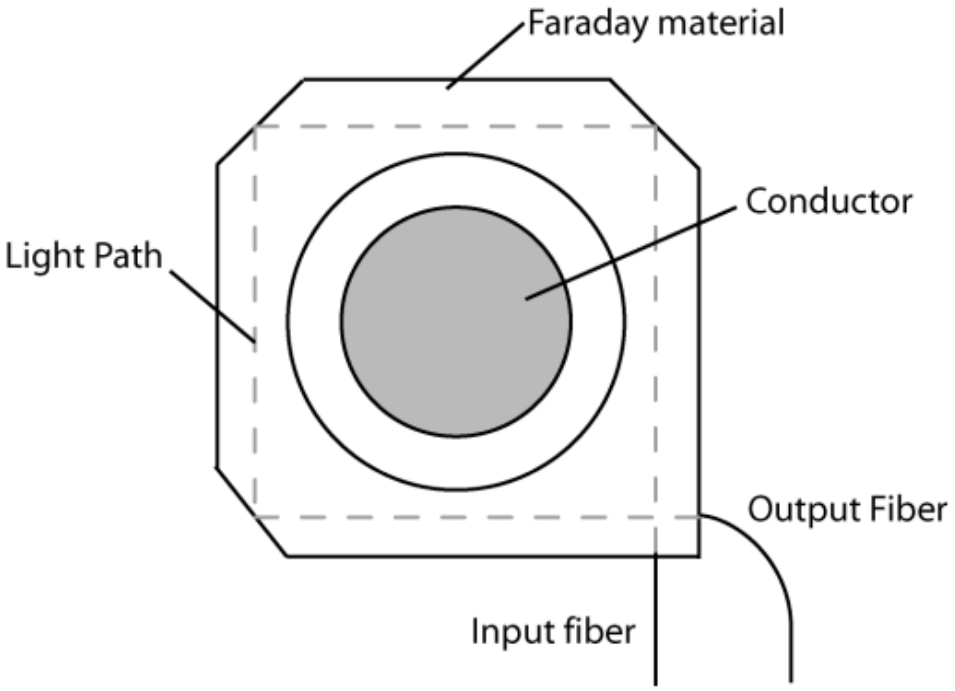

Figure 28: Bulk-glass OPCT.[70]

The bulk-glass based optical current transformer is one of the most used optical current transformer technology. [71] Compared to the other popular technologies of optical fiber based optical current transformers, the bulk-glass may offer some benefits as well as drawbacks. The most notable benefits compared to a fiber optic based transformer are :

- Smaller physical dimensions.
- Higher Verdet parameter.
- Less prone to linear birefringence.

Bulk-glass based transformers are able to be produced in a more compact size, and due to the massive Faraday material it is also sturdier and more resistant to external affections. The material of a bulk-glass usually delivers a higher Verdet constant, increasing its sensitivity compared to a fiber optic based transformer. Linear birefringence is especially pronounced in fiber optic transformers, mainly due to its more resistant design. Linear birefringence may be induced by mechanical stresses on the magneto-optical medium, resulting in photo elasticity which can increase linear birefringence.
The main disadvantages of a bulk-glass sensor is:

- Refraction index of enclosing material matters.
- Reflections inside the bulk-glass may cause a phase shift of the light.
- May be sensitive to shock and vibration.

To propagate around the conductor, the applied light has to reflect on the edges of the bulk-glass to complete a full rotation of the conductor. These reflections is affected by the refraction index of

both the magneto-optical material of the bulk-glass, as well as the refraction index of the material enclosing the bulk-glass. Each bounce will make the light slightly shift due to the refraction index as mentioned in earlier chapters. In a normal situation this refraction index should not affect the current in any notable way, but if the enclosing material is contaminated by something with a different refraction index, like water or dust, the phase shift will be notable. [72]
A counter measure to the possible contamination of refraction index is fully enclosing the bulk-glass in a solid piece of material. This may increase costs of production as well as the physical size and ease of installation. [73]
These designs are also sensitive to shock and vibration, especially the not fully enclosed models. This is due to its dependence on a constant distance from the conductor to measure accurately at all times.[38]

3.2.3 Optical Fiber

Optical fiber based current sensors are similar to the bulk-glass design, except the bulk-glass is swapped for a lower Verdet constant optical-fiber wrapped around the conductor multiple times. A fiber optics based optical current transformer design is shown in figure 29 This design also uses a polarimetric based sensing method.

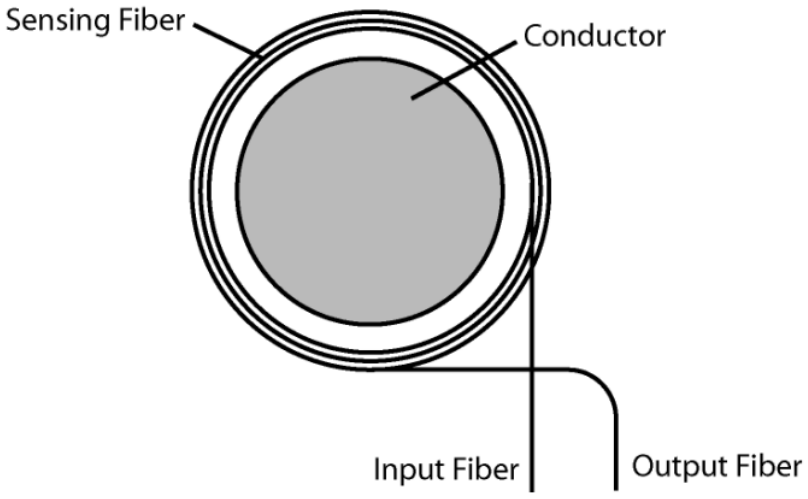

Figure 29: Fiber based OPCT.[70]

Because the Verdet constant of optical fiber is lower than a bulk-glass, the fiber is wrapped multiple times around the conductor to achieve the same level of accuracy. One benefit this gives to the design is the possibility to adjust the sensitivity of the current transformer by varying the amount of turns around the conductor. [74]
The use of multiple turns of optical fiber around the conductor comes with some drawbacks when it comes to robustness. With increasing meters of fiber, the chance of damages due to temperature vibration or thermal stresses increases, as well as possible manufacturing unevenness inducing linear birefringence.
One of the main advantage with using a fully enclosed optical fiber is the negation of disturbance caused by external magnetic fields. In a fully enclosed specification the integral of the magnetic

field equals the current flowing in the primary conductor. [65]

3.2.4 Magnetic Concentrator

A magnetic concentrator is a hybrid design between conventional magnetic current transformer and an optical current transformer. The concentrator is based on a design with a magnetic core partially enclosing a conductor, and an optical sensing element in the remaining gap to fully enclose the conductor. The magnetic core is used to concentrate the magnetic field produced by the conductor into a small point, which is then observed by a optical sensor. To avoid saturation of the core, the small air gap is established. The figure 30 shows the design of such a transformer. [75]

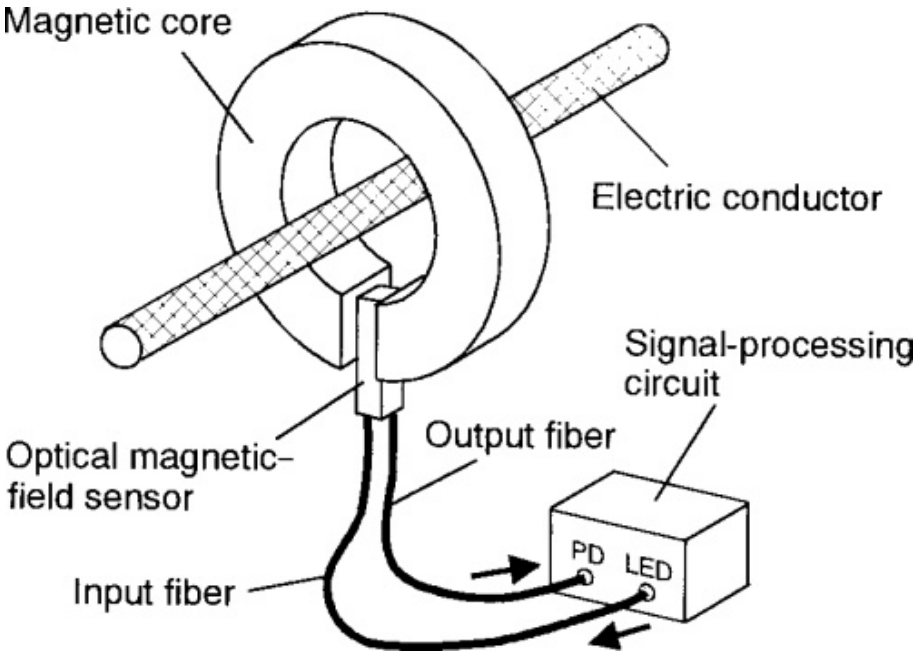

Figure 30: Magnetic concentrator.[75]

This design may come with some drawbacks, and is because of this not the most popular design. Main disadvantages of this design may be:

- Sensitivity to external magnetic fields.
- Sensitivity to lateral movement relative to the conductor.

The design is not fully enclosing the conductor with its magnetic core, resulting in a sensitivity to nearby magnetic fields due to the integral of the magnetic field is not fully proportional with the conductor current. Another drawback comes with the partially open design is the sensitivity to lateral movement, this changes the perceived magnetic field of the magnetic core, resulting in possible error in the measurements.
According to [76] multiple earlier versions of this design has been implemented in the Japanese power grid as a transducer for overcurrent protection systems.

3.2.5 Witness sensor

A witness sensor is a form of non-enclosed bulk-glass optical current transformer. It senses the magnetic field at its current position, therefore possible to relate this magnetic field to the current in the conductor by having a constant distance from the conductor. This requires comprehensive calibration to measure accurate currents. Figure 31 shows the basic principle of the witness sensor.

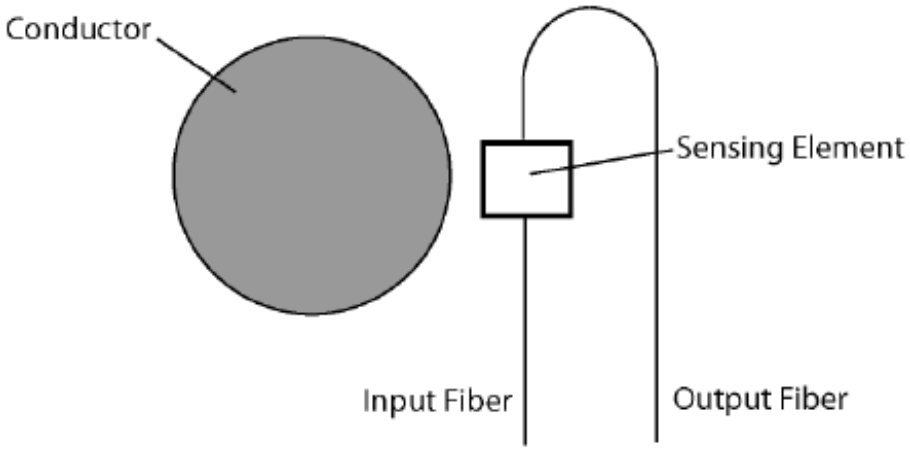

Figure 31: Witness sensor.[75]

A witness sensor might have a low physical volume compared to a fiber-optic or bulk-glass sensor, resulting in a high requirements to the Verdet constant of the magneto-optical material to achieve sufficient sensitivity.
This type of sensor has been used in some earth-fault detection cases. [75]

3.2.6 Interferometric

An alternative to polarimetric measurement is interferometric. In place of measuring the rotation of linearly polarized light through a magneto-optical medium, this technique is based on measuring the phase-shift of circularly polarized light through a magneto-optical medium. As mentioned previously; applying a circularly polarized light to a circular birefringent material will cause a phase shift between the RCPL and LCPL lights. The Faraday effect causes a circular birefringence to the magneto-optical medium, that is linear with the applied magnetic field. This allows the interferometric sensor types to measure the phase difference of RCPL and LCPL lights that has passed through a Faraday rotator. [77]
Examples of interferometric sensors are variations of Sagnac loop interferometers.

Sagnac Loop Interferometer A standard Sagnac loop interferometer is vizualised in figure 32.

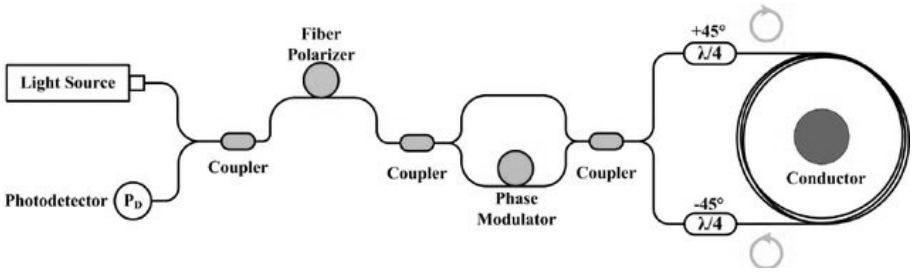

Figure 32: Sagnac Loop Interferometer. [65]

A Sagnac loop interferometer works by injecting a incident light into a coupler. The light then further propagates into a polarizer, making the light linearly polarized. The LP-light is then moved into a coupler and split into two different quarter-wave plates at different angles, +45 and -45 degrees. This turns the LP light into two circularly polarized lights, and the different plates produces right circularly polarized light and left circularly polarized light. Due to the induced circular birefringence in the magneto-optical medium the RCPL and LCPL light will undergo a phase shift during the propagation around the conductor. [6]

The resulting phase shift can be related to the current as shown in equation 16;

$$\Delta\phi_s = 2VNI \tag{16}$$

, where
$\Delta\phi_s$ = Phase shift of light.
V = Verdet constant.
N = Number of turns around the conductor.
I = The primary current.

A drawback with this design is the negative effect of linear birefringence induced by temperature changes or vibration.

Reflective Sagnac Loop Interferometer A further development of the Sagnac loop interferometer is the reflective Sagnac Loop interferometer. This design is illustrated in figure 33. The reflective design is based of the basic sagnac loop interferometer but with a few changes to the sensing fiber. The reflective sagnac produces a circular polarized light to be applied to the sensing fiber, but in this case only in one direction. This circular birefringent light propagates around the conductor, then it hits a mirror and is bounced back towards the photodetector. The great advantage with this design is the counteracting of reciprocal effects, mainly induced by error sources. This means that the linear birefringence error sources picked up on the first rotation around the conductor is counteracted by propagating the same fiber the other way out, leaving only the phase change due to the Faraday effect. This is possible due to the Faraday effect being non-reciprocal as aforementioned. [65]

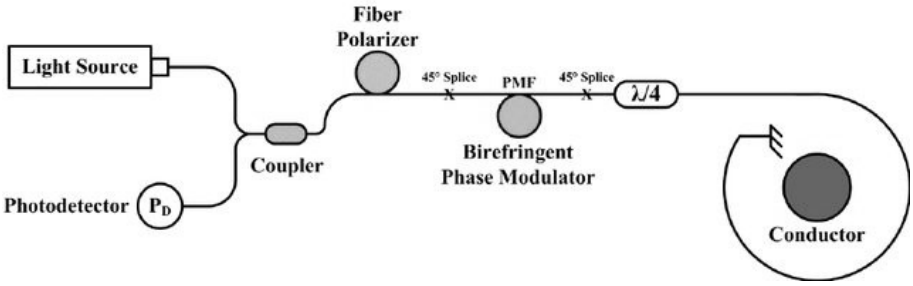

Figure 33: Reflective Sagnac Loop interferometer. [65]

The resulting phase angle of a mirrored interferometric sensor is given in equation 17.

$$\Delta\phi_s = 4VNI \tag{17}$$

As observed by the equation, this sensing method delivers double the sensitivity per turn of optical fiber allowing for shorter distances of optical fiber to reach a sufficient sensitivity level. [69]

3.2.7 Bragg Gratings

The Bragg gratings OPCT is mainly a interferometric sensor, but with altered sensing techniques. A fiber with bragg grating is a a optical filter able to block certain wavelengths. This filter is established by adding different refractive indexes over a short area of a optical fiber, also called fibre bragg gratings or FBG, as shown in figure 34. [78]

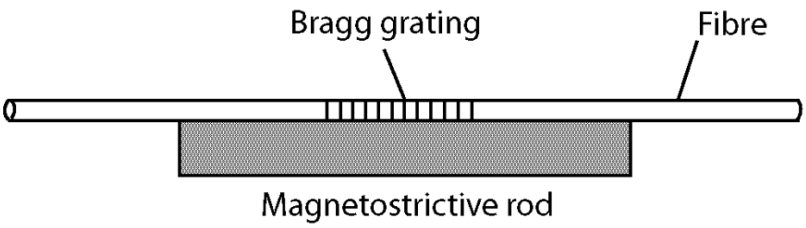

Figure 34: Braggs grating based interferometric OPCT.[79]

The core principle of measuring current with this design is based of the fact that the bragg grating only lets through a small wavelength of light, also called the bragg wavelength : $\mathbf{\Delta bragg}$. Under current load the magneto-optical medium will be under strain changing the refractive index and thereby changing the wavelength let through by the bragg grating. By monitoring this wavelength output, one is able to determine the external magnetic field applied to the magneto-optical medium, and then again the conductor current. [78]
One advantage of bragg gratings is the possibility to easily multiplex multiple signals. [79]

3.3 Error Sources

Optical current transformer designs are sensitive to some external effects. The most common error sources will be explored in this chapter. The focal point is the effect of external error sources on open-core bulk-glass designs.

3.3.1 Vibration

In optical current transformers based on a open core configuration, where the magneto optical medium does not fully, but only partially encloses the conductor, vibration becomes a great source of possible error margins. In a partially enclosed configuration the line integral of the magnetic field in the direction of the light would not equal the conductor current, but rather a proportional amount of the current based on its exposed magnetic field. This proportional amount is dependant on the distance from the conductor but might be highly reduced compared to a closed-core OPCT due to the fact that the magnetic field strength is inversely proportional to the distance from the wire. [80] [81]
Figure 35 shows a modelling experiment done by [81], where the relative error induced by vertical and horizontal displacement of the OPCT in relation to the conductor was examined.

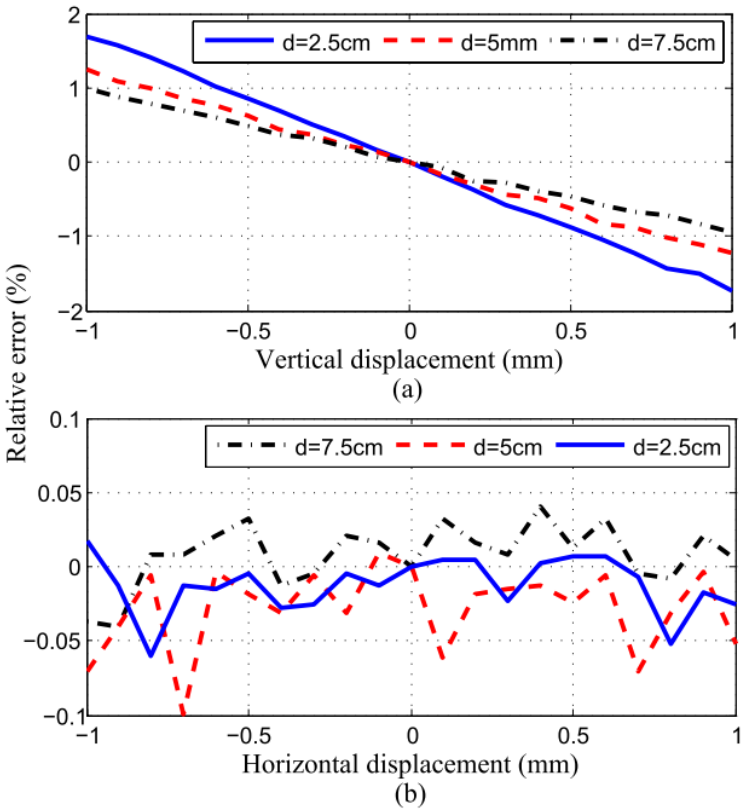

Figure 35: Induced error by horizontal and vertical vibrational displacement. [82]

The results showed that vertical displacement, changing the distance of the OPCT in relation to

the conductor, resulted in a significant relative error. Horizontal displacement, vibration inline with the conductor, showed negligible induced error margins. These error margins are the product of changing the perceived magnetic field distribution of the magneto-optical medium, where the horizontal displacement would result in a small change, and the vertical displacement would result in a great change in perceived magnetic field distribution. These levels of induced error is great enough inhibit the OPCTs possibility to achieve certain accuracy classes. [81]
To reduce the effect of vibrations one can install a closed core OPCT to remove its effect fully, so that the line integral of the magnetic field in the direction of the light always results in the conductor current. A drawback with a closed core installation is the intricacy of the installation, which might increase the overall cost of the installation compared to a open-core design.

3.3.2 Temperature

The Verdet constant of a magneto-optical medium is temperature dependant, making a optical current transformer design vulnerable to fluctuations of the ambient temperature. This is a possible source of significant error margins. [62]
In [83] a experiment was done to examine the error margins generated by changing temperature.

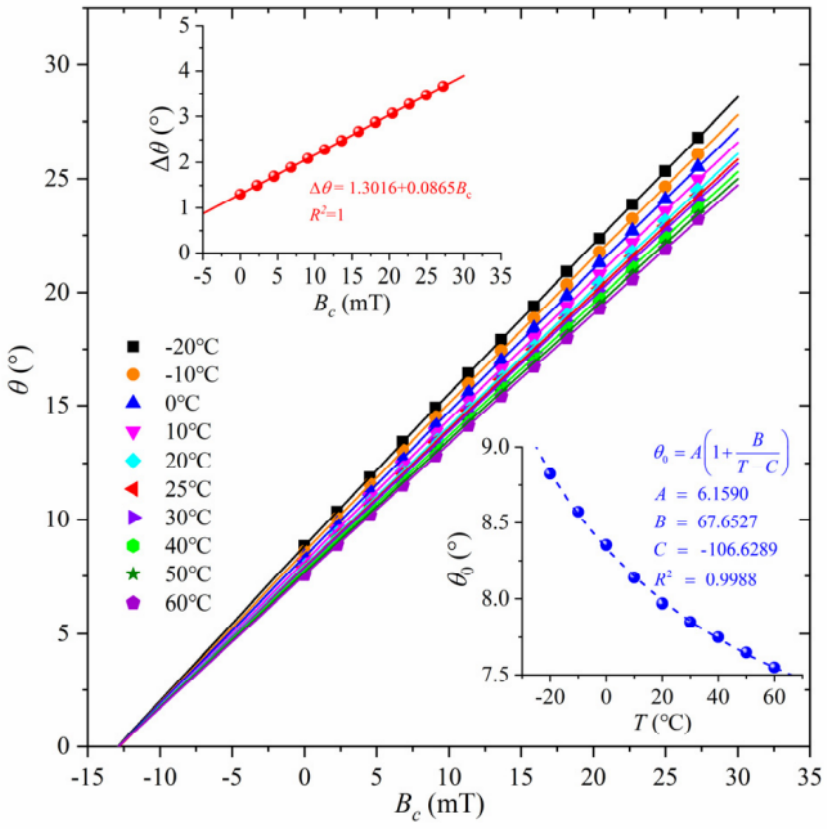

Figure 36: Effect of temperature induced birefringence in optical current transformer.[83]

The experiment mounted the magneto-optical medium in a environment with a temperature controller, and exposed it to a magnetic field by a solenoid. To the magneto-optical medium a light source was applied, and the resulting polarization rotation was recorded. The temperature was changed from -20 to 60 Celsius and the resulting phase rotation change is shown in figure 36.

The experiment showed an average of 0.2% error induced per Celsius. The result also showed that moving the temperature in negative direction would result in a higher output polarization rotation, and increasing the temperature would result in a lower resulting polarization rotation.
There have been successful solutions to this problem by compensating the measured current based on the expected error margins caused by the fluctuation temperatures.

3.3.3 Stray magnetic fields

Stray magnetic fields caused by adjacent conductors or other electrical machines in close proximity can cause high error margins in a open-core optical current transformer. This happens because the overall perceived magnetic field strength observed by the optical current transformer changes. Figure 37 shows the principle of magnetic field amplification caused by close proximity conductors.

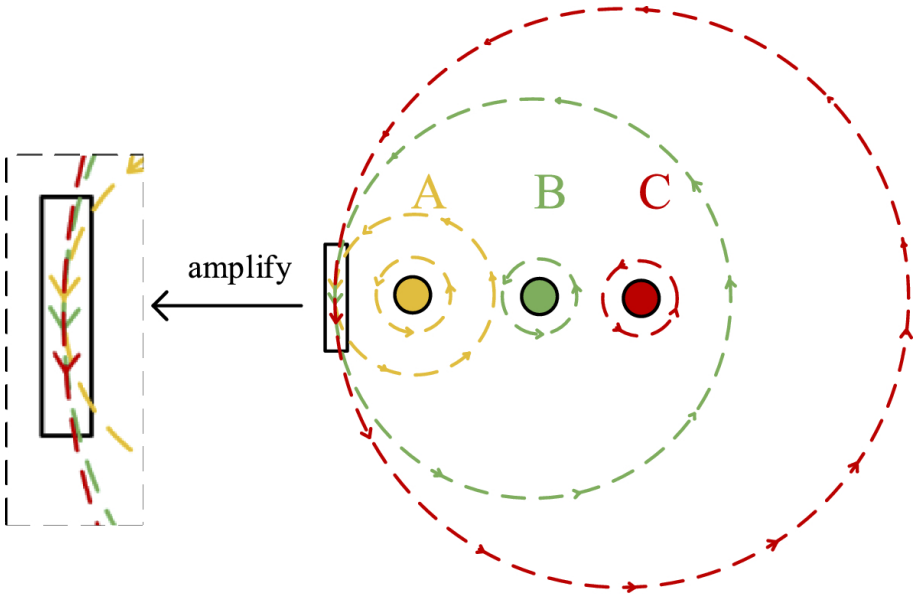

Figure 37: Influence of stray magnetic fields.[84]

The distance between the magneto-optical medium to the conductor highly affects the impact of stray magnetic fields. At a closer proximity the field strength perceived by the sensor is at a higher level, making the overall impact of the external stray field lower compared to the measured primary conductor magnetic field. In [85] a modelling experiment was done by testing the influence of a stray magnetic field as compared to the distance of the OPCT to the primary conductor, and the distance between the conductors.

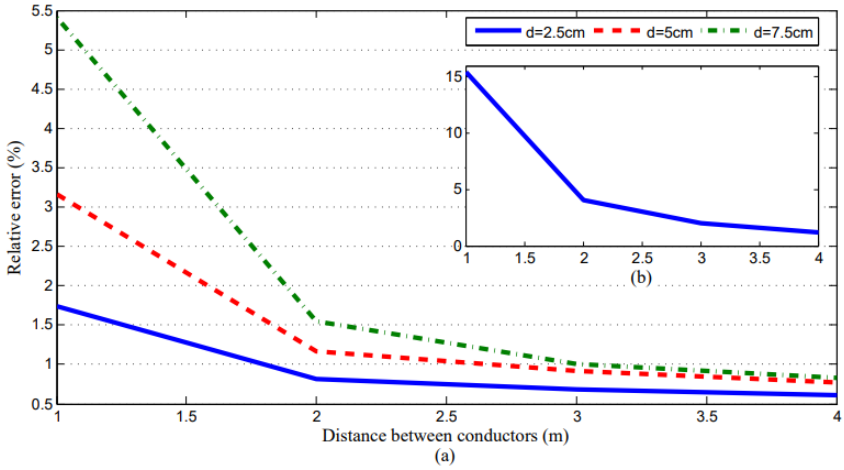

Figure 38: Relative error induced by stray magnetic field at different conductor setups.[85]

The results show that the distance between conductors, and especially distance between OPCT and conductor, may greatly impact overall OPCT performance. The error margins caused by the stray magnetic fields are great enough to inhibit the sensor from achieving higher accuracy classes. [85]

3.4 OPCT Performance

Optical current transformers promises several notable performance improvements as substitute of a conventional current transformer. This chapter explores the main areas of performance improvement promised by the optical current transformer. These areas are split into three groups: Steady state performance, linearity and transient performance.

3.4.1 Steady state performance

Steady state or stationary performance is defined as how precisely a current transformer is able to measure a constant signal over a period of time. A comparison of optical current transformer steady state performance with conventional current transformer performance was done in the article shown in [30]. The experiment applied a ramping current to both current measurement technologies, and the difference was noted. Table 3 shows the measurements from the experiment.

Applied current [A]	Difference [A]	Difference [%]
248	0.4	0.16
313	0.7	0.22
390	0.8	0.20
466	0.8	0.17
543	0.6	0.11
619	0.6	0.09
688	0.4	0.05
762	0.2	0.02

Table 3: Steady state comparison of CT and OPCT. [30]

The peak difference between the two happened at 313A with a resulting 0.22% difference in measured current. This difference is primarily the result of the inaccuracies in the iron core current transformer. Most optical current transformers are classified as 0.2S. [86]

3.4.2 Linearity

Linearity is a measurement device's ability to measure the current proportionally with no non-linear effects occurring. The article [30] also executed a linearity experiment where both of the technologies were examined.
The graph in figure 39 shows the results of the linearity experiment. The optical current transformer was ramped up to 20 times its rated current, while the CT was ramped to 1.1 of its rated current.

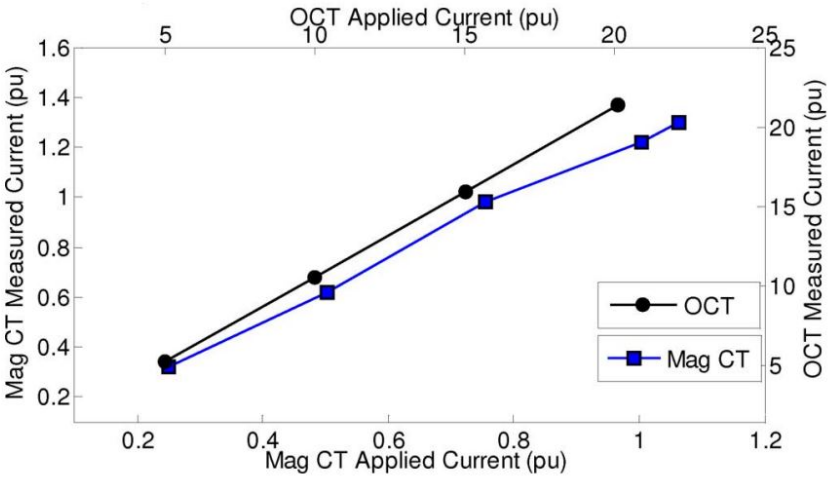

Figure 39: Linearity of OPCT vs CCT.[30]

The experiment shows the optical current transformer as greatly more linear compared to the conventional current transformer. The optical current transformer kept a linear measurement all the way up to 20 times its rated current, while the conventional iron-core transformer lost some linearity while passing its rated current.
This shows the advantage of the non-saturable design of the optical current transformer in place of

the conventional design. The optical current transformer design is not infinitely linear, at a higher current the polarization rotation of the light will surpass 90 degrees, and the measured value will start to decrease with increasing current. This phenomena is shown later in this report in figure 45.[87]

3.4.3 Transient performance

Transient performance of optical current transformers are also a promising field in terms of performance increase. The unsaturable design allows the transformer to be installed in a high short circuit current power system. Optical current transformers are designed to be linear within a certain range, this range is given in the optical current transformer data, similar to a ALF in CCTs. When designing a substation the maximum short circuit current of a optical current transformer has to be taken into account during the design.[30]
When using optical current transformers for protection, their accuracy is also categorized the same way as CCTs: 5P, 10P accuracy classes.[86]
The aforementioned article [30] executed an experiment to examine the performance of an optical current transformer in a transient setting. The premise for the test was to apply the highest possible rated current of the optical current transformer and observe the output response. The test injected a current of 20 times the rated current of the optical current transformer, the resulting transient output wave form is shown in figure 40.

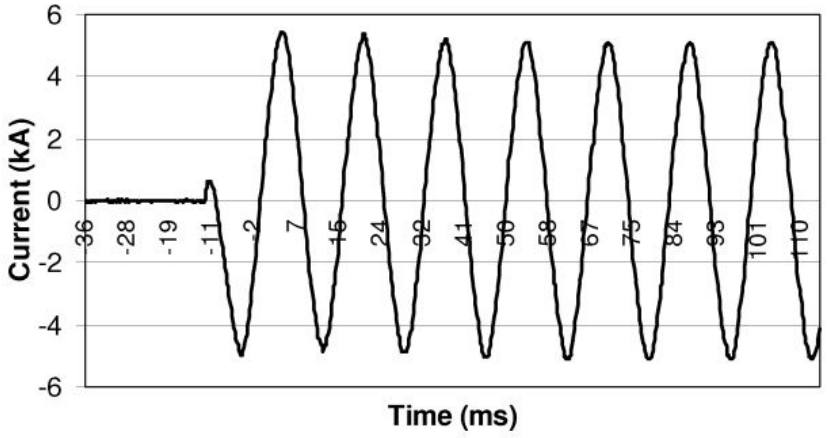

Figure 40: Transient waveform OPCT.[30]

The experiment resulted in a clean sinusoidal output, and the output measurement reached steady state after 3 cycles.
As part of the transient experimental testing, the step response of the optical current transformer was also tested. The goal of this test is to detect the speed of the magneto optical medium and the electronical design. The test used a step current of 300A DC current. The applied signal and resulting optical current transformer response is plotted in the graph 41.

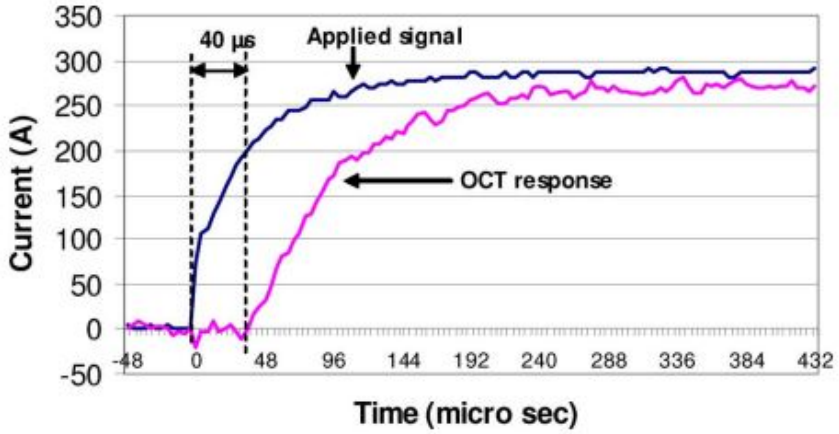

Figure 41: Step response optical current transformer.[30]

The result of the step-response test was a response of 40 microseconds, a satisfactory response time. The experiment also showcased the optical current transformer's possibilities of measuring direct current in a precise manner. [30]
The optical current transformer performance improvements shows notable benefits over conventional iron-core designs. Both protection applications and measurement application would benefit from the transition from iron-core based transformers to optical based transformers. [88] To ensure interoperability and satisfactory real-world performance, a model will be designed and deployed in a real-world scenario.

3.5 Modeling Trends

Optical current transformer models are not overly represented in current literature, especially complete modelling of optical current transformers are rare to come by. A complete model is required to enable faster acceptance tests, interoperability tests and performance tests as well as provide an aid in learning about this technology. A model would also aid the testing of protection relay performance.[89]
Most literature represents only the optical part as a separate stand alone model, without any electrical part. To model the optical part of a optical current transformer it's crucial to be able to represent the Faraday effect. To represent this effect projects in available literature have used different techniques ranging from frequency response data to mathematical modelling set based of Jones matrices and a few articles have used FEM models.
An article published in 2017 [90] makes use of frequency response data to develop an operational amplifier-based low pass filter circuit model, to represent the optical current transformer. This technique manages to model the core functionality of an optical current transformer, but lacking in overall functionality.
An article on complete modelling [91] successfully modelled the optical part of the current transformer using Jones matrices. Jones matrices is a set of matrices, used to represent each optical component in a optical system. By multiplying these matrices together one can calculate the resulting output light states, changing their behavior by regulating the coefficients within the matrices. [66] A representation of optical devices in Jones matrices is shown in figure 42

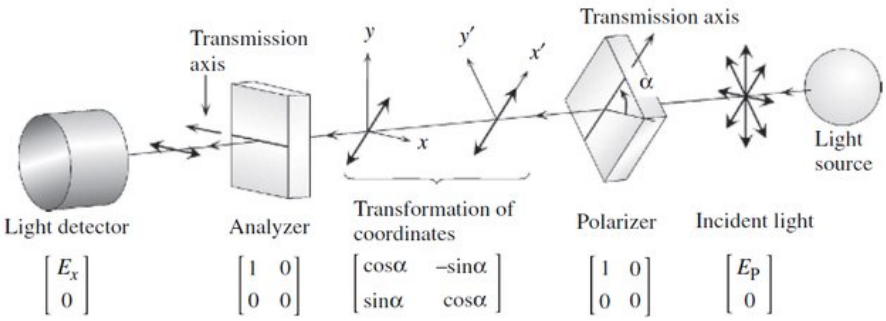

Figure 42: Optical devices represented as Jones matrices.[92]

The advantage of Jones matrices is the ease of use and speed of deployment compared to more intricate modelling methods as FEM. A drawback with using Jones matrices is the limitation to represent some non-ideal effects that optical current transformers are prone to.

Lastly a few articles have been successful in modelling the Faraday effect by using a finite element method. This modelling technique offers the most flexibility to research non-ideal effects of the optical current transformer. The articles [93] and [66] manages to model the Faraday effect by the use of FEM modelling. The Faraday rotational effect from [93] is shown in figure 43. The red arrows represents the polarization rotation through a magneto optical medium. With an applied external magnetic field this polarization rotates, and the red arrow representing the polarization direction changes direction to represent the change, shown in figure 43.

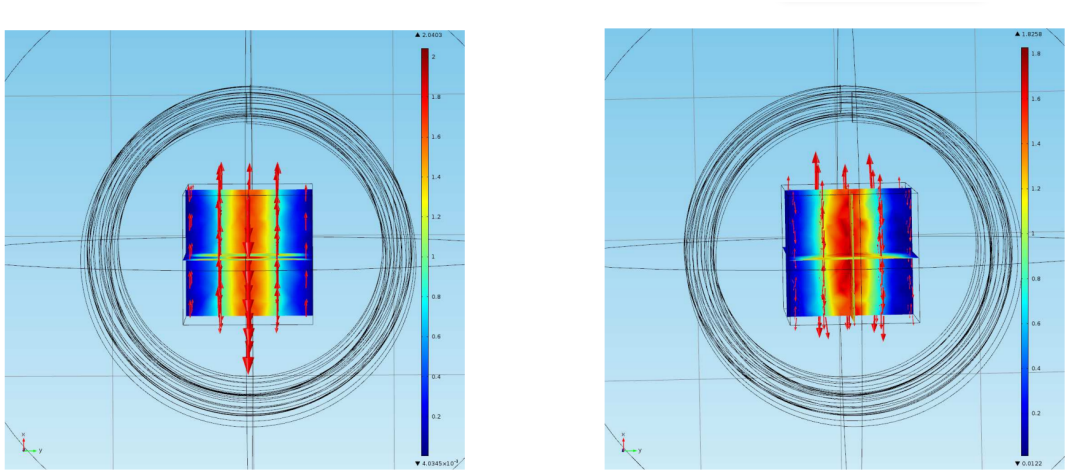

Figure 43: Faraday effect shown modelled in FEM.[93]

Further the authors of [66] have used their model to explore the different non-ideal error sources an optical current transformer is exposed to, validating the optical model for use in testing of non-linear situations. These models are validated compared to physical transducers are are replicating effects precisely. A complete FEM based model is lacking in literature, the continuing chapters will develop a complete FEM based optical current transformer model.

Overall FEM seems like the most promising and flexible modelling technique and will be used in this thesis for the optical current transformer model.

4 Model Development

Developing a complete model for a optical current transformer is a core piece in understanding and exploring its benefits over a conventional design. To model a complete optical current transformer, two components are needed: The optical part, and the electrical part. To model the optical part one has to model the Faraday effect on the magneto-optical medium. The frequency response of the electrical part is used to develop the electrical model. The optical part is defined as all optical components of the transducer, from the source diode to the sensor, the electrical part is the sensing and evaluation electronics surrounding this optical system. [63] This work focuses on developing a complete model of a open-core bulk glass optical current transformer.

The open-core bulk glass optical current transformer is based on linearly polarized light passed through a magneto optical medium, in this case a block of quartz. The linearly polarized light is then affected by the Faraday rotation in a magneto-optical medium, the effect of the Faraday rotation is registered as the resulting polarization rotation of a linearly polarized light. This rotation is then further related to the conductor current of the primary conductor.

As mentioned in previous chapters, the Faraday rotation is defined as the resulting polarization rotation of a light source passing through a magneto optical medium in the direction of a externally produced magnetic field. The resulting rotation of the polarized light is a result of three main factors, the external magnetic field strength and Verdet constant of the magneto optical medium. Equation 18 shows the relationship between the three variables. [63]

$$\theta = V \int \mathbf{B} d\mathbf{l} \tag{18}$$

Where:
B = Magnetic Field Strength
θ = Resulting polarization rotation
V = Verdet constant

The aim of developing a complete model is to both be able to analyze its functionality and performance, examine the ability of modelling the Faraday rotation in FEM, as well as developing a complete model capable of simulating non-ideal situations where other modelling techniques fall short.
The combination of the optical FEM based model, and the electrical model results in the complete optical current transformer model. This complete model will then be based of a transfer function deployed in Simulink for the electrical model, as well as a curve fitted function deployed in the same system in Simulink extracted from the optical model.[94]

4.1 Optical FEM Modelling

The optical model in this thesis will be based on a open-core bulk-glass optical current transformer. The operation of this model is based on the rotation of linearly polarized light. To model the Faraday effect, the following equation relates all optical factors to the resulting output rotation. Equation 19 shows the relationship between optical and electrical parameters of the Faraday effect. [66]

$$\vec{D} = \epsilon\vec{E} + j\epsilon_0\vec{G}x\vec{E} = \epsilon_0(n^2\vec{E} + j\vec{G}x\vec{E}) \tag{19}$$

Where:
$\tilde{\mathrm{D}}$ = Electric Displacement
$\tilde{\mathrm{E}}$ = Electric Field
$\tilde{\mathrm{G}}$ = Gyration Vector
n = Refraction index of the magneto-optical medium.
ϵ = Electric permittivity of the magneto-optical medium.
ϵ_0 = Electric permittivity of free space.

$\vec{G}$ or the gyration vector is the primary driving force of the Faraday rotation. The vector is proportional in the same direction as the external magnetic field. This is done by multiplying a gyration constant with the wave vector. This vector rotates the light polarization in the direction of the external magnetic field. By adapting this formula to the magneto-optical medium in FEM, the Faraday rotation is observed. [66]

The Following constants are used in the model:

- Gyration Constant = 0.05
- Source light intensity 1 V/m
- Refraction index of magneto optical medium = 2.05

The geometry of the model is developed in COMSOL. The geometry and working principle of the optical system is shown in figure 44.

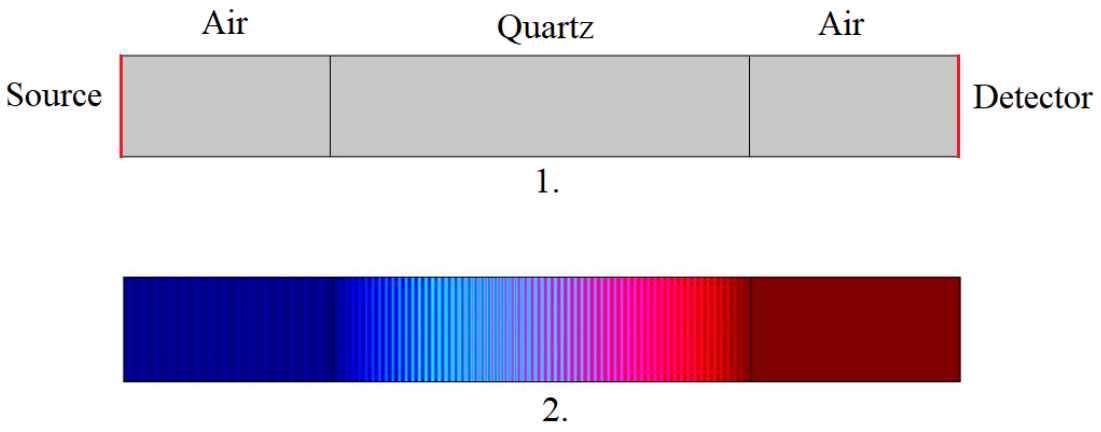

Figure 44: 1: Model Geometry. 2: Faraday effect with a applied external magnetic field. [94]

The geometry is shown in part 1 of figure 44, Part 2 of the figure shows the model functionality of the FEM model. A linearly polarized light highlighted in blue passes through the first air domain and entering the quartz. When inside the quartz the Faraday rotation and high external magnetic field causes the light to rotate in the direction of the magnetic field. In this case the light rotates from a linearly polarized light composed of 100% z-component to a 100% x-component light, marked in red. This sensing is exaggerated to show the principle of the OPCT, at normal loads far lower rotation is observed.
The geometry in part 1 is based on two air domains and one quartz domain. The air domains are only adapted to show the effect of the light entering the quartz. This effect can be seen in part 2 of figure 44.
The quartz is used as the magneto-optical medium and is responsible for the Faraday effect on the source light. On the left side of the geometry there is a source light, injecting a linearly polarized source light at a intensity of $1V/m$. The right side of the geometry contains the detector which detects the resulting polarization rotation of the applied light. To test the model a magnetic field is generated with a simulated conductor current. The resulting wave equations is solved in the frequency domain.
The finite element method solves the magnetic field, by using a amperes law domain solver over the whole model, resulting in the magnetic field strength. The air and quartz domain are solved using wave equation modules. Due to the lack of anisotropic materials in COMSOL version at hand some effects had to be simulated by redefining the quartz's permittivity matrix. [66]
Equation 20 is based on equation 19 and shows the permittivity matrix deployed for the quartz:

$$\vec{D} = \epsilon_0 \begin{bmatrix} n^2 & + & jG \\ 0 & n^2 & 0 \\ -jG & 0 & n^2 \end{bmatrix} \vec{E} \tag{20}$$

To adapt the optical model into the complete model, a curve fitting was generated based of the relationship between applied magnetic field strength and resulting polarization rotation the resulting optical current transformer characteristic is shown in figure 45.

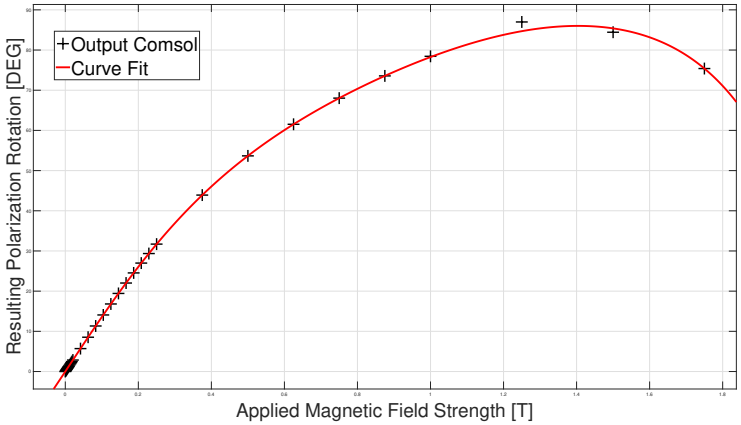

Figure 45: Curve fitting COMSOL Model.

This graph shows the linearity of the optical current transformer over a wide range. The polarization saturation is also represented. Where the polarization rotation surpasses 90 degrees and results in a reduced angle difference between the rotated light and input light, causing a faulty measurement. The model shows linearity up to 0.1 Tesla, at a distance of 0.06m from the conductor this translates to 30kA. This model assumes that all current loads results in a homogeneous magnetic field over the magneto-optical medium.

4.1.1 Optical model Functionality

The optical model functionality was tested by inducing varying external magnetic fields with varying conductor current. Figure 46 shows the polarization of a linearly polarized light traveling through the optical current transformer without any external influences by magnetic fields. The amplitude of the source light is $1V/m$ and stays the same on both sides of the quartz, resulting in no notable loss within the magneto optical medium in a non-affected state. The figure shows the decrease in propagation speed while entering a medium of a higher refraction index, the period length of the light is changed while propagating within the magneto optical medium.

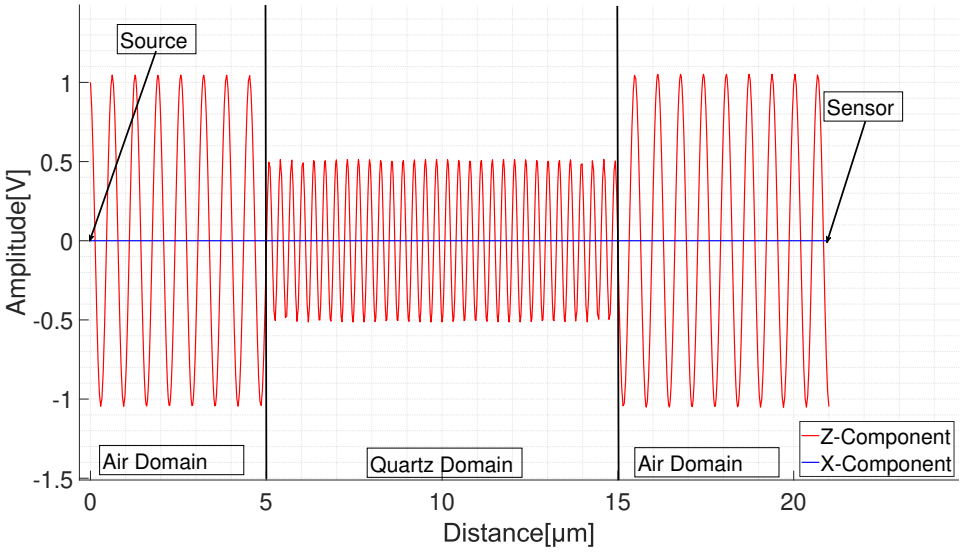

Figure 46: No load condition. **T**=0

Experiments with higher load was also completed to verify the functionality of the model, in these cases the load current is overstated to more clearly visualize the effect of the Faraday rotation. Figure 47 shows a high-load scenario with a magnetic field strength of $T = 1.3$. At this level of external magnetic field the polarization rotation is close to 87 degrees, as shown in figure 48. The load scenario shows the source light of $1V/m$ entering the quartz, while inside the quartz the light is affected by the Faraday effect, which again results in a rotation of the polarization of the linearly polarized light, reducing the Z-component and increasing the X-component.

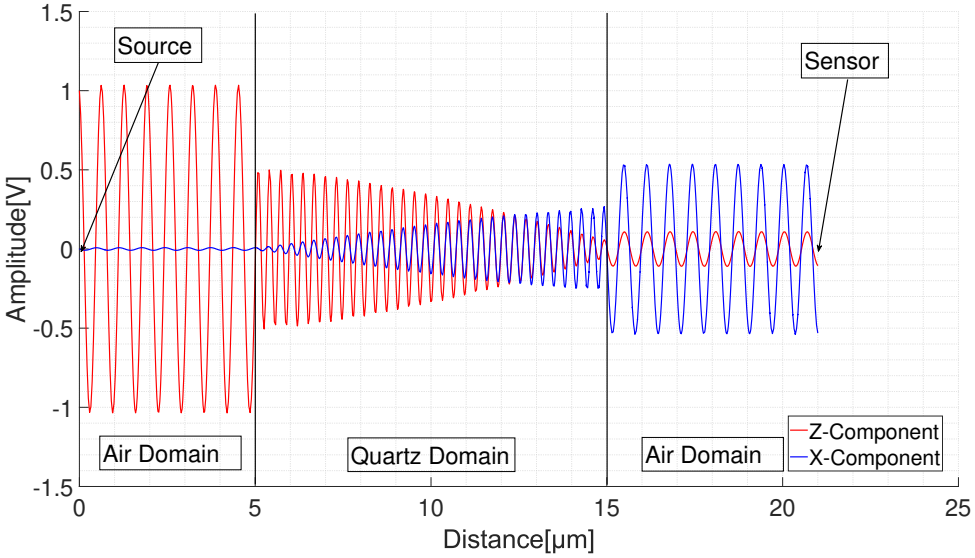

Figure 47: High-load, normal situation. **T**= 1.3

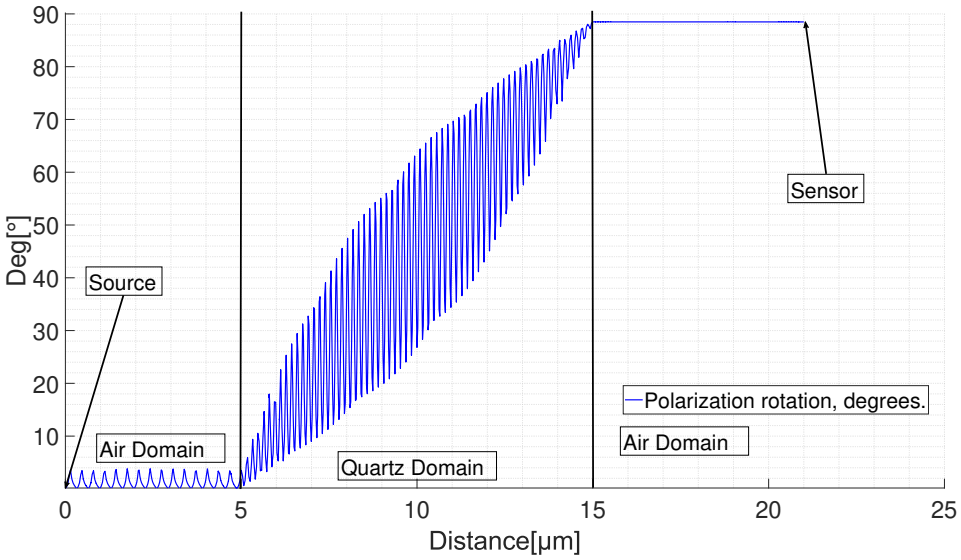

Figure 48: Resulting polarization angle at **T**= 1.3

To extract the load current value of optical current transformer one has to analyze the rotational angle difference between the Z and X-component in the light. Figure 48 shows the angle rotation from approximately 0 degrees to 87 degrees at the output. The resulting output angle is used to relate the rotational angle to the conductor current in the system.

4.1.2 Non-reciprocity verification

As aforementioned in the thesis the non-reciprocity of the Faraday effect is a useful tool for verification of achieved Faraday rotation in a model. To examine the actual occurrence of Faraday rotation in the model, a light was injected at the opposite side of the magneto optical medium and the resulting rotation was observed. The resulting rotation is observed in figure 49.

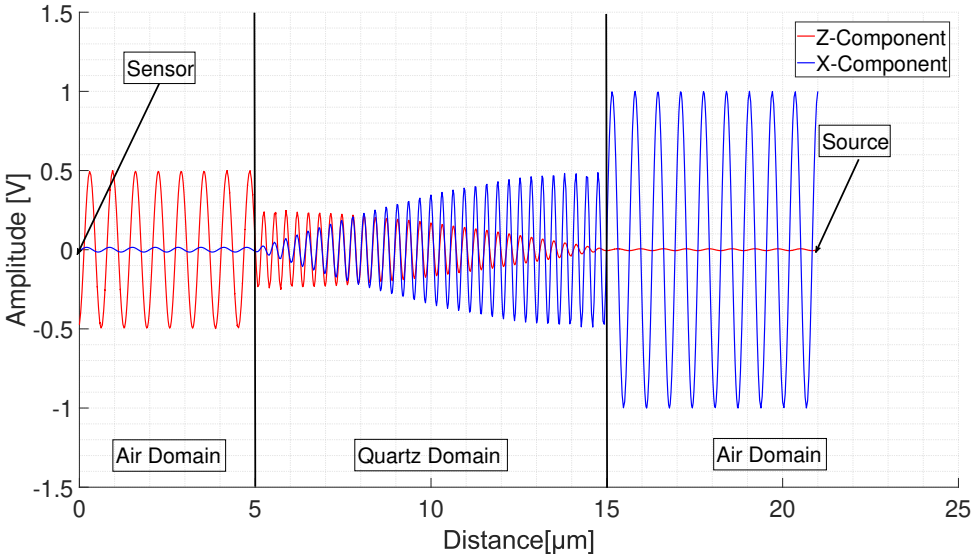

Figure 49: Non reciprocity test at **T**= 1.3

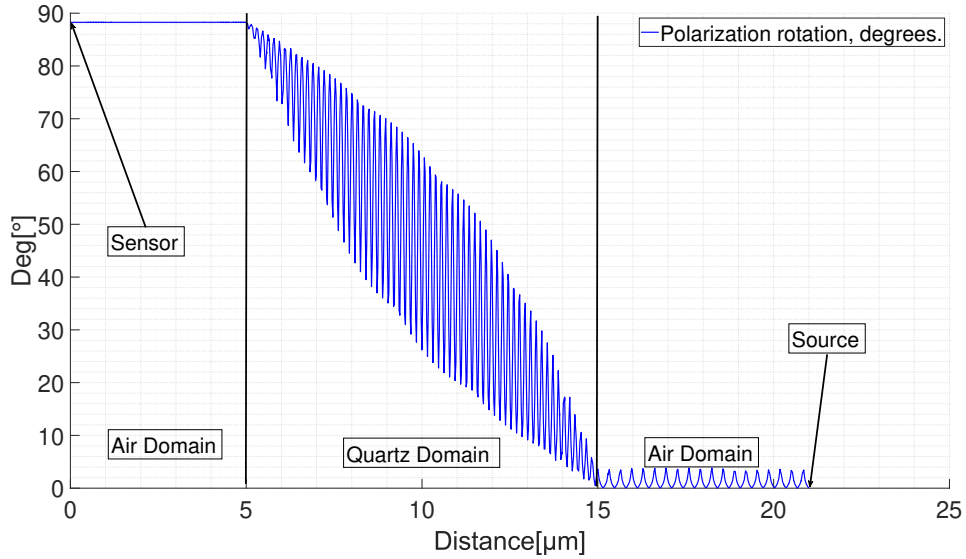

Figure 50: Non reciprocity test at **T**= 1.3

The experiment showed that the rotational direction of the Faraday effect is unchanged and independent of the injection side of the magneto optical medium. With this result its possible to say that the Faraday effect was achieved in FEM.

4.1.3 Varying source light intensity

This design captures the rotation angle by examining the X and Z-component of the applied light. In a bulk-glass open-core optical current transformer this should mean that the rotational angle is independent of the source light intensity. In a real-world scenario this would not be true, depending on the sensing technology of the OPCT. Based on the load test showed in figure 68, a source light intensity test was completed. To perform this test the same preconditions were uphold, except the source light intensity was raised from $1V/m$ to $3V/m$. The results of the experiment is shown in figure 51 and figure 52.

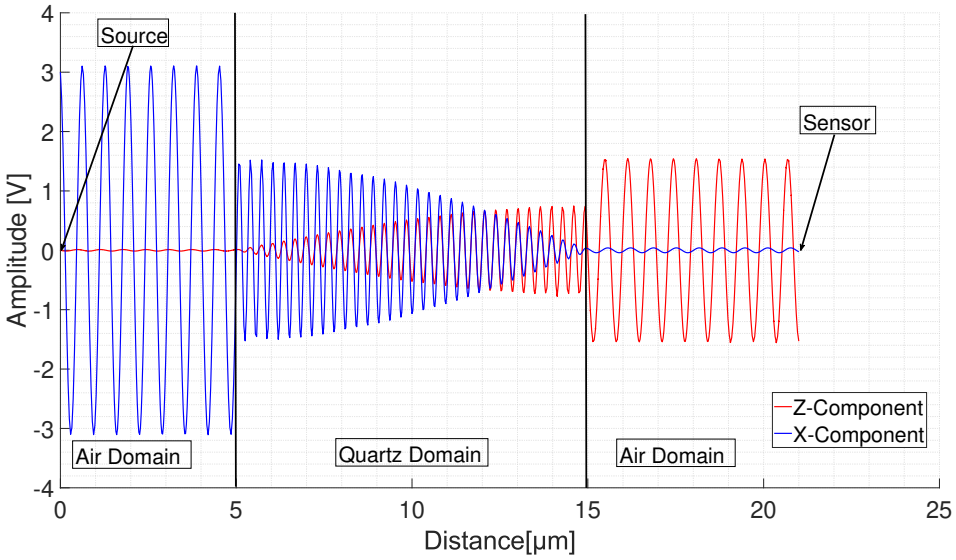

Figure 51: High-load, high intensity source light at $3V/m$, with an external field strength of **T**= 1.3

The behavior observed in figure 52 shows no abnormalities at a intensity of $3V/m$, compared to the regular load situation at $1V/m$ light intensity in figure 68 experiments.

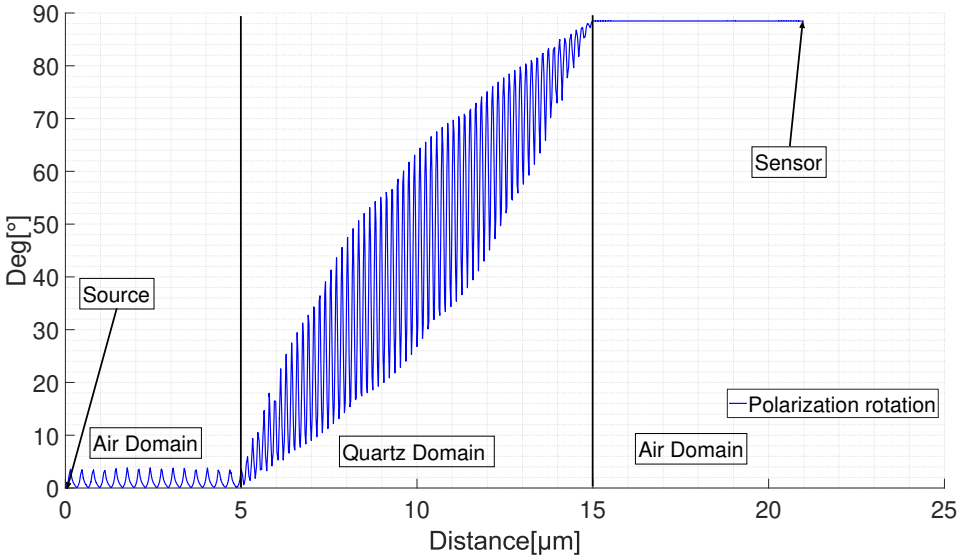

Figure 52: Polarization angle at high-load with source light intensity at $3V/m$. **T**= 1.3

The resulting polarization rotation recorded is identical to the polarization rotation recorded at $1V/m$ light intensity. The results of these experiments show that the output current of the optical model of the OPCT is independent of applied source light intensity for this detection method.

4.2 Electrical Modelling

Due to the lack of a physical optical current transformer electrical circuit, frequency response data is obtained from [90]. The electrical model data shown is experimentally obtained from a real-time apparatus, and the resulting transfer function is compared and verified to the physical optical current transformer. [91]
The transfer function used for the electrical model is shown in equation 21.

$$H(z) = \frac{-0.01102z^5 + 0.01763z^4 + 0.0156z^3 - 0.03298z^2 + 0.01282z^1 + 0.03276}{z^5 - 2.738z^4 + 3.394z^3 - 2.425z^2 + 0.9712z^1 - 0.1669} \tag{21}$$

The transfer function is validated against the experimentally obtained data in figure 53.

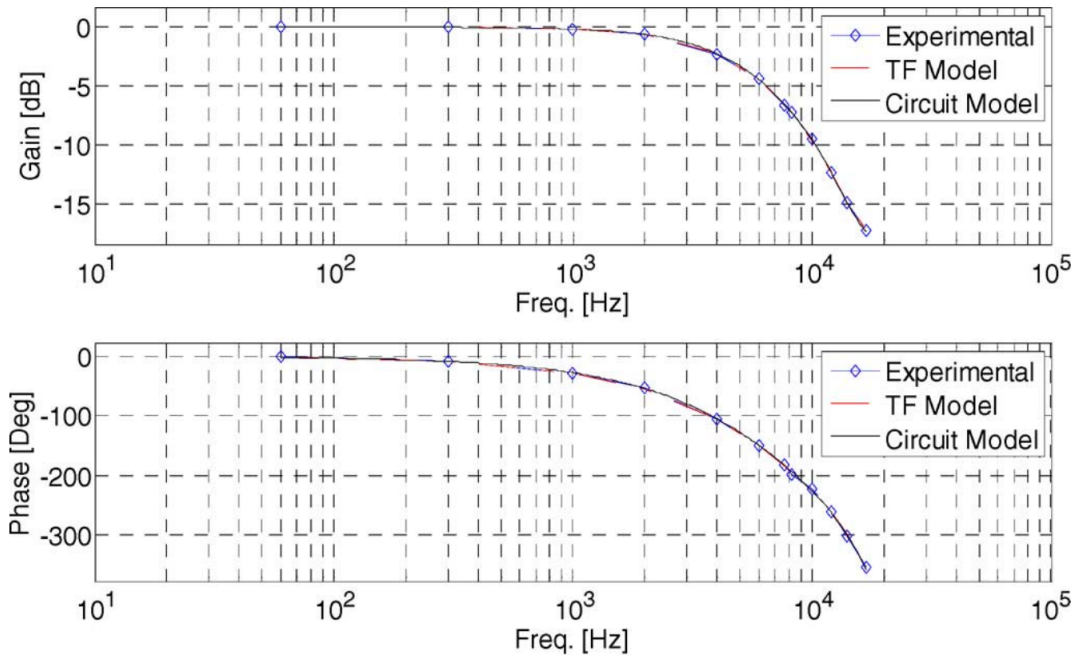

Figure 53: Frequency response comparison of experimental results and model. [91]

The comparison shows a satisfactory representation of the dynamics of the experimentally obtained data. The transfer function is validated against a real device and will be used as an electrical model in the complete model.

4.3 Complete Model

As previously mentioned the complete optical current transformer model is a combination of the optical and electrical sub-models. This combination is done in Simulink. Further this OPCT subsystem is deployed in a Simulink power system model for simulations. A figure of the complete model is shown in 54.

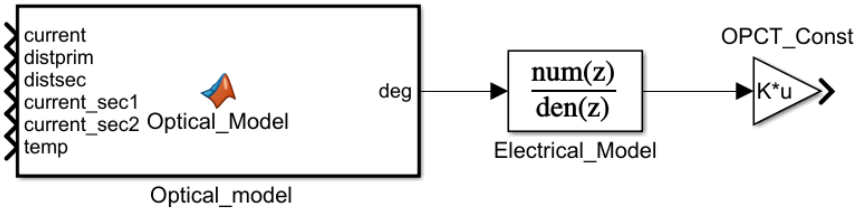

Figure 54: Complete OPCT model represented in Simulink.

The complete model has a few different input parameters to simulate different effects in the system:

- *current* : Input, Primary conductor current
- *distprim* : input, Distance between OPCTs and Conductors.
- *distsec* : Input, Distance between conductors.
- *current_sec1* : Input, Current adjacent conductor 1.
- *current_sec2* : Input, Current adjacent conductor 2.
- *temp* : Input, Temperature of the MO medium.
- *deg* : Output, resulting polarization rotation.

At the farther end of the model, an *OPCT_const* is added, to scale up the change in polarization rotation to the primary current. This is done by multiplying the rotational angle with a factor, because the optical current transformer is linear and proportional over its dimensioned operating range. Changing the distance of the OPCT from the conductor, or the Verdet constant of the magneto optical medium, would result in a need to re-evaluate the OPCT constant.
This model expects the conductor design to be inline as shown in figure 55.

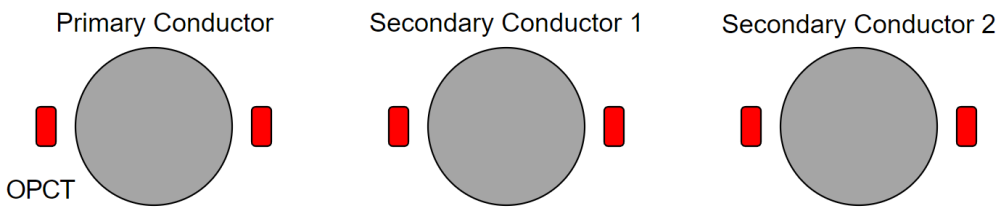

Figure 55: Setup of Conductors and optical current transformers.

Figure 55 showcases the architecture used for the conductors and OPCT in this model. Each conductor has two optical current transformers to compensate for external magnetic fields. All conductors are installed inline of each other. Default distance parameters used for this setting is $distprim = 0.06$ m, $distsec = 1$ m and the default ambient temperature is set to $temp = 20$C.

5 Results

To execute testing of the complete OPCT model, multiple scenarios are generated in the power system model. These scenarios are exported as transient files and played back as IEC61850 Sample values to a Siemens 7UT82 transformer differential protection relay. The reactions and COMTRADE files recorded by the transformer differential protection is examined for each scenario.

5.1 Lab Setup

A certain amount of lab equipment is required to perform the experiments as mentioned. In this case a protection relay test set, GPS clock, network switch acting as a process bus and a protection IED was needed. The actual lab setup is shown in figure 56.

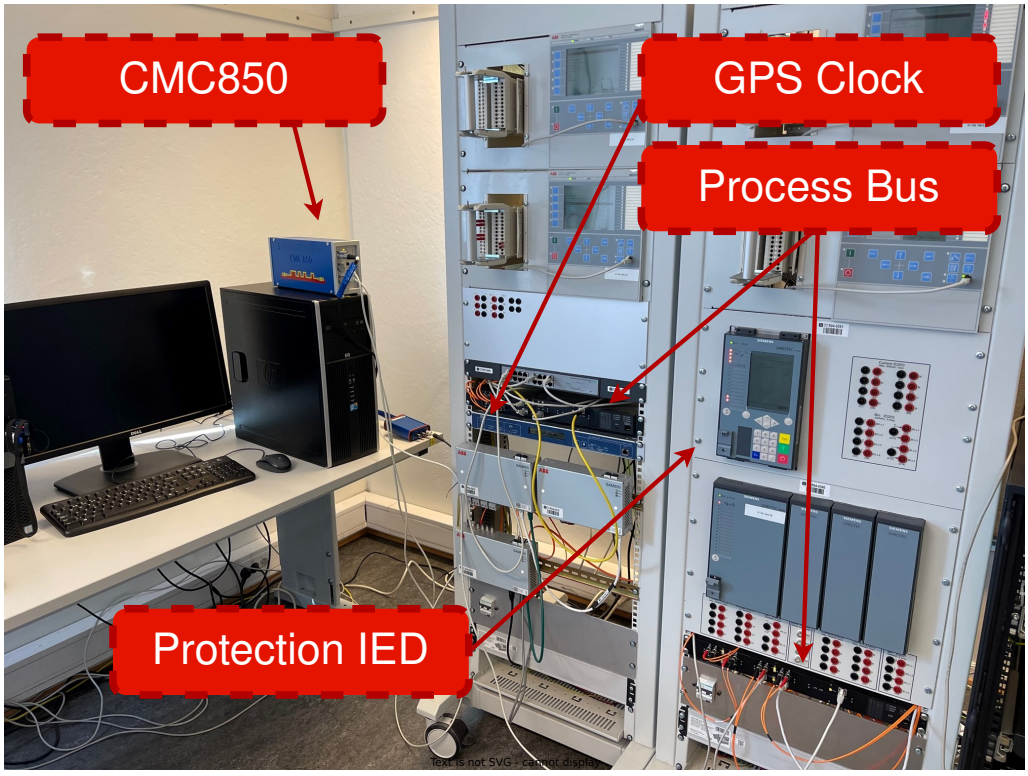

Figure 56: Laboratory setup.[94]

The optical current transformer performance was analyzed by injecting a stream of sample value measured values, these values are based on COMTRADE files generated by the model. In order to translate COMTRADE files generated by the power system model to Sample value injections a OMICRON CMC850 protection relay test set is utilized. Furthermore the *advanced transplay* module by OMICRON is used to replay the COMTRADE files as IEC61850 compliant Sample

Values.[95][96]
The Siemens IED is configured as a Sample Value client, subscribing to the stream of Sample Values generated by the OMICRON. A crucial component in Sample Value transmission is a healthy time synchronization, this is handled by a GPS clock over a NTP-Protocol.
The protection relay was parameterized based on guidance from a differential protection guide [44]. The final settings of the differential protection is shown in table 4.

Function	**Setting**
Slope 1	0.1
Turningpoint 1	1.2In
Slope 2	0.25
Turningpoint 2	4In
Idiff>	0.8
Idiff>>	7.5In
Idiff>>>	15In

Table 4: Differential protection settings 7UT82.

These parameters are parameterised slightly optimistically for conventional current transformers to show the performance difference between OPCT and CCT. These settings resulted in the differential protection characteristic shown in 57.

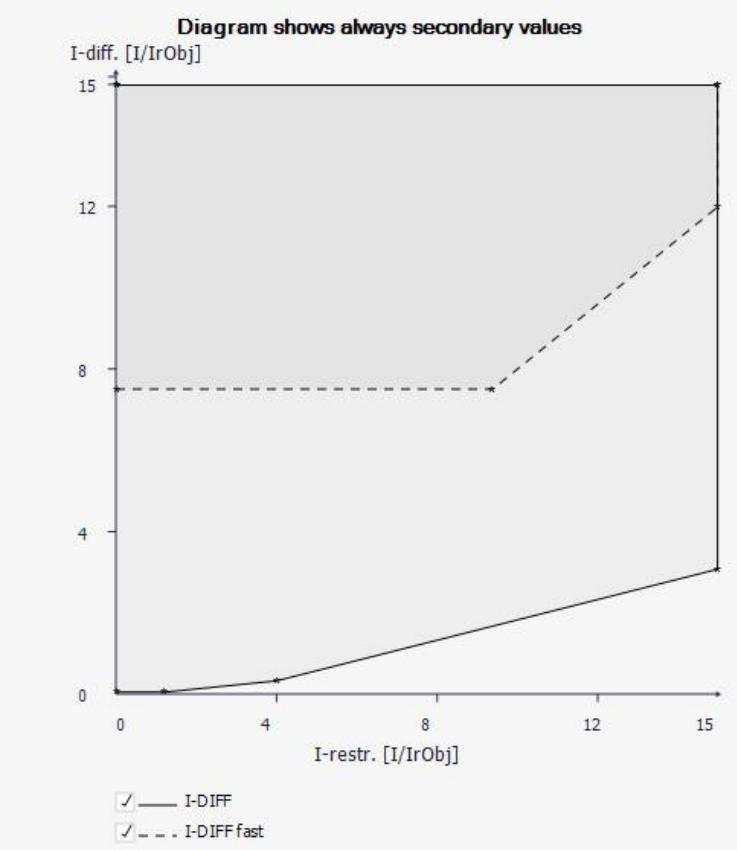

Figure 57: Resulting Differential protection characteristic.[97]

To verify the Sample Value streams OMICRON SV-Scout [98] and Wireshark were used. Both are able to capture the Sample Value stream packets to show the stream of packets in a network. A screen dump of a Wireshark verification of the lab SV streams are shown in figure 58.

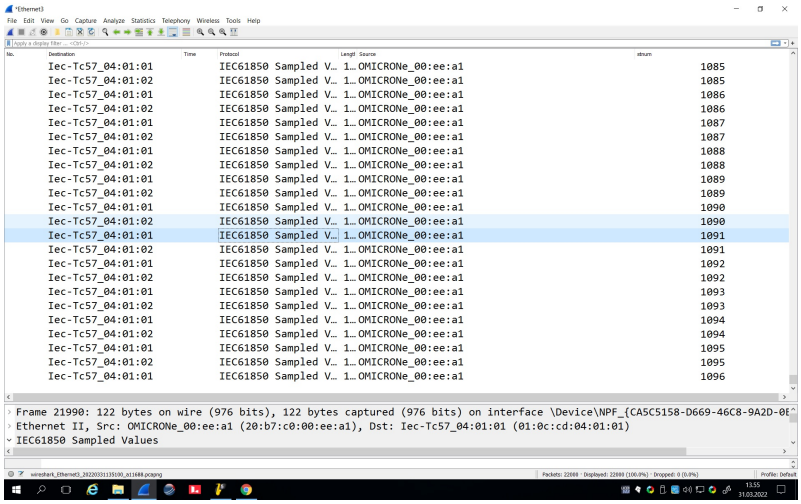

Figure 58: Wireshark Packet Capturing process bus Lab.

The use of Wireshark eases the troubleshooting and verifies the actual stream of packets happening. Any faulty time sync would be hard to spot in Wireshark due to the cryptic standard of the BER ASN.1 data structure.

5.2 Simulation Model

To generate COMTRADE files for use in the lab, the following power system model was used, as shown in figure 59.

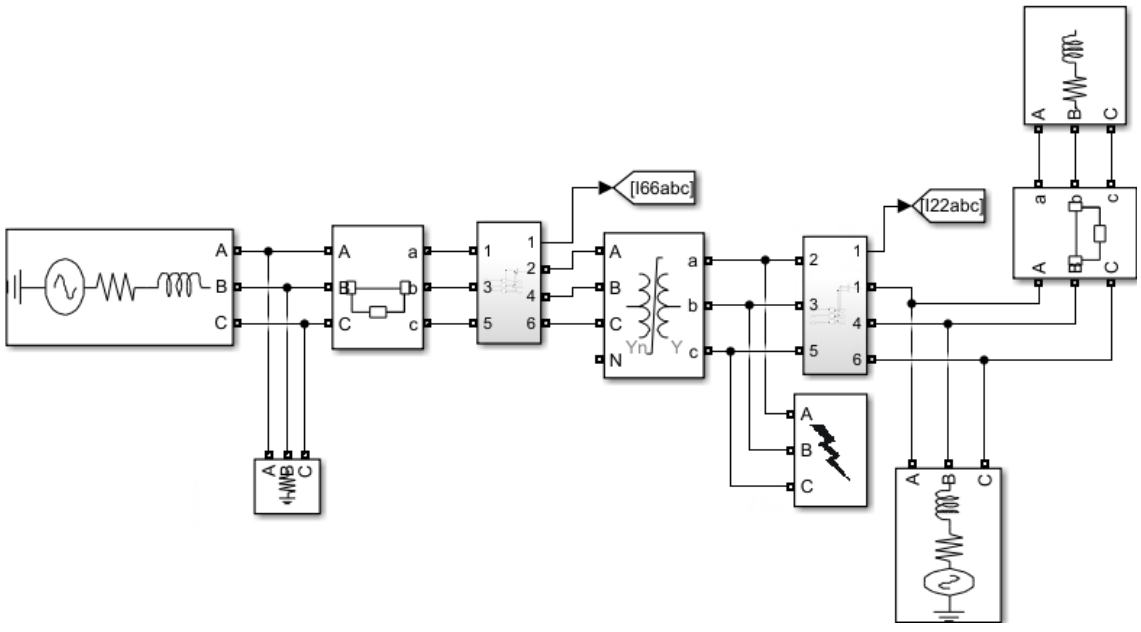

Figure 59: Power system model for simulation in Simulink.

The power system model consists of one power transformer, two circuit breakers, one load and two sources. On each side of the power transformer an optical current transformer and a conventional current transformer were added in series, and their outputs both generated COMTRADE files simultaneously. This was done to be able to analyze and compare their generated output wave forms. The model has capabilities of simulating normal load scenarios, inrush scenarios as well as external and internal transformer faults, covering the main focal points of this thesis.

5.3 Performance Results

The performance results of the experiments are products of different scenarios. The performance results includes accuracy rating, differential protection performance as well as the most common error sources: Vibration, temperature and adjacent magnetic fields, covering core non-linearities. The performance results are evaluated with a conventional current transformer as reference, this is done to lay groundwork for evaluating the use of OPCT in place of CCTs. Interoperability between the two is also examined in the performance results.

5.3.1 Accuracy Rating

The accuracy rating of the developed optical current transformer model is evaluated in relation the IEC61869 standard. [24] The OPCT is evaluated for ratio error, with methods mentioned in previous chapters.
The ratio error was examined by applying a steady load current at an expected rated current level, this current level was chosen as 600A for this power system. Figure 60 shows the current applied on the primary side as reference, as well as the current measured by the optical current transformer on the secondary side.

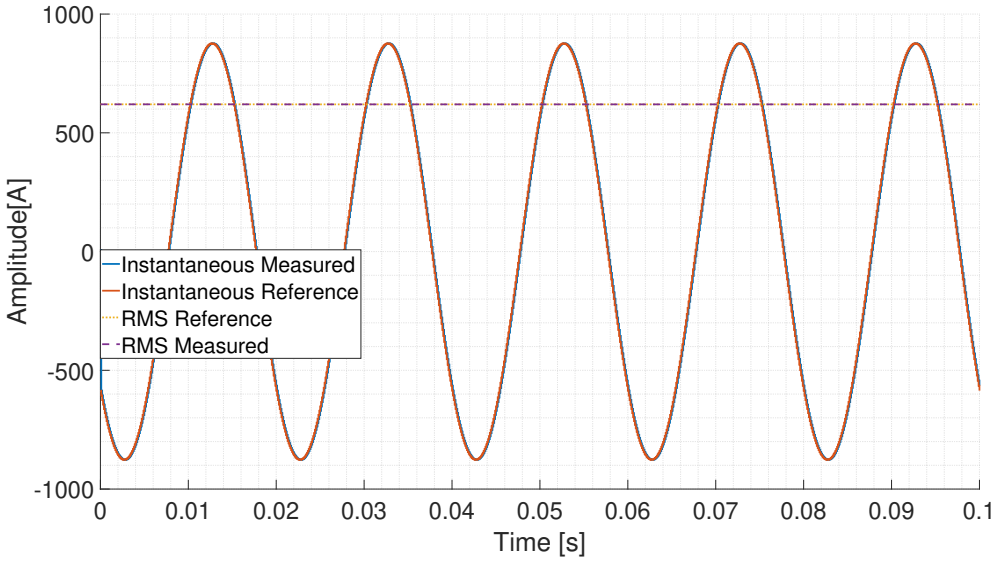

Figure 60: Applied instantaneous current and RMS current.

The ratio error was found using the formula shown in equation 2. Inserting this equation as a function in the measurement resulted in the following ratio error shown in figure 61.

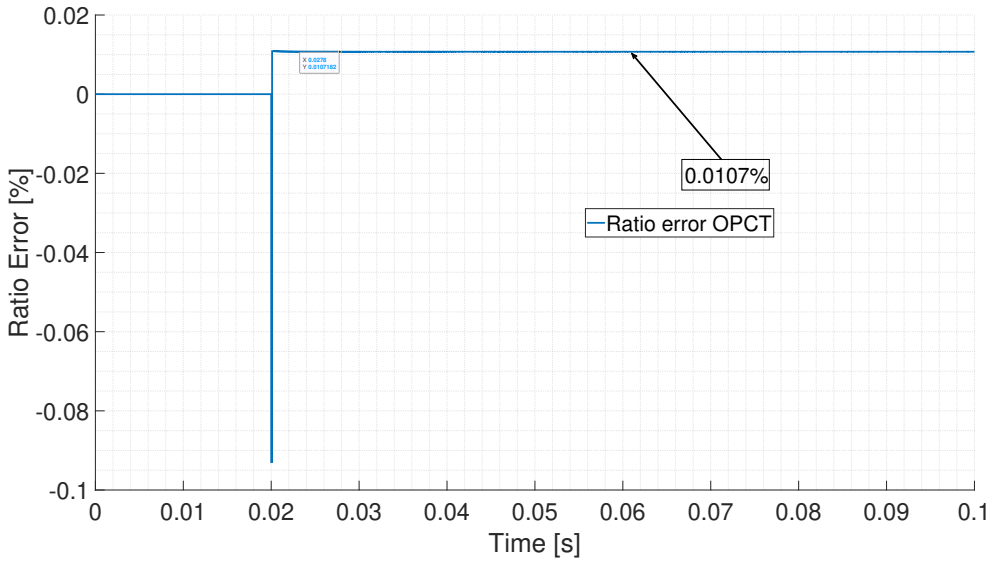

Figure 61: Resulting OPCT Ratio Error.

The accuracy test shows the optical current transformer to be accurate at a level of 0.0107% at a RMS current of 620A. This is within the IEC classification of 0.2S at rated current. To achieve the standard accuracy categorization given to most optical current transformers **0.2S**, the current transformer has to be accurate withing rated current, as well as at 1% of rated current.
The artifact of ratio error dropping in the figures at **T=0.02** is a result of the time steps of the RMS calculation, the RMS calculated after **T=0.02** is the true RMS of the current.

To evaluate the second step of the accuracy rating a 1% rated load is applied to the system, in this the result is a RMS current of 6.2A. The applied current as well as measured current is shown in figure 62, both RMS values and instantaneous values are shown.

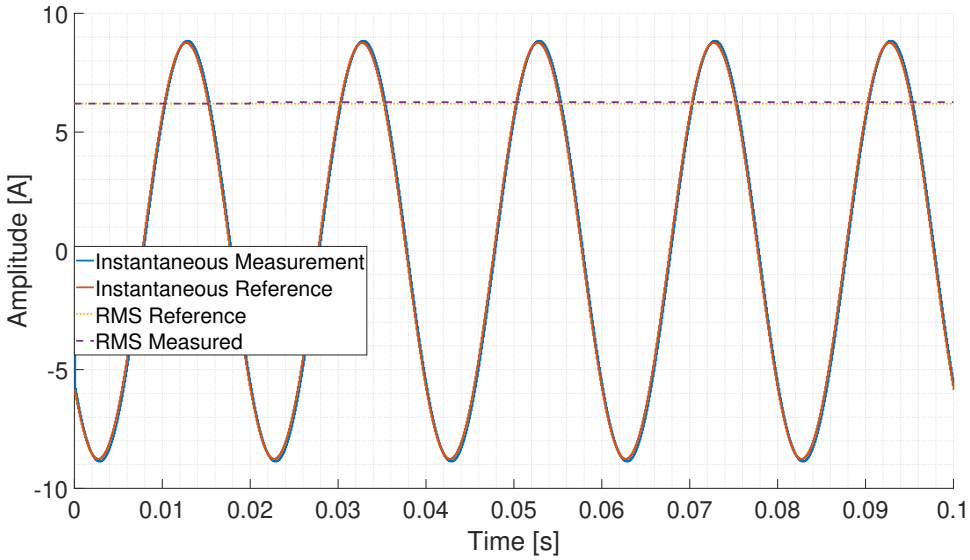

Figure 62: Applied Instantaneous current and RMS current.

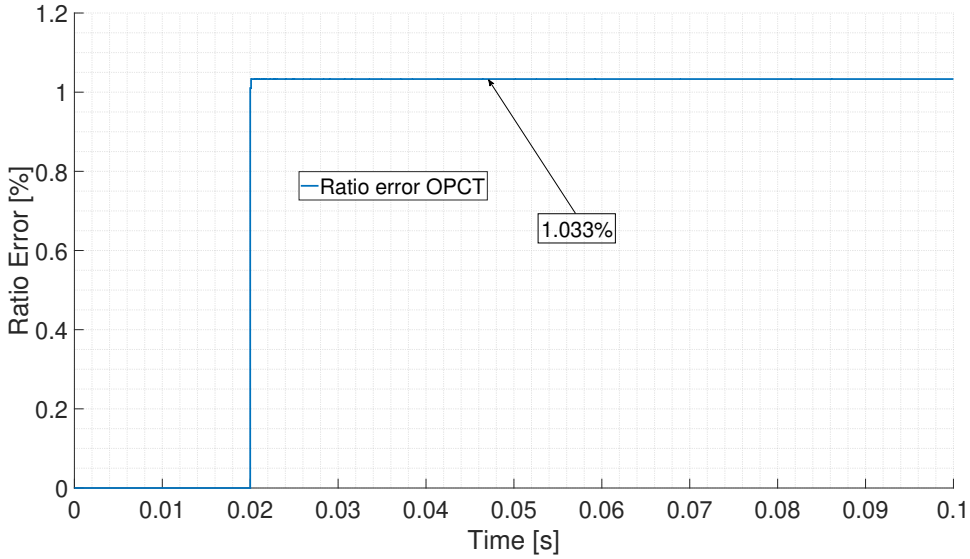

Figure 63: Resulting OPCT Ratio Error.

This load resulted in a ratio error of 1.033% as shown in figure 63. This error is beyond the limitations of the expected accuracy rating. To increase the sensitivity of the optical current transformer the transformer's distance to the conductor was decreased to increase overall sensitivity. Doing this resulted in the ratio error shown in figure 64.

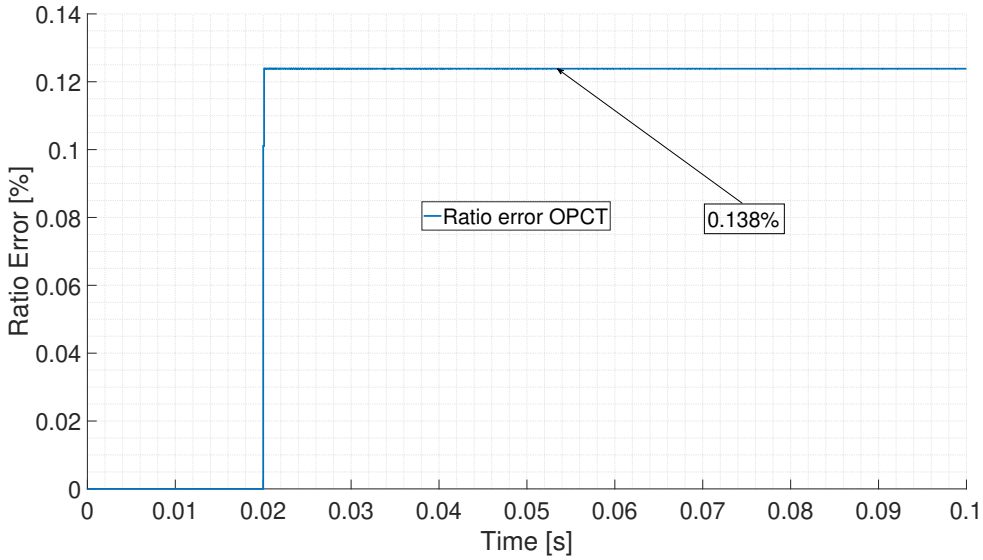

Figure 64: Resulting OPCT Ratio Error, with tuned optical current transformer distance.

The resulting ratio error after the tuning of the setup resulted in a value of 0.138% at 1% of rated current. Based on these test the current transformer can be classified as **0.2S**, based on the IEC61869 Standard. [24].

5.3.2 Distance from Conductor

The optical current transformer experiences an exponential decrease in magnetic flux with an increasing distance from the source, resulting in a possible significant change in output current based on the distance to the conductor.

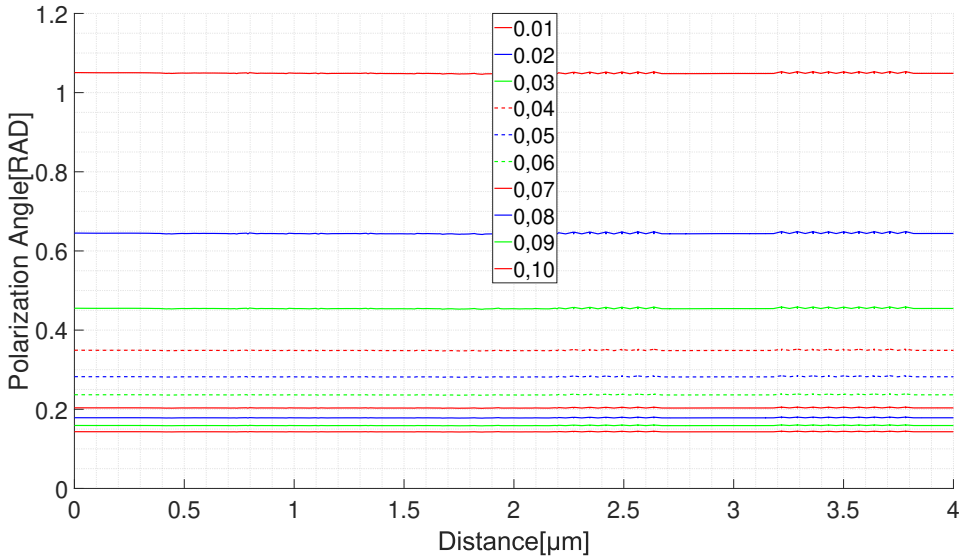

Figure 65: Measured output angle with constant current and varying distance from primary conductor.

Figure 65 shows multiple configurations installed with distances of 0.01m to 0.1m with 0.01m steps. The configurations were all exposed to the same level of magnetic field strength, but the output polarization angle varied significantly with distance from the conductor increasing, due to the inversely proportional decrease in magnetic field strength per distance unit.
This effect has drawbacks and advantages. By reducing the distance from the conductor one increases the magnetic field strength the MO material is exposed to per ampere, flowing through the conductor. By doing this the optical current transformer becomes more sensitive to conductor current, and less exposed to stray magnetic fields generated by external sources. But the increase in perceived magnetic field strength also results in a lower linear range.
The distance from the conductor has to be kept constant to ensure precise measurements in a open core configuration. Another way of negating this effect is installing multiple OPCT per phase to compensate for the movement.

5.3.3 Temperature

Magneto-optical material is sensitive to temperature changes because that the Verdet constant is temperature dependent. This could act as a significant source of error if uncompensated. The article represented in [83] obtained the error margin caused by temperature changes in a magneto optical medium experimentally. This experiment showed that a change in one Celsius resulted in an error margin of 0.2%. This dynamic was adapted to the Simulink model to be able to account for and show the effects of uncompensated temperature changes.

Figure 66 is the results of an experiment done on the complete optical current transformer model

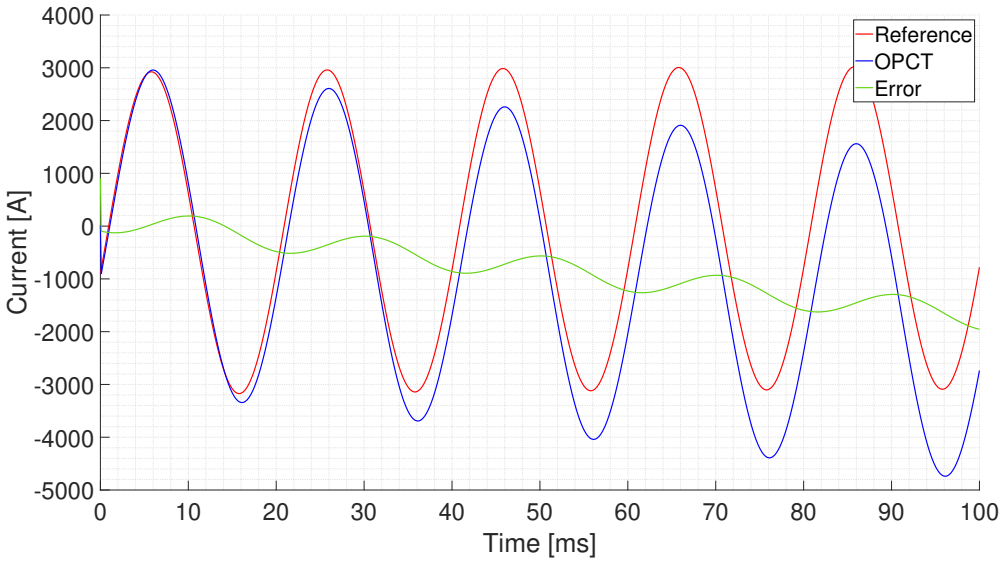

Figure 66: Temperature ramped from $20°C$-$40°C$.[94]

with the temperature error margin adapted. The Figure shows a ramping temperature from default $20°C$ to a peak of $40°C$. This resulted in a great error margin during high load. The induced error caused a incorrect trip of the transformer differential protection. To counteract the effect of the fluctuating temperatures and keep the system reliable, a temperature compensation has to be implemented.

5.3.4 Vibration

Vibrations can affect two crucial factors of a optical current transformer; the physical distance from the conductor and the perpendicularity of the light source in relation to the MO material, causing birefrigence.
Horizontal vibrations that may change the physical position of the OPCT in relation to the conductor results in an error margin close to the one which is represented in figure 65. The optical current transformer model was exposed to horizontal vibrations of 600Hz. [99] The test results are shown in figure 67.

The experiment showed significant changes in measured value during the vibration. The vibration level moved the OPCT far enough to result in incorrect operation of the protection relay. To counteract this effect, a closed core optical current transformer or multiple open-core OPCTs per phase is suggested.
Vibrations also have the potential to cause internal vibrations in the OPCT, changing its internal structure. In a normal situation the MO-material and source light are perpendicular to each other so as to eliminate the effect of induced double refraction when light hits the optical material at an angle. If the vibrations change the angle of the two components in relation to each other, a double refraction or birefringence happens, skewing the measurements. In figure 68 the source and MO are kept perpendicular, in figure 69 the source light changes to a offset of 2 degrees due to vibration.

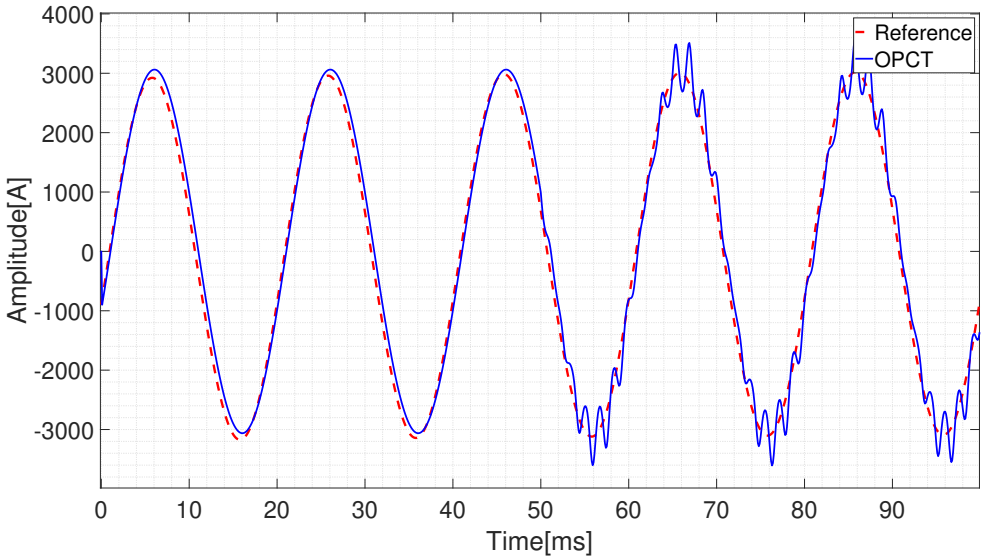

Figure 67: Horizontal vibrations 600Hz, vibrations start at t=50 ms.

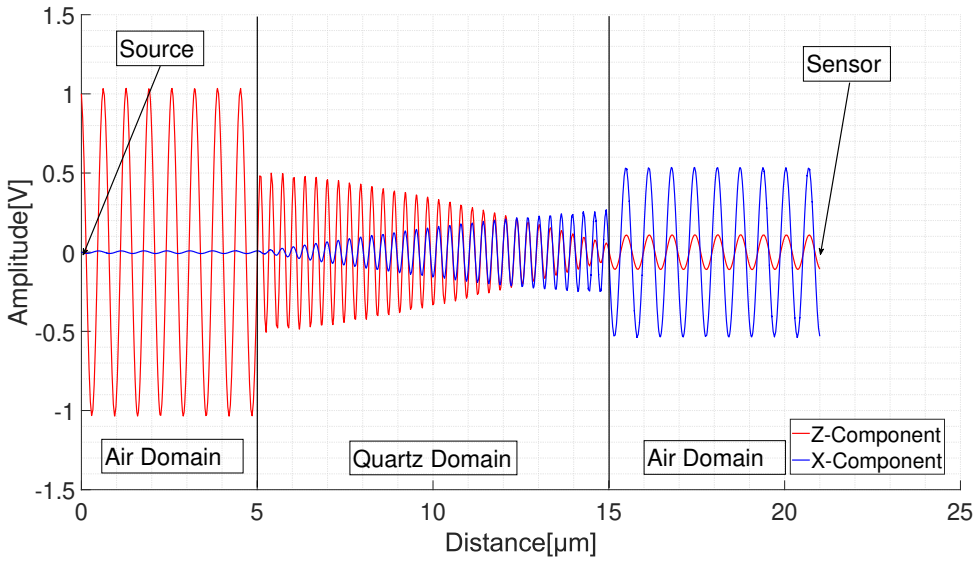

Figure 68: Standard polarization angle through optical model, perpendicular angle between MO and source light.

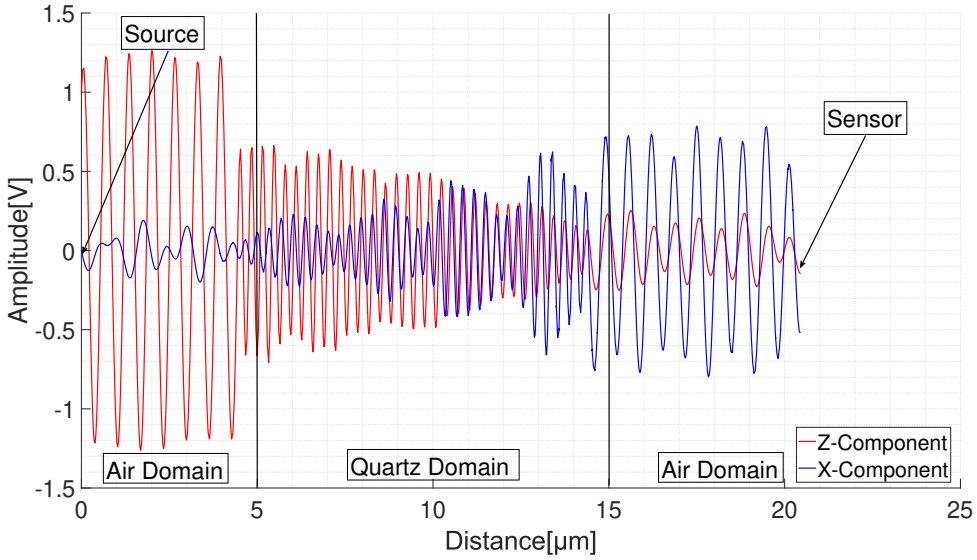

Figure 69: 2 degree offset between MO and source light.

This offset of 2 degrees results in a great induced error in the OPCT as shown in figure 69. These two degrees results in a overall error margin of 15%, putting the OPCT out of any accuracy class. The vibration simulations shows the severe effects vibrations can have on OPCTs, especially open core designs. The results further substantiates the use of closed-core current transformers.

5.3.5 External Magnetic Fields

Stray magnetic field induced by other sources than the primary measured source may greatly influence the measurements of a open-core OPCT. As a compensation for this effect two OPCT have been deployed per phase. These optical current transformers work together to separate the stray magnetic field from the primary magnetic field. To show the severe error that results from not compensating for this effect, the second OPCT was disabled for each phase and a load was applied to the system. To exaggerate the effect and showcase the effect of distance from the conductor this experiment was done with a radius from the OPCT to the conductor of 0.06m and 0.24m. [100]

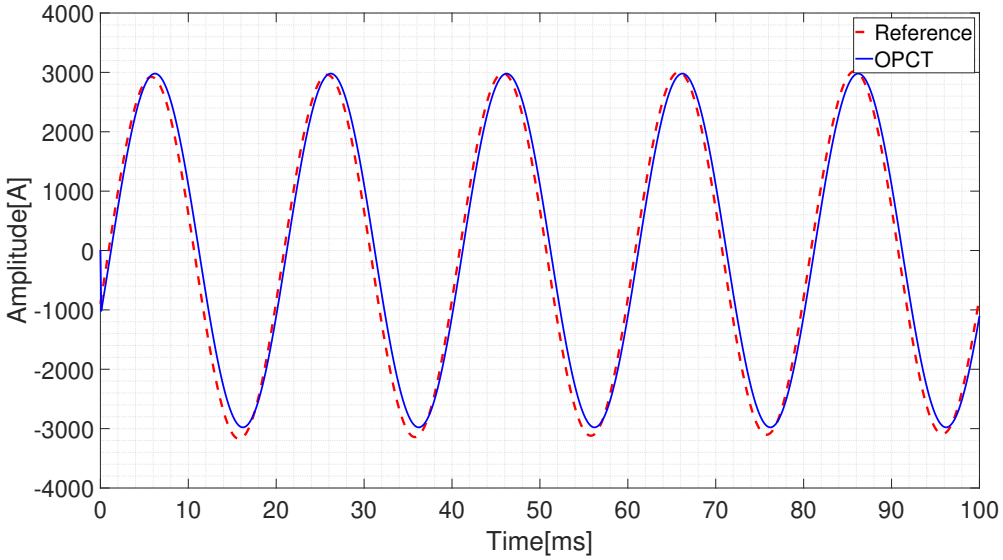

Figure 70: Uncompensated External fields, primary distance = 0.06m.

Figure 70 showcases the effect of a uncompensated stray magnetic field at a distance of 0.06m from the primary conductor. The close proximity of the OPCT to the conductor limits the error margin considerably. This resulted in a very low generated error margin, and no incorrect operation of the switchgear.

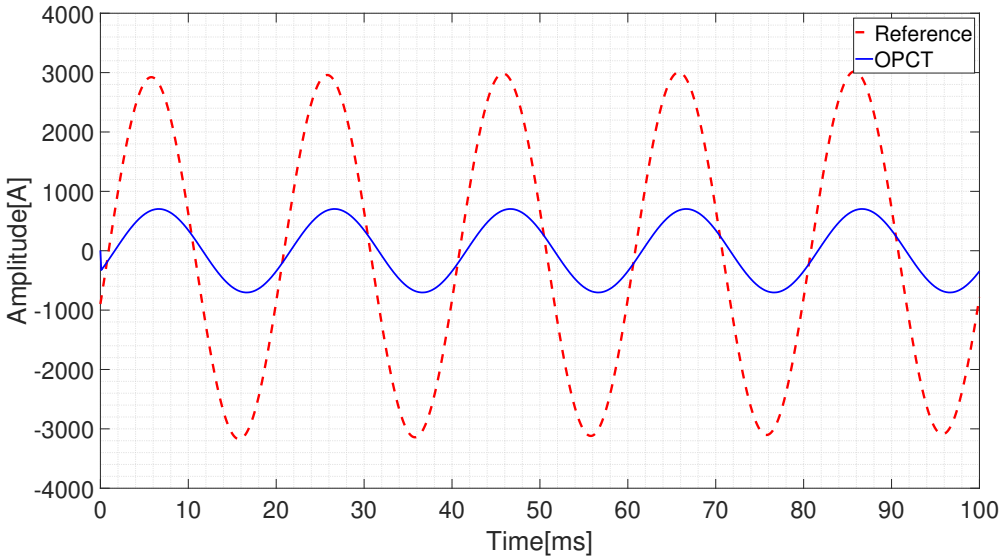

Figure 71: Uncompensated External fields, primary distance = 0.24 m.

Figure 71 showcases the effect of a uncompensated stray magnetic field at a distance of 0.24m from the primary conductor. The substantial distance from the conductor severely reduces the impact of the primary conductor, and increases the percent error margin of the stray magnetic fields. These stray magnetic fields has to be handled either by compensation in an open-core design or by implementing closed-core optical current transformers in place of the open-core ones.

5.3.6 Differential Protection Performance

Differential protection performance is a focal point of these experiments. The performance was analyzed by running a conventional current transformer and an optical current transformer through the same scenarios and comparing and analyzing the resulting output current wave forms. Mainly external faults were analyzed with different combinations of current measurement technologies. Internal faults kept a consistency between the two technologies, with no inconsistent control system reactions.

External fault experiments showed a performance gap between the two, mainly because of the saturable core of the conventional current transformer. A test with conventional transformers on both sides of the transformer is shown in figure 72 and 73.

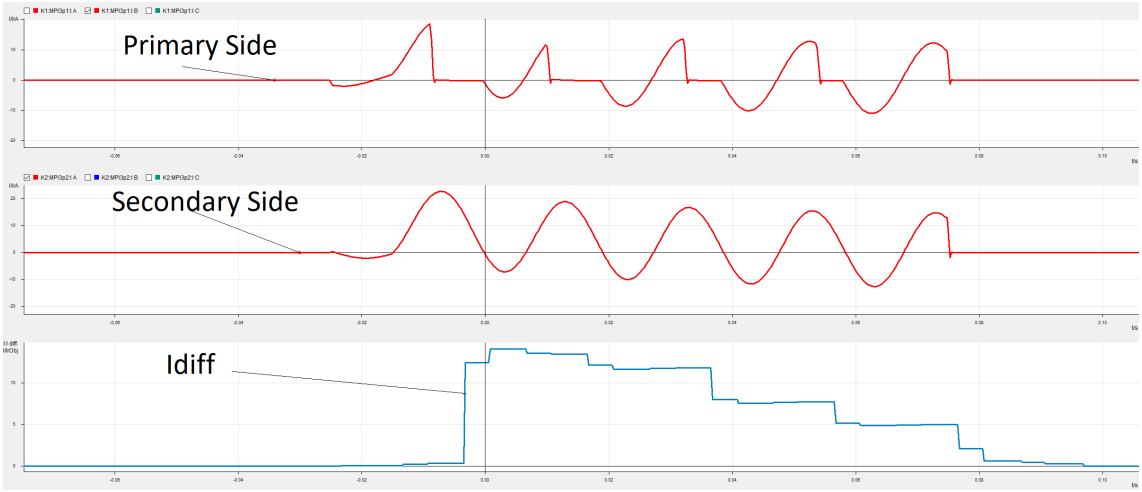

Figure 72: External fault, Measured currents CCT-CCT setup.

Figure 72 shows the effects of core saturation on at the primary side of the transformer. The peaks are clipped, and the overall RMS value of one side is reduced. The secondary side does not saturate, causing a large perceived differential current *Idiff* between the two sides.

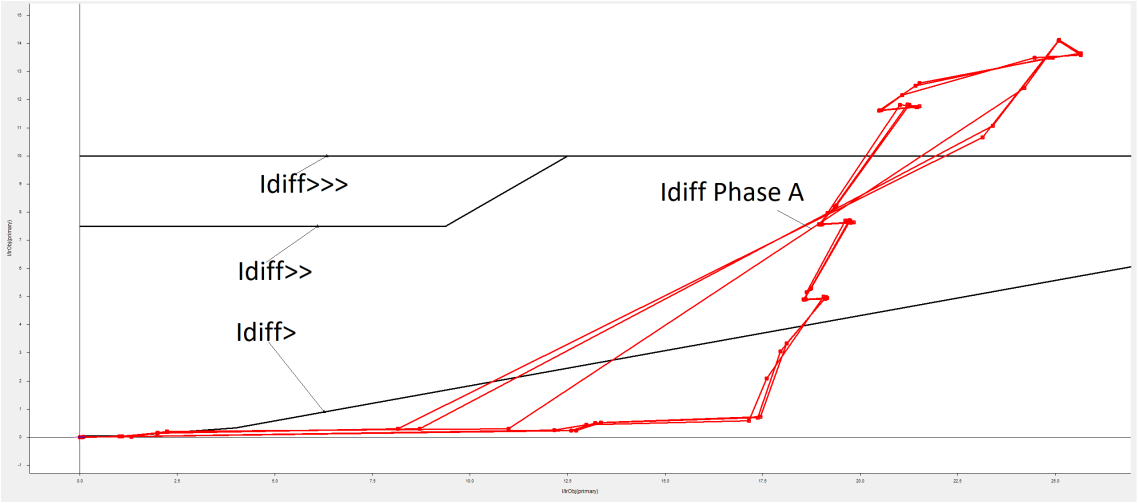

Figure 73: External fault, Differential current CCT-CCT setup.

Figure 73 shows the circular diagram of the differential current, plotted on the differential protection characteristic. An external fault should never be detected as an internal fault in a differential protection. In this case the transformer differential protection trips on $Idiff >>>$ and $Idiff >$ due to the falsely generated differential current between the two measurements that results from core saturation of one side.

Optical current transformers are unsaturable, and have a greater linearity than conventional transformers. The following experiment is equal to the one above, but with optical current transformers on each side of the transformer. Figure 74 shows the waves forms, figure 75 shows the wave forms plotted on the differential characteristic.

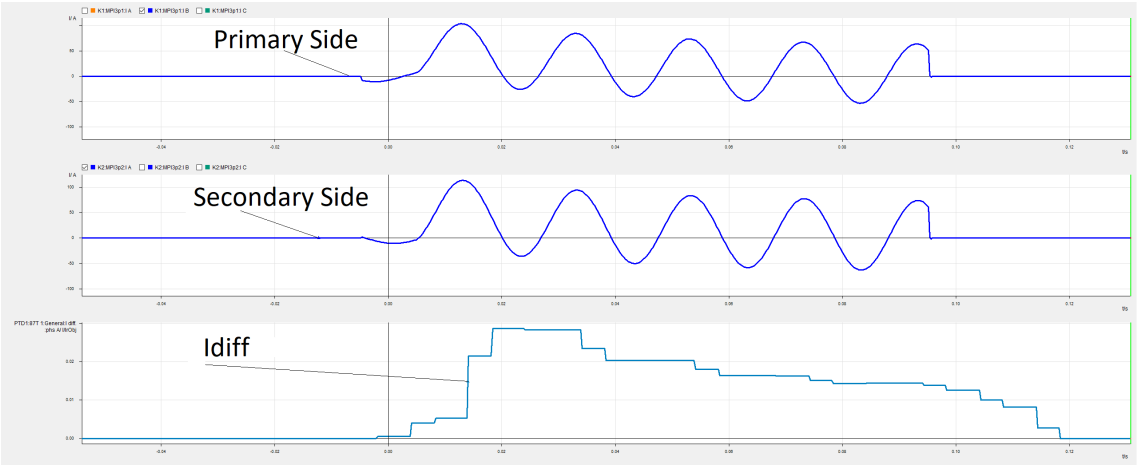

Figure 74: External fault, Measured currents OPCT-OPCT setup.

In figure 74 the wave forms on each side of the transformer are co-ordinated, with almost no differential current. The $Idiff$ in the figure is scaled down by a magnitude if 500 compared to the conventional current transformer test.

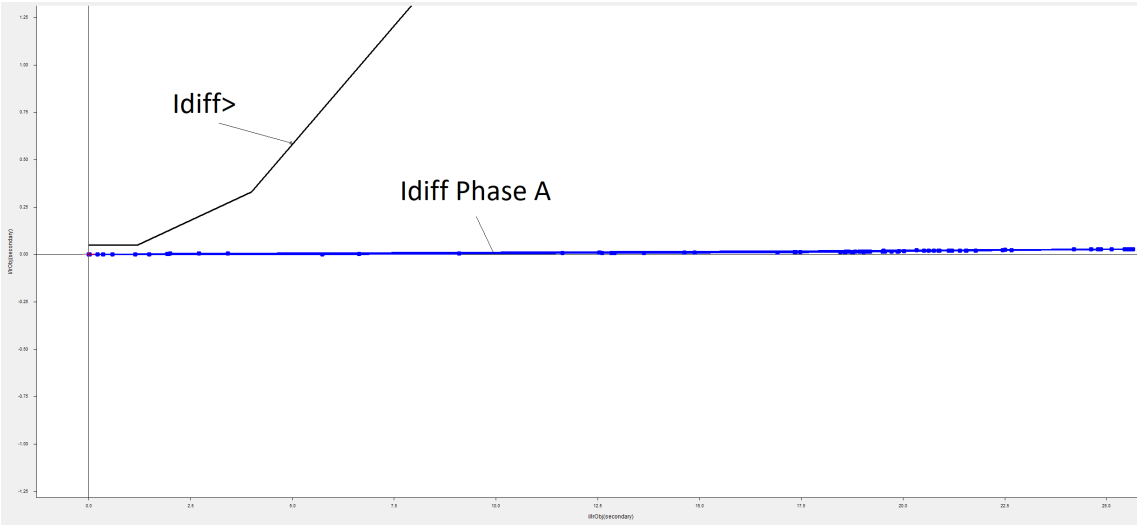

Figure 75: External fault, Differential current OPCT-OPCT setup.

Figure 75 further substantiates the claims of linearity. The differential currents of the two OPCTs does not exceed the $Idiff >$ setting, but rather keeps a linearly low value. This configuration does

not incorrectly trip the same external fault as the CCT configuration did.

5.3.7 Interoperability Differential protection

An experiment was done to analyze the interoperability of the two technologies. An external fault was added close to the transformer, and the current measurement technology was split into a conventional current transformer for the primary side and a optical current transformer for the secondary side. The wave form of the experiment is shown in figure 76, the resulting circular diagram is shown in 77.

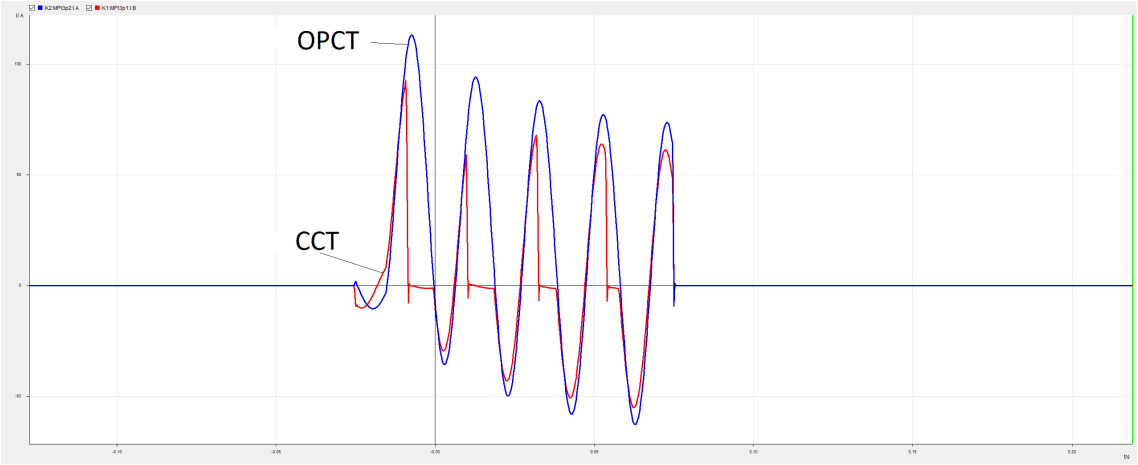

Figure 76: Current measurements OPCT-CT differences at same load.

Figure 76 shows a optical current transformer behaving close to the reference waveform while the conventional current transformers core is saturating and skewing the measurements of the primary side. The difference between the two measurements at high current results in a large $Idiff$ current.

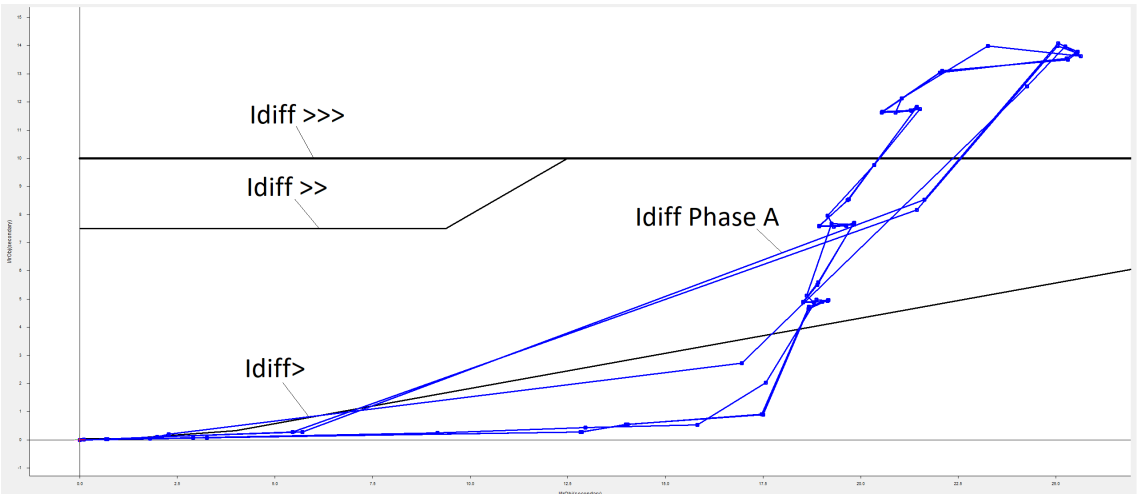

Figure 77: Differential current External fault OPCT-CT.

Figure 77 shows the circular diagram of the differential current and the differential protection characteristic. The differential current is great enough to trip the protection relay due to the core saturation. The differential current is almost identical to the one of double CCT configuration. This

experiment results in a need to have the equal performance on each side of the power transformer to reap the benefits of an increased performance. A benefit gained by substituting one conventional current transformer with a OPCT is eliminating any chance of saturation.

6 Conclusion and Further Work

6.1 Conclusion

The digital substation enables the use of several beneficial functions as IEC61850 communication protocols, along with optical current transformers with IEC 61850 Sample Value streams as output medium. The optical current transformer itself can also provide many benefits compared to a conventional current transformer. These include; reduced maintenance requirements, lower operational costs, increased safety for personnel and a striking increase, especially with regards to linearity, as well as improved overall accuracy.

A drawback with the open-core bulk-glass optical current transformer is the increased vulnerability to external stresses and a price increase due to a more intricate design compared to a conventional current transformer. The open-core design is especially vulnerable to stray magnetic fields and vibrations as shown in this work. The error sources in this thesis are mostly corrected by moving to a closed-core design, this seems like a more sensible technology to adopt.

Based on the optical model demonstrated in this work it's possible to verify the finite element method as an effective means to model not only an open-core bulk-glass optical current transformer, but also to simulate the Faraday effect and other non-ideal effects successfully.

The primary outcome of this thesis is the construction and verification of FEM modelling. FEM modelling is shown to be a promising method of modelling optical effects in an optical current transformer—effects that are challenging to recreate through other modelling techniques. The complete model replicates expected results when put under external stresses such as vibration, temperature changes and stray magnetic fields.

These external effects are shown to affect the performance of the OPCT significantly, and to achieve reliable operation these must be compensated for.

The resulting complete model of the optical current transformer shows significant performance increase over a conventional current transformer in a differential protection setting. These results are mainly due to the increased linearity and accuracy of the optical current transformer. This performance increase enables the protection relay parameters of the differential protection to be more conservative, resulting in a higher sensitivity and sophistication of the differential protection parameter-set.

In a differential protection setting the interoperability of an optical current transformer and a conventional current transformer shows no apparent performance increase over a setup with only conventional technologies. The main benefit gained by substituting one conventional current transformer with a OPCT is the elimination of any chance of core saturation at the given current levels. The performance increase in a differential setting is significant when deploying the optical design as measurement device for all side of a transformer.

6.2 Further Work

This project only covered optical current transformers of the type bulk-glass open-core designs. A natural step for further research and development of the model created in this thesis would be to cover other optical current transformer designs. This would enable the comparison and interoperability test of OPCT designs.
The model was not compared to a physical optical current transformer due to the absence of a OPCT. A verification against a similar open-core bulk-glass optical current transformer would further validate the design of the model and could provide important information about the model design.
A direct comparison between finite element method modelling and Jones matrice modelling could further illuminate the advantages of FEM as the preferred modelling technology.

Comparing the optical current transformer model to other non-conventional current sensing technologies could narrow down the actual performance increase an optical current transformer would provide as compared to other non-conventional sensing technologies. Especially Rogowski coils seem promising after the literature review, due to their increase in linearity over a conventional current transformer.

References

[1] Chendan Li et al. 'Grid architecture for future distribution system — A cyber-physical system perspective'. In: Oct. 2017, pp. 5235–5239. DOI: 10.1109/IECON.2017.8216906.

[2] Tamilmaran Vijayapriya. 'Smart Grid: An Overview'. In: *Smart Grid and Renewable Energy* 02 (Jan. 2011), pp. 305–311. DOI: 10.4236/sgre.2011.24035.

[3] Myungchin Kim, Sung Lee and Sungwoo Bae. 'Decentralized Power Management for Electrical Power Systems in More Electric Aircrafts'. In: *Electronics* 7 (Sept. 2018), p. 187. DOI: 10.3390/electronics7090187.

[4] electrical engineering portal. *$MV_CTSetup$*. 2021. URL: https://electrical-engineering-portal.com/wp-content/uploads/2020/01/iec-nema-ratings-current-transformers-cts-medium-voltage-switchgear.jpg (visited on 12/03/2022).

[5] Ji-Lei. Yi Yuan. Yubo and Yi. Yang. *IEC 61850-Based Smart Substation : Principles, Testing, Operation and Maintenance*. 2019.

[6] Ingvill Urdal Rian. 'Application of Optical Current Transformers in Digital Substations'. In: (2018).

[7] Defeng Chen et al. 'The Differentiation Analysis between Smart Substation and Comprehensive Automation Substation'. In: 2016.

[8] Chenglei Sun, Ying Zhang and Shiguang Qu. 'Research on Secondary System of Smart Substation'. In: *IOP Conference Series: Materials Science and Engineering* 394.4 (Aug. 2018), p. 042118. DOI: 10.1088/1757-899x/394/4/042118. URL: https://doi.org/10.1088/1757-899x/394/4/042118.

[9] Norges vassdrags- og energidirektorat. 'Fra Brettet til det Smarte Nettet Ansvar for driftskoordinering i kraftsystemet'. In: (2020).

[10] Aashir Waleed et al. 'Effectiveness and Comparison of Digital Substations Over Conventional Substations'. In: *Advances in Science, Technology and Engineering Systems Journal* 4 (Aug. 2019), pp. 431–439. DOI: 10.25046/aj040452.

[11] ABB. *ABB Digital substations concepts and applications*. 2017. URL: https://clc-iq.com/blog/2018/06/01/online-reputation-and-management/ (visited on 12/03/2022).

[12] Alexander Apostolov. 'Efficient maintenance testing in digital substations based on IEC 61850 edition 2'. In: *Protection and Control of Modern Power Systems* 2 (Dec. 2017), p. 37. DOI: 10.1186/s41601-017-0054-0.

[13] Vikas Shrivastava and CHRIS SALTER. 'FUTURE TRENDS TO SMART GRID AUTOMATION ARCHITECTURE BY IEC 61850'. In: Jan. 2018.

[14] Inc. SISCO. 'Overview and Introduction to the Manufacturing Message Specification (MMS)'. In: ().

[15] Rannveig.S.J. Loken. 'Testing of IED in a Digital substation'. In: *The Journal of Engineering* 2018 (July 2018). DOI: 10.1049/joe.2018.0172.

[16] André Oppegård. 'Modelling Optical Current Transformers in a digital substation'. In: (2021).

[17] International Telecommunication Union. 'OSI networking and system aspects - Abstract Syntax Notation One (ASN.1)'. In: (2002).

[18] Seyed Reza Firouzi et al. 'Interpreting and implementing IEC 61850-90-5 Routed-Sampled Value and Routed-GOOSE protocols for IEEE C37.118.2 compliant wide-area synchrophasor data transfer'. In: *Electric Power Systems Research* 144 (Mar. 2017), pp. 255–267. DOI: 10.1016/j.epsr.2016.12.006.

[19] Carl Kriger, S. Behardien and John Retonda. 'A Detailed Analysis of the GOOSE Message Structure in an IEC 61850 Standard-Based Substation Automation System'. In: *International Journal of Computers, Communications Control (IJCCC)* 8 (Oct. 2013), pp. 708–721.

[20] Grid Software Inc. 'GSE – GOOSE/GSSE Reference Manual'. In: (2014).

[21] ISO. 'Industrial automation systems — Manufacturing Message Specification — Part 1: Service definition'. In: (203).

[22] Byong-Kwan Yoo et al. 'Communication Architecture of the IEC 61850-based Micro Grid System'. In: *Journal of Electrical Engineering and Technology* 6 (Sept. 2011). DOI: 10.5370/JEET.2011.6.5.605.

[23] John D. McDonald. *Electric Power Substation Engineering,* 2006.

[24] NEK. 'Instrument transformers, Part 2:Additional requirements for current transformers'. In: (2012).

[25] Beckhoff Automation. *Basics current transformers.* https://infosys.beckhoff.com/english.php?content=../content/1033/sct0xxx/8933287307.html&id=. 2012.

[26] Elzbieta Lesniewska. 'Influence of the Selection of the Core Shape and Winding Arrangement on the Accuracy of Current Transformers with Through-Going Primary Cable'. In: (2021).

[27] Pallav Bera and Can Isik. *Intelligent Protection Classification of Transients in Two-Core Symmetric Phase Angle Regulating Transformers.* June 2020.

[28] Chen Baixin et al. 'Modeling and optimization of magnetic core TSV-inductor for on-chip DC-DC converter'. In: Nov. 2018, pp. 1–8. DOI: 10.1145/3240765.3240829.

[29] Stig Holst, Janez Zakonjsek and Ab. 'Transient Behaviour of Conventional Current Transformers used as Primary Transducers and Input Elements in Protection IEDs and Stand Alone Merging Units'. In: Jan. 2013.

[30] Sadik Kucuksari and George Karady. 'Experimental Comparison of Conventional and Optical Current Transformers'. In: *Power Delivery, IEEE Transactions on* 25 (Nov. 2010), pp. 2455–2463. DOI: 10.1109/TPWRD.2010.2050010.

[31] Ritwik Chowdhury et al. 'Determining CT Requirements for Generator and Transformer Protective Relays'. In: Oct. 2019.

[32] Donald G. Pellinen et al. 'Rogowski coil for measuring fast, high-level pulsed currents'. In: *Review of Scientific Instruments* 51.11 (1980), pp. 1535–1540. DOI: 10.1063/1.1136119. eprint: https://doi.org/10.1063/1.1136119. URL: https://doi.org/10.1063/1.1136119.

[33] Morteza Rezaee. 'Design Modification of Rogowski Coil for Current Measurement in Low Frequency'. In: *Iranian Journal of Electrical and Electronic Engineering* 6 (Dec. 2010).

[34] Mohammad Hamed Samimi et al. 'The Rogowski Coil Principles and Applications: A Review'. In: *IEEE Sensors Journal* 15 (Oct. 2014), pp. 651–658. DOI: 10.1109/JSEN.2014.2362940.

[35] Slawomir Tumanski. 'The Research of Vibration Monitoring System for Transformer Based on Optical Fiber Sensing'. In: *CRC Press.* 2011, p. 175.

[36] Marco Buzio. 'Fabrication and calibration of search coils'. In: *CAS 2009 - CERN Accelerator School: Magnets, Proceedings* (Apr. 2011).

[37] Harshad Mishra. 'Magnetic field sensor based on micro-structured magnetoelastic surface acoustic waves devices'. PhD thesis. Nov. 2019.

[38] Sascha Liehr. 'Optical Measurement of Currents in Power Converters'. In: (Apr. 2006).

[39] Dr. Steve Arar. *Hall Effect Current Sensing: Open-Loop and Closed-Loop Configurations*. https://www.allaboutcircuits.com/technical-articles/hall-effect-current-sensing-open-loop-and-closed-loop-configurations/. 2021.

[40] Gokhan Gokmen, Yelda Karatepe Mumcu and Nazm Ekren. 'Neuro network solution to the design of a Hall effect current transformer'. In: July 2008, pp. 184–188.

[41] rs-components. *hall-effect-sensors-guide*. https://ie.rs-online.com/web/generalDisplay.html?id=ideas-and-advice/hall-effect-sensors-guide. 2021.

[42] Michael Caruso et al. 'A New Perspective on Magnetic Field Sensing'. In: *Sensors (Peterborough, NH)* 15 (Dec. 1998).

[43] Takafumi Koseki et al. 'Measurement and modeling of nonlinear magnetic core characteristics of a fluxgate direct current sensor for wide-range current monitoring'. In: Dec. 2009, pp. 1–6. DOI: 10.1109/ICEMS.2009.5382643.

[44] Arcteq. 'AQ-T257 Instruction manual V2.01'. In: (2019).

[45] Armando Guzman et al. 'A current-based solution for transformer differential protection - Part I: Problem statement'. In: *Power Delivery, IEEE Transactions on* 16 (Nov. 2001), pp. 485–491. DOI: 10.1109/61.956726.

[46] Umer Ehsan et al. 'A Detailed Testing Procedure of Numerical Differential Protection Relay for EHV Auto Transformer'. In: *Energies* 14 (Dec. 2021). DOI: 10.3390/en14248447.

[47] Wikipedia. *Polarization waves*. http://en.wikipedia.org/w/index.php?title=Polarization%20(waves)&oldid=1057469350. 2021.

[48] Radek Pelc, Wolfgang Walz and J. Doucette. *Neurohistology and Imaging Techniques*. Sept. 2020. ISBN: 978-1-07-160426-7. DOI: 10.1007/978-1-0716-0428-1.

[49] J. Tioh, R.J. Weber and Mani Phd. 'Magneto-optical switches'. In: Oct. 2010, pp. 97–135. ISBN: 9781845695798. DOI: 10.1533/9780857090416.97.

[50] Shyam Singh. 'Refractive Index Measurement and its Applications'. In: *Physica Scripta* 65 (Feb. 2006), p. 167. DOI: 10.1238/Physica.Regular.065a00167.

[51] Adam Malik et al. 'Determination of refractive index on three mediums based on the principle of refraction of light'. In: *Journal of Physics: Conference Series* 1806 (Mar. 2021), p. 012003. DOI: 10.1088/1742-6596/1806/1/012003.

[52] Asmaa Jawad, Isaa Kadhim and Adnan Al-Ithawi. 'A New Technique for Measuring the Refractive Index'. In: *International Journal of Nanoelectronics and Materials* 11 (Oct. 2018), pp. 427–434.

[53] Ulf Lund. *Refraction at interface*. https://en.wikipedia.org/wiki/List_of_refractive_indices#/media/File:Refraction_at_interface.svg. 2014.

[54] V. Kumar and Jitendra Singh. 'Model for calculating the refractive index of different materials'. In: *Indian Journal of Pure and Applied Physics* 48 (Aug. 2010).

[55] Michael W. Abramowitz Mortimer; Davidson. *Optical Birefringence*. https://www.olympus-lifescience.com/en/microscope-resource/primer/lightandcolor/birefringence/. 2022.

[56] Mellon College of Science. *An Introduction to Optical Activity*. http://www.chem.cmu.edu/groups/bominaar/Test7.html.

[57] Sherif Hindi. 'Birefringence of bio-based liquid crystals'. In: *BioCrystals Journal* 1 (Mar. 2016), pp. 13–25.

[58] Newport Corporation. *Introduction to Waveplates*. https://www.newport.com/n/introduction-to-waveplates.

[59] Necdet Onur Urs et al. 'Advanced magneto-optical microscopy: Imaging from picoseconds to centimeters - imaging spin waves and temperature distributions (invited)'. In: *AIP Advances* 6.5 (2016), p. 055605. DOI: 10.1063/1.4943760. eprint: https://doi.org/10.1063/1.4943760. URL: https://doi.org/10.1063/1.4943760.

[60] E. Prati. 'PROPAGATION IN GYROELECTROMAGNETIC GUIDING SYSTEMS'. In: *Journal of Electromagnetic Waves and Applications* 17.8 (2003), pp. 1177–1196. DOI: 10.1163/156939303322519810. eprint: https://doi.org/10.1163/156939303322519810. URL: https://doi.org/10.1163/156939303322519810.

[61] Stefaan Vandendriessche. 'The influence of magnetic fields on light–matter interaction'. PhD thesis. May 2014. DOI: 10.13140/2.1.3201.7608.

[62] David Vojna et al. 'Verdet constant of potassium terbium fluoride crystal as a function of wavelength and temperature'. In: *Opt. Lett.* 45.7 (Apr. 2020), pp. 1683–1686. DOI: 10.1364/OL.387911. URL: http://opg.optica.org/ol/abstract.cfm?URI=ol-45-7-1683.

[63] Luciano Casado Joseb Zubia. 'Design and Development of a Low-Cost Optical Current Sensor'. In: (2013).

[64] V.A Kotov A.K Zvezdin. 'Modern Magnetooptics and Magnetooptical Materials'. In: 1997.

[65] Ricardo Silva et al. 'Optical Current Sensors for High Power Systems: A Review'. In: *Applied Sciences* 2 (July 2012), pp. 602–628. DOI: 10.3390/app2030602.

[66] Mohammad Hamed Samimi et al. 'Open Core Optical Current Transducer: Modeling and Experiment'. In: *IEEE Transactions on Power Delivery* 31 (Oct. 2015), pp. 2028–2035. DOI: 10.1109/TPWRD.2015.2490720.

[67] Optique Ingenieur. *Polarimetric Current sensors*. http://www.optique-ingenieur.org/en/courses/OPI_ang_M06_C04/co/etude.html. 2022.

[68] Truong Giang Nguyen. 'A REVIEW ON PROBLEMS AND COUNTER-MEASURES IN DESIGN AND FABRICATION OF OPICAL CURRENT SENSORS'. In: Nov. 2016.

[69] Silvio Ziegler et al. 'Current Sensing Techniques: A Review'. In: *Sensors Journal, IEEE* 9 (May 2009), pp. 354–376. DOI: 10.1109/JSEN.2009.2013914.

[70] T. Takahashi Genji; Sato. *Japanese Patent 1983: Optical Current Transformer*. 1983.

[71] Mohammad Hamed Samimi, Amir Abbas Shayegani Akmal and H. Mohseni. 'Optical Current Transducers and Error Sources in Them: A Review'. In: *IEEE Sensors Journal* 15 (Sept. 2015), pp. 4721–4728. DOI: 10.1109/JSEN.2015.2428652.

[72] Simon P. Bush and David A. Jackson. 'Numerical investigation of the effects of birefringence and total internal reflection on Faraday effect current sensors'. In: *Appl. Opt.* 31.25 (Sept. 1992), pp. 5366–5374. DOI: 10.1364/AO.31.005366. URL: http://www.osapublishing.org/ao/abstract.cfm?URI=ao-31-25-5366.

[73] G. A. Woolsey, N.E. Fisher and D. A. Jackson. 'Control of the Critical Angle of Reflection in an Optical Current Sensor'. In: *12th International Conference on Optical Fiber Sensors*. Optical Society of America, 1997, OWC24. DOI: 10.1364/OFS.1997.OWC24. URL: http://www.osapublishing.org/abstract.cfm?URI=OFS-1997-OWC24.

[74] Jianhua Wu and Xiaofeng Zhang. 'Recent Progress of All Fiber Optic Current Transformers'. In: Sept. 2020, pp. 134–143. DOI: 10.1109/IFEEA51475.2020.00036.

[75] Nobuki Itoh et al. 'Small optical magnetic-field sensor that uses rare-earth iron garnet films based on the Faraday effect'. In: *Appl. Opt.* 38.10 (Apr. 1999), pp. 2047–2052. DOI: 10.1364/AO.38.002047. URL: http://opg.optica.org/ao/abstract.cfm?URI=ao-38-10-2047.

[76] Stephen R. Forrest (Panel Chair) Larry A. Coldren Sadik C. Esener Donald B. Keck Frederick J. Leonberger Gary R. Saxonhouse Paul W. Shumate. 'Optoelectronics in Japan and the United States'. In: (1996).

[77] R. Wang et al. 'Optical fiber current sensor research: Review and outlooks'. In: (2016).

[78] Gao Wenjing et al. 'Multi-Wavelength Ultra-Weak Fiber Bragg Grating Arrays for Long-Distance Quasi-Distributed Sensing'. In: *Photonic Sensors* (July 2021). DOI: 10.1007/s13320-021-0635-4.

[79] Dejun Feng et al. 'Experimental study on fiber Bragg grating electric current sensor'. In: *Proceedings of SPIE - The International Society for Optical Engineering* (Aug. 2000), pp. 26–27. DOI: 10.1117/12.390558.

[80] Boston University Andrew Duffy Department of Physics. 'Essential Physics'. In: Sept. 2009, pp. 14–15.

[81] Hans Høidalen and Magne Runde. 'Continuous Monitoring of Circuit Breakers Using Vibration Analysis'. In: *Power Delivery, IEEE Transactions on* 20 (Nov. 2005), pp. 2458–2465. DOI: 10.1109/TPWRD.2005.855486.

[82] Mohammad Hamed Samimi, Amir Abbas Shayegani Akmal and H. Mohseni. 'Optical Current Transducers and Error Sources in Them: A Review'. In: *IEEE Sensors Journal* 15 (Sept. 2015), pp. 4721–4728. DOI: 10.1109/JSEN.2015.2428652.

[83] Qing Jia et al. 'Temperature Compensation of Optical Fiber Current Sensors with a Static Bias'. In: *IEEE Sensors Journal* 22 (Jan. 2022), pp. 352–356. DOI: 10.1109/JSEN.2021.3128937.

[84] Zhao Xiaojun et al. 'Clustered magneto-optical current sensor to eliminate the interference of a phase-to-phase magnetic field'. In: *Opt. Continuum* 1.2 (Feb. 2022), pp. 197–214. DOI: 10.1364/OPTCON.447649. URL: http://opg.optica.org/optcon/abstract.cfm?URI=optcon-1-2-197.

[85] Mohammad Hamed Samimi et al. 'Effect of Nonideal Linear Polarizers, Stray Magnetic Field, and Vibration on the Accuracy of Open-Core Optical Current Transducers'. In: *Sensors Journal, IEEE* 14 (May 2014), pp. 3508–3515. DOI: 10.1109/JSEN.2014.2328873.

[86] IEEE. 'IEEE guide for application of optical instrument transformers for protective relaying'. In: (2018).

[87] Jianping Wang, Ferry Viawan and Thomas Werner. 'Effects of sensor technology on differential protection'. In: *10th IET International Conference on Developments in Power System Protection (DPSP 2010). Managing the Change*. 2010, pp. 1–5. DOI: 10.1049/cp.2010.0313.

[88] Hongbo Li et al. 'Transient Performances Analysis and Experiment for Optical Current Transformer'. In: *Unifying Electrical Engineering and Electronics Engineering*. Ed. by Song Xing et al. Springer New York, 2014.

[89] Sadik Kucuksari. 'Development of Models for Optical Instrument Transformers'. In: (2010).

[90] Hafiz Ashraf et al. 'Modeling and Simulation of Optical Current Transformer using Operational Amplifiers'. In: Mar. 2017. DOI: 10.1109/ICEE.2017.7893440.

[91] Sadik Kucuksari and George Karady. 'Complete Model Development for an Optical Current Transformer'. In: *Power Delivery, IEEE Transactions on* 27 (Oct. 2012), pp. 1755–1762. DOI: 10.1109/TPWRD.2012.2203155.

[92] Merve Karakaya. 'CHARACTERIZATION OF MOLECULAR BEAM EPITAXIALLY GROWN CDTE LAYERS OVER GAAS BY SPECTROSCOPIC ELLIPSOMETRY'. PhD thesis. Dec. 2014. DOI: 10.13140/RG.2.2.20652.87682.

[93] Li Xin Cao, Yan Song Li and Jun Liu. 'Research on the Modeling of the Faraday Effect Based on the OCT Used in Power System'. In: *Design, Manufacturing and Mechatronics*. Vol. 551. Applied Mechanics and Materials. Trans Tech Publications Ltd, July 2014, pp. 275–279. DOI: 10.4028/www.scientific.net/AMM.551.275.

[94] Irina Oleinikova André Oppegård Mohammad Khalili Katoulaei. 'Complete FEM-based model of a bulk-glass optical current transformer'. In: (2022).

[95] Omicron Energy. *OMICRON CM-Line Catalog*. https://www.omicronenergy.com/download/document/41220528-3C40-4FD5-A0AE-0CF5A1ACB75D/. 2022.

[96] NEK. 'Communication networks and systems for power utility.' In: (2020).

[97] Siemens. '7UT6X Manual'. In: (2019).

[98] Omicron Energy. *SVScout*. https://www.omicronenergy.com/en/products/svscout/.

[99] Li Min et al. 'The Research of Vibration Monitoring System for Transformer Based on Optical Fiber Sensing'. In: *2018 IEEE 3rd Optoelectronics Global Conference (OGC)*. 2018, pp. 126–129. DOI: 10.1109/OGC.2018.8529978.

[100] Chun-Yan YANG et al. 'Study of the Electronic Current Transformer's Additional Error Testing'. In: Jan. 2017. DOI: 10.2991/eeeis-17.2017.21.